EXPERIMENTS ON UNSTAGGERED CASCADE SYMMETRICAL AIRFOILS FOR APPLICATION IN TURBINES OPERATING IN BIDIRECTIONAL WIND

A thesis submitted

in partial fulfillment of the requirements

for the degree of

MASTER OF TECHNOLOGY

by

R. KALIMUTHU

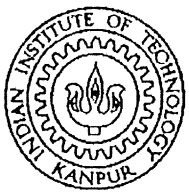

to the

DEPARTMENT OF AEROSPACE ENGINEERING
INDIAN INSTITUTE OF TECHNOLOGY KANPUR

March 1997

CERTIFICATE

It is certified that the work contained in this thesis entitled *"EXPERIMENTS ON UNSTAGGERED CASCADE SYMMETRICAL AIRFOILS FOR APPLICATION IN TURBINES OPERATING IN BIDIRECTIONAL WIND"* by *R. KALIMUTHU* has been carried out under my supervision and that this work has not been submitted elsewhere for a degree.

Professor K. Ghosh
Department of Aerospace Engineering
Indian Institute of Technology
Kanpur

March, 1997

Dedicated

to

My Beloved Parents & Sisters

Abstract

An unstaggered cascade consisting of only three symmetrical airfoils (NACA 0015) was fabricated for experimental purpose. Wind tunnel tests were carried out to examine the aerodynamic characteristics of the airfoils in this configuration. Pressure distribution over the cascade airfoils were measured for different angles of attack with different space chord ratios and for two different Reynolds Numbers(Re.Nos : 3.31×10^5, 4.6×10^5). With the help of pressure plots, lift and drag were calculated.

Wake measurements were made by means of wake survey rake and total drag was calculated. From the experimental studies, it was found that due to cascade effect the stall was delayed and some lift was obtained upto angle of attack 25^o.

The C_l vs α curve for an airfoil in the middle of the cascade has lower slope, compared to a single airfoil. As the angle of attack increases drag also increases, upto angle of attack 15^o. After that the drag decreases due to cascade effect. Thus the cascade effect improves lift-drag ratio for angles of attack above 15^o.

Acknowledgement

I am greatfully indebted to Prof. K. Ghosh, my thesis supervisor, for his excellent guidance and invaluble suggestions which enabled me to successfully finish my work.

My sincere thanks to Mr. Mohan, technical officer, of low speed A/D Lab and Mr. Rameswar who helped me to solve lot of technical problems while fabricating the model and carrying out the tests. I also thank Mr. Bhattacharya and his men of the Aerospapce workshop for their help in model fabrication. I thank Dr. K. Poddar, who helped me to solve lots of problems while experimentation.

My special thanks to Dr. E. Rathakrishnan for his help in technical and personal matters. I express my gratitude to Prof. N.G.R. Iyengar and Dr. C. Venkatesan for their support.

I extend my thanks to Saravanan(vandi), Sriram(low tech), KSrini(Dad), Satya(cc),Pandi, Uday(VANDI), KSiva(perusu), Joye(D'JIFF), Srini(gun), Araja(thollai), Kalya, Pachai(KR), S. Rajesh(thalaiva), Karum(dada), Bharathi(hema), Dr. Elango, Dr.N. Balakrishnan, Dr. Shanmugaraj, Rajesh(chem), and all others who made my stay at IIT a very memorable one.

My heartfelt thanks to Prof. K. Padmanaban., Prof. K.V. Narayanan., Prof.(Mrs.) C. Srihari Nagore., Mr.M. Paramasivam., Dr.N. Marisami., Mrs. Mohana and Mr. K. Nagarajan who encouraged me to pursue higher education. I also thank my friends Jayasri,Thirugnanam, Ilyas in MIT,Madras

I can never forget the love and help rendered by Veerakumar(thambi), Thangs, Ramaraj, Sriganesh, Mrs.Dhana, Malar, Mrs.Chitra, Muthamizh and Kanna for having moulded my future.

I would not have been who I am now, had it not been for my sister Mrs. Kaleswari and her husband Mr. Rajamanickam. They are responsible for guiding me through various critical stages of my life. I sincerely thank them for their kindness.

My thanks to all my relatives who helped me all through my life. I can never be able to repay the love and affection of my parents and sisters.

THE AUTHOR

Contents

NOMENCLATURE

Material Constants

ρ_a	density of air
ρ_w	density of water
μ	coefficient of viscosity of air

Flow quantities

$p_{o\infty}$	free- stream total pressure
p_∞	free- stream static pressure
p_{si}	surface static pressure
p_w	static pressure at the wake region
p_{ow}	total pressure at the wake region
q_∞	dynamic pressure
C_p	coefficient of pressure
V_∞	free-stream velocity
V_1	out flow velocity
V_w	velocity at wake region
$Re = \frac{\rho\, V_\infty\, C}{\mu}$	Reynolds Number
Ω	angular velocity of the turbine

Gemometric quantities

S/C	space chord ratio
C	chord length
S	wing area
b	wing span
G	gap between planes of the biplane turbine
Θ	angle between planes of the biplane turbine
t	pitch between two blades(see Fig.1.3)

Aerodynamic quantities

β	stagger angle
α	angle of attack
L	lift
D	drag
F_N	normal force of the airfoil
F_C	axial force of the airfoil
F_T	tangential force of the turbine blade
F_X	axial force of the turbine blade
C_l	lift coefficient
C_d	drag coefficient
C_{dp}	pressure drag coefficient
C_{ds}	skin friction drag coefficient
C_{F_C}	axial force coefficient of airfoil
C_{F_N}	normal force coefficient of airfoil
C_{F_T}	tangential force coefficient of turbine blade
C_{F_X}	axial force coefficient of turbine blade

List of Tables

List of Figures

Chapter 1

INTRODUCTION

1.1 Turbomachinery - Problem Outlook

Two dimensional cascade tests and analysis have historically played a key role in the development of axial-flow compressor , axial-flow turbine and pump design. Various organizations contributed numerous cascade tests from which a wealth of design informations can be obtained. A successful investigation of the cascade problem needs systematic experimental research, as it was done for the single airfoil. In this work we wish to investigate the aerodynamic performance of the symmetrical airfoil in unstaggered cascade formation. The idea of the present research work is that a deeper knowledge of the complex flow phenomena, as they occur in turbomachines cannot be acquired without experimental research. The first step in the investigation of the flow through cascades is the incompressible flow through a two dimensional cascade. The main problem in investigation of the two dimensional cascade is to find the relation between the geometric and aerodynamic parameters of the cascade. The geometric parameters are the profile of the blade with the maximum camber,leading edge radius, thickness ratio etc. The geometry of the cascade is given by space chord ratio, angle of stagger β etc. Present experiment deals with symmetrical airfoils, with thickness ratio t/c = 15 %, in unstaggered cascade formation with different space chord ratios. These

parameters define the geometry of the cascade depending on the arrangements of the blades in the cascade.

The aerodynamic parameters of the cascade are

inflow and outflow velocity,

and angle of inflow and angle of outflow ,

deflection of the flow deviation ,

pressure difference across the cascade ,

chord wise pressure distribution over the blade,

resultant aerodynamic force on the blade

the tangential component of force , and the axial component of force,

loss of total pressure in the cascade,

The following parameters can be set at any required value within appropriate range.

- inflow angle
- inflow velocity

The following quantities are measured as the function of these parameters,

- 1. pressure distribution on the blade
- 2. the total pressure behind the cascade

1.2 Application To Wave Energy – A brief Outlook

One of the most promising way of utilizing sea wave is provided by the oscillating water column(OWC) wave energy device which is pollutant free and economically viable. The OWC device provides the simplest and possibly the most reliable means of converting irregular wave motion into high speed rotational movement required for electric power generation. For countries surrounded by the sea such as the British Isles, Japan, India,Portugal, Australia

and other island countries, wave energy conversion is an attractive technological proposition. The United Kingdom and Japan are pioneers in developing the wave energy and leading several activities.

1.3 The Wells Turbine

In the oscillating water column(OWC) device, the flow of air, displaced by the free surface within a chamber open at a immersed bottom, drives a turbine. The requirement of transforming the reciprocating airflow into unidirectional rotational motion is met without the need for any rectifying valves, by a turbine invented by Wells(1976).

The Wells turbine is a self rectifying axial flow air turbine suitable for extracting the energy from reversed cyclic airflows. These conditions are encountered in the OWC caisson of wave energy converters. The Wells air turbine consists of several symmetrical airfoil blades set around a central hub as shown in Fig.1.1 with their chord planes oriented normal to the axis of rotation.

1.3.1 Principle of operation

According to classical airfoil theory, an airfoil, which is set at an angle of incidence alpha in a fluid flow, generates a lift force L, normal to the free stream and also a drag force D which is in the direction of the free stream. These lift and drag force can be resolved into tangential and axial components F_T ,F_X respectively. The tangential and axial components are expressed as follows and also shown in Fig. 1.2

$F_T = L\ sin\ \alpha - D\ cos\ \alpha$

$F_X = L\ cos\ \alpha + D\ sin\ \alpha$

The tangential and axial force coefficients are C_{F_T} and C_{F_X} for a 2D airfoil. The force F_T is responsible for the power output, the force F_X results in an axial thrust along the axis of the rotor which has to be absorbed by the bearing. The turbine can start from rest (α = 90 degree) and accelerate to a running condition if the solidity of blades is higher than a certain minimum value.

For symmetrical airfoil, the direction of tangential force F_T is the same for the both positive and negative values of $'\alpha'$. If such airfoil blades are positioned around an axis of rotation, this will always rotate in a single direction regardless of the direction of airflow. Therefore the turbine does not need rectifying valves in a bi-directional flow, the Wells turbine itself is a self rectifying turbine. That is why Wells wind turbine is well suited for wave energy conversion from OWC devices.

There are two types of Wells turbine, mono-plane Wells turbine and bi-plane Wells turbine. Mono-plane turbine consists of symmetrical airfoil blades set around a central hub and bi-plane Wells turbine consists of two such rows of blades separated by a gap(Fig 1.3). One mono-plane Wells turbine is installed at Trivandrum in India.(Raghunathan 1995)

1.4 The Cascade Wells Turbine

Ghosh(1996a) has suggested a cascade turbine for the OWC wave energy device. This turbine is the subject of the present study.The two view of the present cascade Wells turbine and Wells turbine are shown in Fig.1.4. Cascade turbine consists of two cascades at the top and bottom of the nacelle(Fig.1.4b) Each cascade consists of 6 blades lined up in the axial direction as in Fig.1.4b Whereas a typical Wells turbine consists of 12 blades in a single circular row. Ghosh(1996a) has shown that the Working principle is same as VAWT(Vertical Axis Wind Turbine). Moreover the cascade effect allows a large angle of attack without stall in five upstream rows.

1.5 Objective of the Present Work

From the past studies on Gas turbines (compressor or turbine cascade) Pressure distribution of cambered airfoil cascades are available. From studies on Wells turbine, pressure distribution of tandem cascades of symmetrical airfoils is also available. Tandem cascade is also known as a cascade of 90 degree stagger angle. But little information about cascade of zero stagger symmetrical airfoils is available . So Present work is related to cascade studies of symmetrical airfoils. Schematic diagram of present cascade are shown in Fig 1.4.

The aerodynamic parameters of the cascade are

inflow and outflow velocity V_∞ , V_1,

and angle of attack α,

S/C space chord ratio,

pressure difference across the cascade $\delta p = p_w - p_\infty$,

chord wise pressure distribution over the blade p(x),

resultant aerodynamic force on the blade L,D,

loss of total pressure in the cascade δp_o,

The following parameters can be set at any required value within appropriate range.

- inflow angle = α
- inflow velocity =V_∞

The aim is

- to find the pressure distribution around the cascade airfoils with different space chord ratios at different angles of attack and Reynolds Numbers,
- to find optimum space chord ratio needed for achieving high L:D, for angles of attack from 15^o *to* 27.5^o,
- to find the total pressure behind the cascade ,

- to find the total drag which is calculated by wake survey method,
- to find the separation points at different angles of attack and different space chord ratios for cascade airfoils.

Chapter 2

LITERATURE SURVEY

The theory of the flow past cascade or infinite series of airfoils, regularly spaced is of importance in connection with the design of compressor, turbine and pump blades. Large amount of low speed cascade and high speed cascade data are available about cambered airfoil. Very little amount of experimental data are available about unstaggered cascade of symmetric airfoils. Schlichting(1954) made some investigations on unstaggered symmetric airfoil cascade.

One of the most popular device in wave energy conversion is the water to air junction which is called oscillating water columns proposed by Masuda in Japan. The popularity of the oscillating water column is derived from this simplicity which is a good feature of engineering design(Salter 1989). Dr. A.A. Wells invented a new design of turbine (which is called Wells turbine) at the Queen's University of Belfest. A practical problem encountered with the Wells turbine is its difficulty to run up to operational speed when started from rest. This phenomenon where the turbine accelerates up to a certain speed which is much lower than the operational speed, is termed crawling. In order to avoid crawling , a high solidity and a low hub to tip ratio rotor is therefore required(Raghunathan 1982). Typically a hub to tip ratio of 0.6 and a solidity of 0.6 is required to overcome crawling. The blades in tandem cascade have better starting characteristics than an isolated blade, but will have

a lower ultimate efficiency at the operating condition(Raghunathan 1981).

There are many reports which describe the performance of the Wells turbine both at starting and at running conditions. According to their results, the wells turbine has inherent disadvantage, that is, lower efficiency, poor starting and a high axial thrust in comparison with conventional turbines. In order to overcome these weak points, an impulse turbine with self-pitch-controlled guide vanes for wave energy conversion has been proposed(Kim et al 1988).

Ghosh(1996a , 1996b) suggests two novel cascade configurations of the wind turbine of the oscillating water column device. A probable configuration for guide vanes has been discussed (Ghosh1996b) by him. He suggested an alternative novel configuration which has a stator cascade in the middle with rotor cascades on either side. This turbine is unlikely to stall even in high velocity winds created by large waves. It operates at a relatively low tip speed ratio. However, the object of the study here is not this cascade, but a symmetrical airfoil cascade for a turbine of high tip speed ratio.(Ghosh1996a) It is argued that the cascade effect would delay onset of stall in the five upstream blades.

Chapter 3

EXPERIMENTAL SETUP AND PROCEDURE

For the purpose of present study, we selected NACA 0015 symmetrical airfoil. For this testing configuration, the dimension of the blades were selected according to the available space of the wind tunnel test section. The cascade is tested in closed circuit 2D wind tunnel.

3.1 Fabrication of Airfoils

Present study deals with cascade aerodynamics, so more than two airfoils were needed to do the experiment. Three airfoil blades were fabricated in Aero Workshop, IIT, Kanpur. The template was made, and used for checking the airfoil profile(NACA 0015). All the three blades were made out of wood. The span-wise location of pressure holes station were same for the all three blades and the station distance is $2.5 inches$ from one end of the airfoil. Stainless steel tubes having 1.6 mm outer diameter and $1 mm$ inner diameter were selected for pressure measurements. The bottom and top airfoils have same number of pressure tubes.(Fig.3.1)&(Tabular. 3.1) Middle airfoil has more number of pressure tubes because this airfoil has the required cascade effect. They were placed at different chord-

wise distances on both upper and lower surfaces of the airfoil. A large number of pressure tubes were placed on the upper surface and fewer pressure tubes were placed on the lower surface. The distribution of pressure tubes are at close intervals near leading edge of the airfoil because pressure variation is rapid at this place. The remaining portion of the airfoil which has a small curvature,has a lesser number of pressure tubes. Each pressure tube has length of $3inches$ and was fixed onto the groove by araldite. It should be noted that the airfoil blades were 2 dimensional, so there was no need to fix longer length of presure tube on to the groove of the airfoil. After that, pressure holes were made on all tubes by $1mm$ diameter drill bit. Finally, the surface of airfoil were smoothened and polished by varnish. Details of dimension of blades and pressure tubes locations are shown in Fig 3.1

3.2 Circular Model Base Disc

The circular disc, made of wood, has dimensions of 20 inch dia and 1 inch thickness. A rectangular piece of wood $7inches \times 14inches$" was cut out from the center of the disc. In its place two MS metal strips were fixed, which were used for changing the space between the two airfoils. The circular disc was used for mounting the blades to simulate the hub effect on the test model. The model with base shown in Fig 3.2.(photograph). A schematic diagram of Expeimental Set up is shown in Fig.3.3.

3.3 Wind Tunnel

The experimental test were conducted in 2D arm of a 5D closed-circuit Wind Tunnel in Low Speed Aerodynamics Laboratory at IIT,Kanpur. The low speed tunnel is a large venturi where the airflow is driven by two centrally located fans each connected to 15 hp motor drive. The schematic diagram of the 5D wind tunnel is shown in Fig 3.4. The airflow with pressure p_1 enters into the nozzle at velocity V_1, and area is A_1. The nozzle converges to a smaller area A_2 at the test section, where the velocity increases to V_∞, and the pressure

decreases to p_∞. After flowing over the model, the air is passed into a diverging duct(diffuser), where the area increases to A_3, the velocity decreases to V_3 and the pressure increases p_3 . Since , it is a closed circuit tunnel, the air from the exhaust is returned directly to the front of the tunnel. The tunnel test section dimensions are given below.

- Test section Width = 1 ft
- Test section Height = 4 ft
- Test section Length = $5\frac{1}{2}$ ft

3.4 Wake Survey Rake

Pressure distribution is used to determine the lift , pressure drag and moment coefficients for the airfoils that are tested in a wind tunnel.Pressure distribution does not give the viscous drag. The total drag coefficient , in contrast, is usually obtained by measuring the momentum loss(or energy) of the air behind the airfoil. Data for this are obtained by a pressure-measuring device called a wake survey rake. Wake rake has a profile of symmetrical airfoil and made out of wood. It has 35 pitot probes and 5 static probes fixed equally spaced. Diagram shown in Fig 3.5(photograph) and Fig.3.3. The distance between trailing edge of the airfoil and total pressure probe of wake rake is 4.3 C.

3.5 Digital Micromanometer

In this experiment Furness controls limited FC012 pressure scanner with two Digital Micromanometers were used for measuring the model static pressure. It has a selection box with 60 channels. A digital micromanometer has a maximum range of $\pm 200\ mm$ of H_2O.

The stainless steel tubes of the blade model were connected to FC012 pressure scanner through plastic tubes. The static pressure at every location was noted down just by selecting

the channel in pressure scanner. This scanned pressure value shows in digital micromanometer. The micromanometer gives the difference between model surface static pressure and free stream static pressure in mm of H_2O. The pitot-static probe was connected to another digital micromanometer which displayed directly the speed in m/s or difference between total pressure and free stream static pressure in mm of H_2O. Digital Micromanometer with Pressure Scanner are shown in Fig.3.6.(photograph) and Fig.3.3.

3.6 Water Manometer

Water multimanometer has 40 tubes which were used for measuring the wake total and static pressure. 5 tubes were connected to static pressure tubes and 35 tubes were connected to total pressure tubes of wake rake. Water manometer gives the pressure values in mm.

Before conducting the experiment the pressure holes were checked for any blockage by passing compressed air. In the first set of readings, we found that two pressure tubes were blocked in the pressure scanner and these were cleared. The Wind tunnel was run at different speeds, as decided and the measurements were done for the different angles of attack of interest and different space chord ratios. Water multimanometer is shown in Fig 3.7(photograph).

3.7 Experimental Procedure

3.7.1 Calculation of coefficient of Pressure

Coefficient of pressure is defined as

$$C_p = \frac{p_{si} - p_\infty}{0.5\ \rho\ V_\infty^2} = \frac{p_{si} - p_\infty}{p_{o\infty} - p_\infty}$$

Where

p_{si} - the static pressure of airfoil at particular pressure tube,

p_∞ - free stream static pressure,

$p_{o\infty}$ - free stream total pressure,

In these experiments , static head(measured with reference to p_∞) and dynamic head were measured separately. So the ratio between static and dynamic head is coefficient of pressure. Coefficient of pressure are plotted vs X/C. We found that we did not get the reading for exact stagnation point (where C_p is +1) in many cases. To overcome this, the location of stagnation point in lower surface of the airfoil was taken from Shevell(1989) for NACA 0012. upto $\alpha = 10^o$. For greater values of α, this stagnation point is located by extrapolating the curve. This is the defect of this experiment. Hence larger number of pressure tubes are needed in the lower surface of the airfoil, for further experiments.

3.7.2 Calculation of Lift and Drag from Pressure Measurement

The aerodynamic forces on the airfoils are due to only two basic sources(Anderson 1991),

1. Pressure distribution over the airfoil p(x),
2. Shear stress distribution over the airfoil τ

The net effect of p(x) and τ distribution integrated over the complete body surface is a resultant of aerodynamic force R and it can be split up into two components (sets of which are shown in Fig 3.8.) L is the lift component of R perpendicular to V_∞, D is the drag component of R parallel to V_∞ , some times R is split into components perpendicular & parallel to chord C.

F_N - normal force component of R perpendicular to chord C,

F_C - axial force component of R parallel to chord C,

The geometrical relation between L, F_N and D, F_C are

$$L = F_N \cos\ \alpha - F_C \sin\ \alpha \tag{3.1}$$

$$D = F_N \sin\ \alpha + F_C \cos\ \alpha \tag{3.2}$$

We note that θ in Fig 3.9 is given by $tan^{-1}(dy/dx)$ and s is the distance along the airfoil curvature. The total normal and axial forces per unit span are obtained

$$F_N = -\int_0^C (p_u \cos\ \theta + \tau_u \sin\ \theta)\, ds_u + \int_0^C (p_l \cos\ \theta - \tau_l \sin\ \theta)\, ds_l \tag{3.3}$$

$$F_C = \int_0^C (p_u \sin\ \theta + \tau_u \sin\ \theta)\, ds_u + \int_0^C -(p_l \sin\ \theta + \tau_l \cos\ \theta)\, ds_l \tag{3.4}$$

In these experiments, we measured static pressure only, the shear stress term will be zero because we have neither measured nor calculated shear stress τ The equation 3.3 & 3.4 becomes,

$$F_N = -\int_0^C (p_u \cos\ \theta)\, ds_u + \int_0^C (p_l \cos\ \theta)\, ds_l \tag{3.5}$$

$$F_C = \int_0^C (p_u \sin\ \theta)\, ds_u - \int_0^C (p_l \sin\ \theta)\, ds_l \tag{3.6}$$

Eqn 3.5 & 3.6 can be written in nondimensional form. From the geometry shown in Fig 3.9.

$$\theta = tan^{-1}(dy/dx) \qquad \Delta x = \Delta s \times \cos\ \theta \tag{3.7}$$

$$\Delta y = (\Delta s \times \sin\ \theta) \tag{3.8}$$

$$Area\ \ S = C \times (1) \tag{3.9}$$

substituting eqn 3.7 & 3.8 into 3.5 & 3.6 and dividing by $q_\infty\ S$ and using eqn 3.9. We obtain the following integral forms for force coefficient

$$C_{F_N} = \frac{1}{C}\left[\sum_{i=0}^{C} C_{pl} \times \Delta x_i - \sum_{i=0}^{C} C_{pu} \times \Delta x_i\right] \tag{3.10}$$

$$C_{F_C} = \frac{1}{C}\left[\sum_{i=0}^{C} (C_{pu}\frac{dy_u}{dx} \times \Delta x_i - \sum_{i=0}^{C} C_{pl}\frac{dy_l}{dx} \times \Delta x_i\right] \tag{3.11}$$

The lift and drag coefficient can be obtained from equation 3.1 & 3.2

$$\begin{aligned} C_l &= C_{F_N} \cos \alpha - C_{F_C} \sin \alpha \\ C_d &= C_{F_N} \sin \alpha + C_{F_C} \cos \alpha \end{aligned} \tag{3.12}$$

C_l is the lift coefficient

C_d is the pressure drag coefficient

3.8 Calculation of Drag by the Wake Survey Method

The total drag of the cascade drag may be obtained by comparing the momentum in the air head of the model with momentum behind the model (Alen Pope 1947).

$$D = \frac{Mass}{sec} \times change\ in\ velocity \tag{3.13}$$

$$D = \int\int \rho \left(V_\infty V_w - V_w^2\right) da \tag{3.14}$$

Where,

V_∞ is the free stream velocity,

V_∞ is the wake region velocity,

da is the small area of the wake perpendicular to stream,

$$C_d = \frac{D}{0.5\ \rho\ V_\infty^2\ S}$$

$$C_d = 2 \int\int \left[\frac{V_w}{V_\infty} - \frac{V_w^2}{V_\infty^2}\right] \frac{da}{S} \tag{3.15}$$

Also,

$$V_\infty = \sqrt{\frac{2\ q_\infty}{\rho}}, \qquad V_w = \sqrt{\frac{2\ q_w}{\rho}} \tag{3.16}$$

$$C_d = 2 \int \left(\sqrt{\frac{q_w}{q_\infty}} - \frac{q_w}{q_\infty} \right) \frac{da}{S} \tag{3.17}$$

For a unit section of the airfoil $S = C \times 1$, and the area $da = dy \times 1$, where y is measured perpendicular to the free stream.

$$C_d = 2 \int \left(\sqrt{\frac{q_w}{q_\infty}} - \frac{q_w}{q_\infty} \right) \frac{dy}{C} \tag{3.18}$$

The total drag is $C_d = C_{dp} + C_{ds}$. Where,

C_{dp} is the pressure drag, C_{ds} is the skin friction drag.

Chapter 4

RESULTS AND DISCUSSIONS

4.1 C_P Distribution of Cascade Airfoil

The surface pressure measurement for the cascade airfoils were done by means of digital micromanometer for angles of attack of 0^o *to* 27.5^o, and S/C = 0.5, 0.7, 0.9 for two different Reynolds Numbers($Re\ No = 3.31 \times 10^5$ at $V_\infty = 25\ m/s$, $Re\ No = 4.6 \times 10^5$ at V_∞ = 35 m/s).

4.1.1 C_p for S/C = 0.5, $\alpha = 0^o$ *to* 27.5^o, at V_∞ = 25 m/s & 35 m/s.

The C_p distribution curve could not be closed in most cases and area under the curve was compared by eye estimation.

- In C_p,distribution, shown in Figs. 4.1 & 4.2 it is seen that top airfoil upper surface nearly behaves like a single airfoil of NACA 0015(Abbott et al(1959)). Bottom airfoil lower surface shows slightly different pressure from a single airfoil. There may be half a degree error in setting of this airfoil. The C_p of the lower surface of top airfoil and

the upper surface of bottom airfoil are interfered with due to cascade effect and they have greater acceleration of the flow, manifested in greater negative pressures. The two surfaces of middle airfoil have almost identical pressure distribution, that means its producing almost zero lift at an angle of attack 0^o . Also we perceive greater acceleration of the flow on both the surfaces compared to a single airfoil. This is due to cascade effect.

- Figs 4.3 & 4.4, the separation occurs on upper surface of the top airfoil near trailing edge(TE). Bottom airfoil produces more positive lift compared to other airfoils in cascade. This is to be expected since separation is suppressed on the upper surface of the bottom airfoil due to cascade effect. The upper surface of middle & bottom airfoils are comparable. But the lower of the middle has more accelerated flow due to cascade effect. Hence middle airfoil produces less lift than bottom airfoil. For the sake of convenience from now on we shall refer to the airfoils as top af, middle af & bottom af.

- The top af in Figs. 4.3 &4.4 produces almost no lift, since the lower surface has more than usual acceleration of flow due to cascade effect.

- In Figs 4.3 to 4.10, the separation point gradually moves towards leading edge(LE) of top af, as the angle of attack increases from 0^o *to* 17.5^o. And lower surface of the middle af have positive value of C_p. The C_P of lower surface of bottom af are consistently larger compared to other af lower surfaces. Between $\alpha 15^o$&17.5^o, the lift (area between upper & lower surface curves) of top af seems to reach a maxima. This signifies onset of stall.

- At high angles of attack, 20^o in Fig 4.11(a), top af has stalled completely at V_∞= 25 m/s . Considering upper surface alone in Fig 4.11(a) , it can be seen that pressure recovery has almost stopped at the leading edge. But at V_∞ = 35 m/s in Fig 4.12(a) the same upper surface has slight pressure recovery. This may be due to increased Reynolds Number. The same trend is happening upto $\alpha = 22.5^o$. But at high angles of attack, C_p of upper surfaces of middle af and bottom af have higher negative values. This is because of cascade effect.

4.1.2 C_p for S/C = 0.7, $\alpha = 15^o$ *to* 27.5^o, at V_∞ = 25 m/s & 35 m/s.

- Considering Fig 4.19(b), upper surface of middle af has negative pressure of greater magnitude when compared to Fig 4.7(b). This is because of increase in S/C (S/C = 0.7). That means that the flow accelerates more , and middle af produces more lift. Comparing Fig 4.19(a) and 4.7(a), the lift of both are same. The separation point occurs near the mid chord. In Fig 4.20, the upper surface of the top af has same pressure recovery as Fig 4.19. The upper surface of middle af has lower negative pressure when compared to 4.19(b). Fig 4.21(a) top af at $\alpha = 17.5^o$, at V_∞ = 25 m/s, upper surface C_p distribution is almost flat along the chord length. It seems that top af has stalled. Fig 4.21 bottom af produces more lift compared to other af in cascade. In Fig 4.22(a) V_∞ = 35 m/s upper surface negative pressure is high. This may be due to increased Reynolds Number. Fig 4.22(c) bottom af upper surface negative pressure is high at LE when compared to Fig 4.21(c). This may be due to increased Reynolds Number. Fig 4.23(a) top af has stalled completely at V_∞ = 25 m/s. But in Fig 4.24(a) top af , upper surface negative pressure is high in a small zone near the leading edge. This is due to increased Reynolds Number. In Fig 4.24(b) middle af upper surface has

lower negative pressure compared to Fig 4.23(b). This is due to lesser flow acceleration.

- At high angles of attack, $\alpha = 20^o$ *to* 27.5^o, the same trend happens. One thing should be noted that negative pressure magnitude of the upper surface of the middle af is increased near leading edge, when compared to S/C = 0.5, $\alpha = 17.5^o$ *to* 27.5^o (Fig 4.21 to Fig 4.30). This is because of increasing S/C ratio and it behaves a little like a single af.

4.1.3 C_p for S/C = 0.9, $\alpha = 15^o$ *to* 27.5^o, at V_∞ = 25 m/s & 35 m/s.

- For angles of attack from 15^o to 20^o, similar trends as for S/C - 0.7 are observed.
- Fig 4.35 $\alpha = 20^o$, top af has stalled and middle and bottom af pressure distribution has higher negative on the upper surface. But in Fig 4.36(a) upper surface of top af pressure is starting to decrease and then recover, this indicates that stalling is not total yet. The same trend is happening upto $\alpha = 22.5^o$. When α is increased to 25^o top af(Fig 4.39) stalls completely. The middle and bottom af also begin to stall. In Fig 4.39, the middle af and bottom af have also stalled in the sense that the upper surface flow separates at the leading edge. But even then the cascade effect brings some benefit and keeps the upper surface pressure coefficient at a higher negative, when compared to that of top af. Thus the middle and bottom af produce some lift and less drag. The same trend continues from Fig 4.39 to Fig 4.42.

4.2 Velocity Profile from Wake Measurement

Wake region velocity profile vs location of total pressure probes in the wake rake are plotted for all the angles of attack($\alpha = 0^o$ *to* 27.5^o). Bezier approximation curve was used to get

ɜmooth velocity profile. These experiments were done in 2D closed circuit wind tunnel. ɹke rake was mounted in test section which is used for single af wake measurement, but ɜsent experiment is about cascade afs. Wake rake height is not quite sufficient for these ɔeriments.

2.1 Velocity profile for S/C = 0.5, $\alpha = 0^o$ *to* 27.5^o

- In Fig 4.43 (a) & (b), at $\alpha = 0^o$, the maximum loss of velocity is at region of top af and bottom af. When the angle of attack is increased upto 15^o the loss of velocity is more behind the bottom af when compared to the other afs(Fig 4.44 to Fig 4.47). This is because more upstream flow seems to be deflected towards the top of the cascade. When $\alpha = 20^o$, the momentum loss is more behind top af. This is because of top af stalls. The momentum loss is lesser for middle af. This happens upto angles of attack 22.5^o (Figs 4.48 & 4.49). In Fig 4.50 to Fig 4.51 beyond $\alpha = 25^o$, the trend is entirely different, that is middle af has a greater momentum defect.

2.2 Velocity profile for S/C = 0.7, $\alpha = 15^o$ *to* 27.5^o

- The velocity profiles are shown in Fig 4.52 to Fig 4.57. At V_∞ is 25 m/s the loss of velocity is more towards the top af than bottom af. In Fig 4.52(b) top and bottom af has almost equal amount of momentum loss. In fig 4.53(a), at V_∞ is 25 m/s the top af wake is lossing more momentum. Consider Fig 4.53(b) the maximum loss of momentum is in between top and middle afs at $\alpha = 17.5^o$. Fig 4.54(a) is not correct, may be this is due to experimental error. The momentum defect is increased at high angles of attack like $\alpha = 20^o$ *to* 27.5^o (Fig 4.55 to Fig 4.57). When compared to Fig 4.43 to Fig 4.52, it seems that velocity loss in the case of S/C = 0.7 is more. This

because of increased blockage of the tunnel due to increased width of the cascade.

.2.3 Velocity Profile for S/C = 0.9, $\alpha = 15^o$ *to* 27.5^o

- Considering Fig 4.58 (a) , the momentum defect has a single maximum in wake region. Fig 4.58(b) is not correct , may be this is because of experimental error. In Fig 4.59 Fig 4.60, Fig 4.61, momentum defect is large. Velocity profile seems to be a parabolic curve. At high angles of attack like $\alpha = 25^o$ & 27.5^o the momentum defect is more between top af and middle af.

.2.4 Drag Calculated by Wake Survey Method

- Drag calculated by wake survey method , in Figs 4.64 and 4.65 are plotted from the experimental result. Drag increases when the angle of attack increases from 0^o *to* 15^o, after that drag decreases when α increases for $V_\infty = 25m/s$, & $V_\infty = 35m/s$, S/C = 0.5. For NACA 0015 single af , drag increases with α (Critzes et al (1955)). When comparing single af and present cascade afs, the drag is lesser in cascade afs for higher angles of attack. We have measured wake measurement for S/C = 0.7 & 0.9 at $\alpha = 15^o$ *to* 27.5^o with two different Reynolds Numbers. From Fig 4.64 and Fig 4.65 , we see that same trend is happening like S/C = 0.5. But with different drag values.

.3 C_l vs α

- C_l vs α are plotted only for S/C = 0.5, α = 0 , 5 , 10 degrees. For these angles of attack, C_p distribution has a closed curve(Fig 4.66 (a),(b),(c)). The C_l vs α are plotted in different graphs for top af , middle af and bottom af. Top af gives negative lift at

$\alpha = 0^o$. After α is increased lift is also increasing . As the velocity is increased from 25 m/s to 35 m/s, the lift also increases. Middle af produce positive lift and bottom af is also producing more positive lift compared to other afs.

.4 Conclusion

he following conclusion were obtained,

- In unstaggered symmetrical cascade af stall was delayed & some lift was obtained upto $\alpha = 25^o$
- The C_l vs α curves for middle af & bottom af have lower slope, compared to a single af.
- As the angle of attack increases drag also increases upto $\alpha = 15^o$, after that the drag decreases.

.5 Further Studies

- The same experiments should be performed with more pressure tubes near the LE of the af and lower surface of all the afs. So that C_p distribution curve can be closed and one can calculate the lift and drag.

References

.. Abbott,I.H., and A.E.von Doenhoff(1959), Theory of wing sections, Dover publications, nc., New York,1959.

:. Schiltching,H.(1954), Problem and Result of Investigation on cascade flow. Journal of \eronautical Sciences - March 1954, pp 163-180.

·. Wells,A.A.(1976), Fluid Driven Rotary Transducers, British Patent 1595700.

. Kim,T.W., et al(1988), Proceeding of Second KSME-JSME Fluid Engineering Conference /ol.1., pp 277-281.

. Salter,S.H.(1989), World progress in wave Energy -1988. International Journal of Ambint Energy, Vol 10, No 1, January , pp 3-24.

. Raghunathan,S. et al(1981), Wind tunnel test on Airfoils in Tandem Cascade . AIAA, /ol 19, No 11, pp 1490-1492.

. Raghunathan,S.,Tan.C.P.(1982), Performance of the Wells turbine at starting. Journal of Energy. Vol 6, No 6, Nov-Dec , pp 430-431.

. Raghunathan,S.(1995), The Wells Air turbine for wave energy conversion, Progress. \erospace, Vol 31, 1995, pp 335-386.

. Ghosh(1996a) Cascade Wind turbine for the oscillating water column wave energy device. 'art I. Progress of World Resource Energy Conference, 1996, pp 1219-1222.

0. Ghosh(1996b) Cascade Wind turbine for the oscillating water column wave energy evice Part II. Progress of World Resource Energy Conference, 1996, pp 2181-2184.

1. Anderson,Jr. John D.,(1991), Fundamentals of Aerodynamics, Second Edition, McGraw-[ill Company, New York.

2. Shevell,Richard S.,(1989), Fundamentals of Flight, Second Edition, Prentice-Hall, En-lewood Cliffs, New Jersey 07632.

3. Alen Pope.,(1954), Wind Tunnel Testing, Second Edition, John Wiley & Sons Inc., 'ew York.

4. Critzes,C.C., Heyson,H.H., & Boswinekle RW(1955), Aerodynamic characteristics of ACA 0015 Airfoil Section at angles of attack from 0^o *to* 180^o, NACA Technical Note 3361.

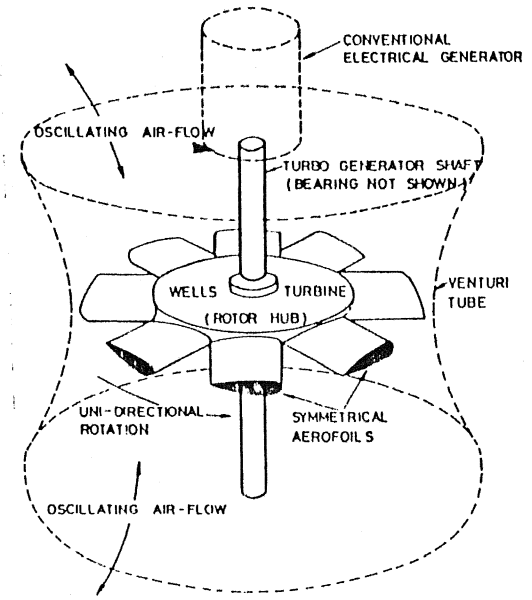

Figure 1.1: Schematic of Wells Turbine

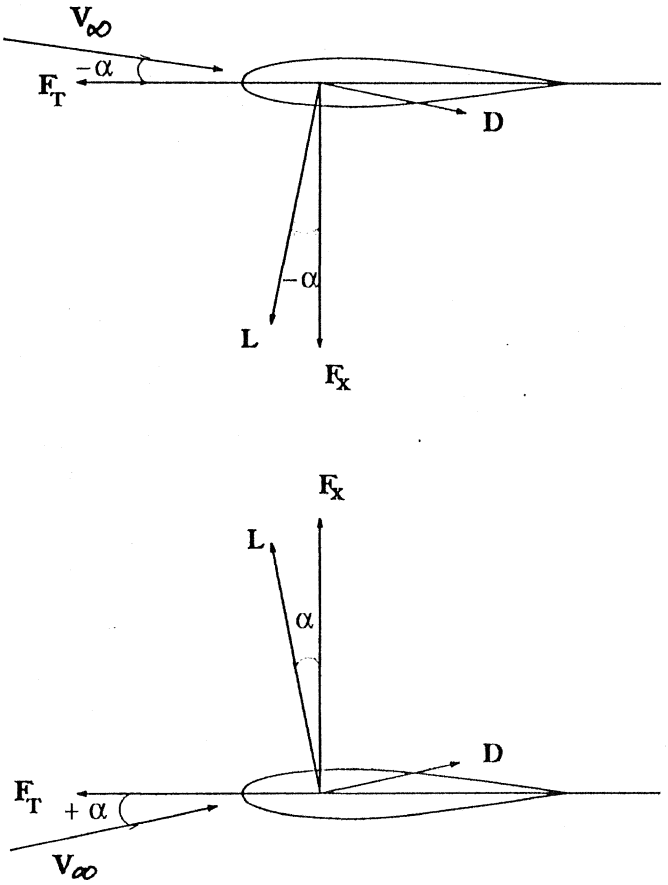

Figure 1.2: Tangential and Axial forces of Turbine Blade

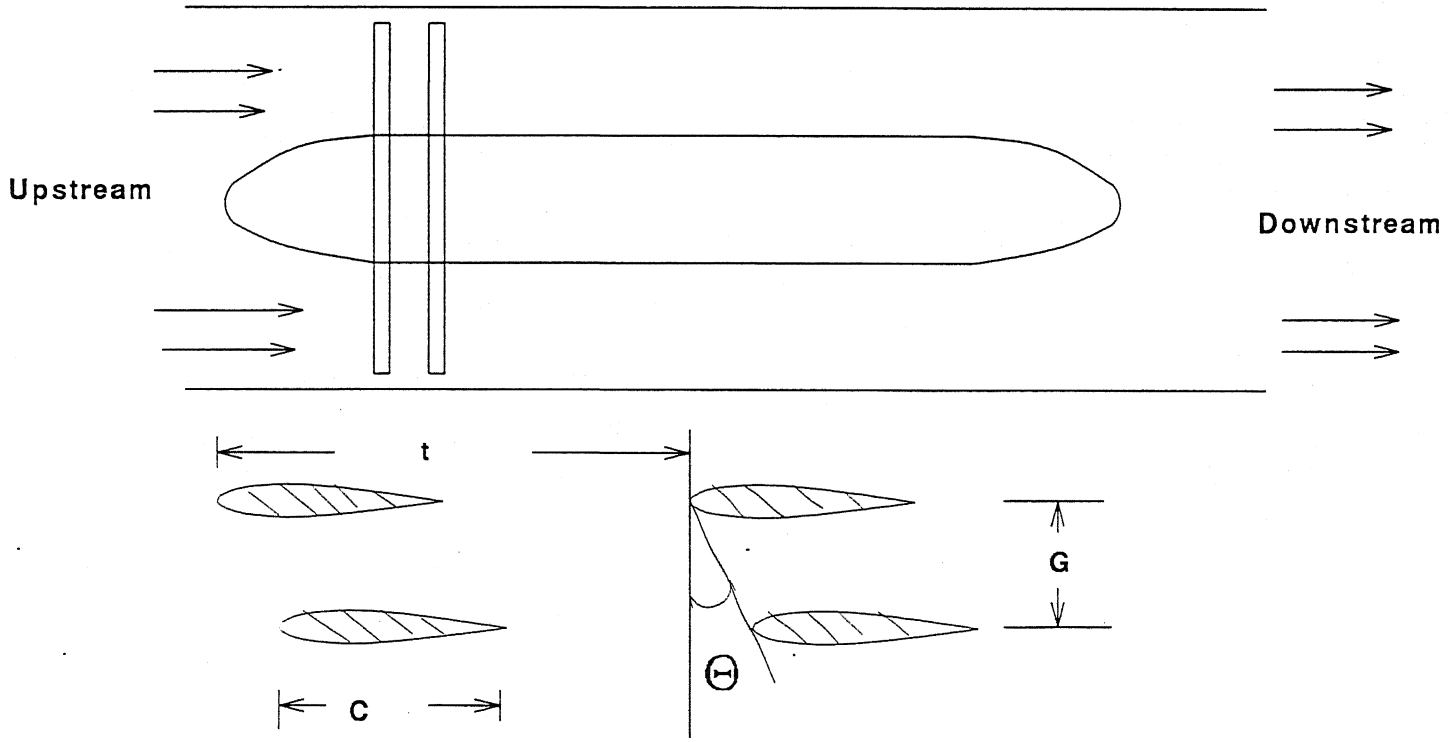

Θ Angle of circumferential position of blades in biplane
C Chord
G Gap between planes of the biplane turbine
t Axial distance between two planes

Figure 1.3: The biplane Wells Turbine

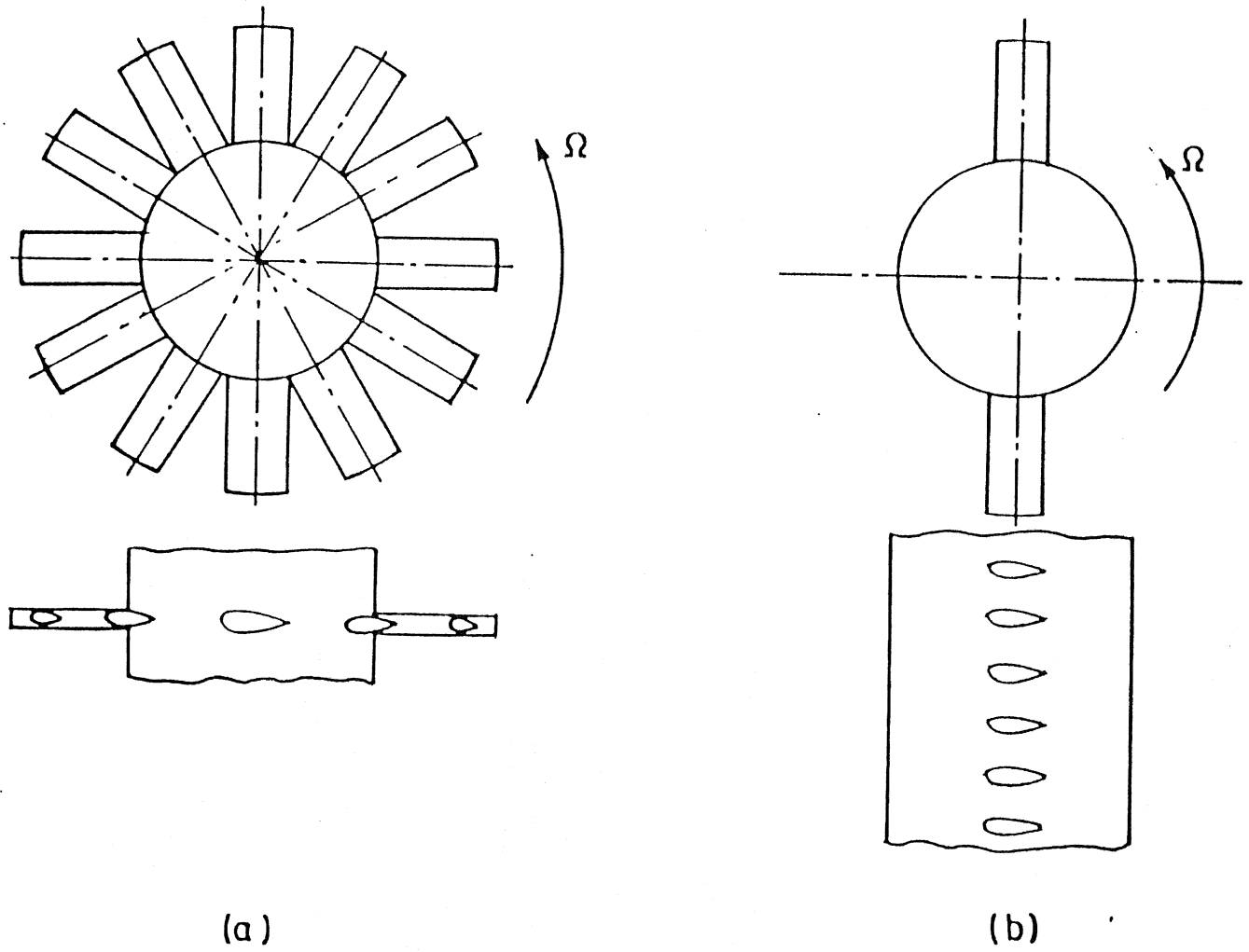

Figure 1.4: Comparison of (a) Wells turbine, (b) Present Cascade Turbine

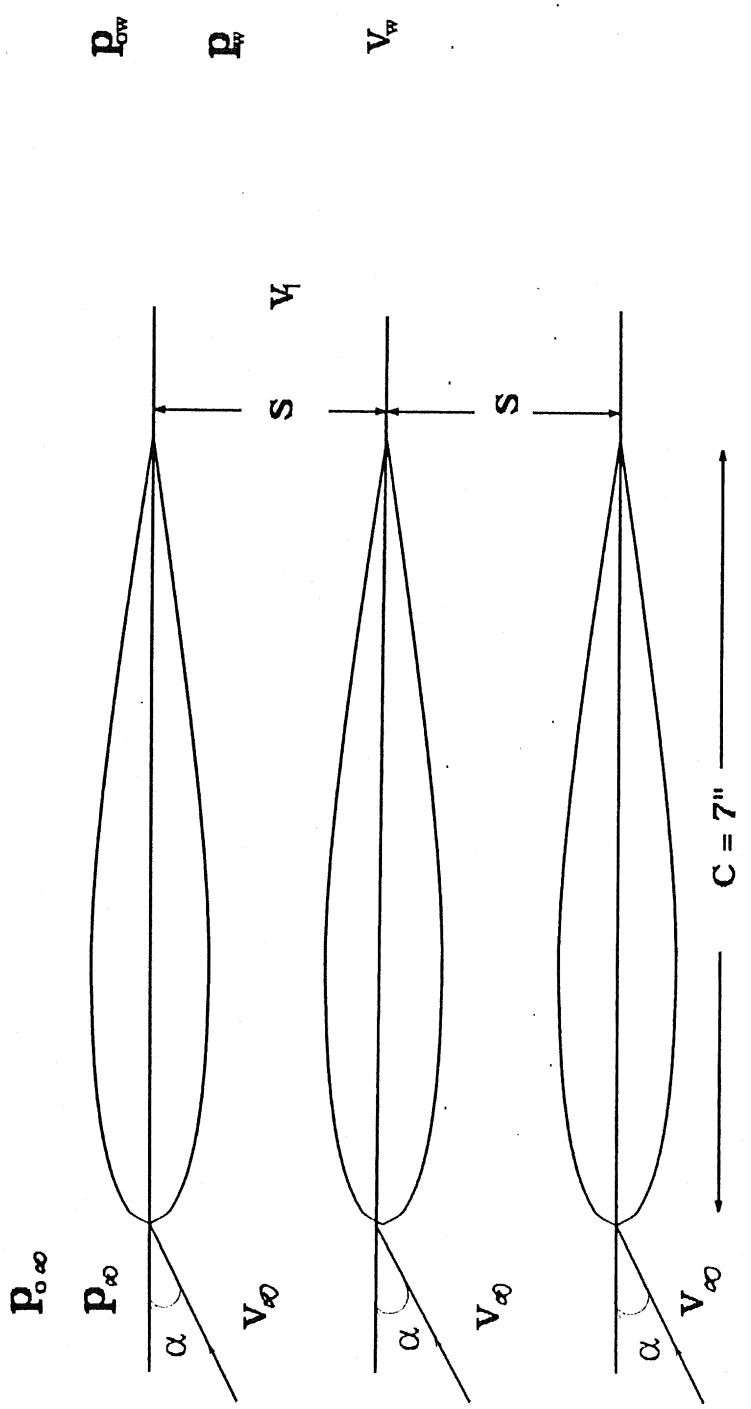

Figure 1.5: Present Cascade of NACA 0015 Airfoils

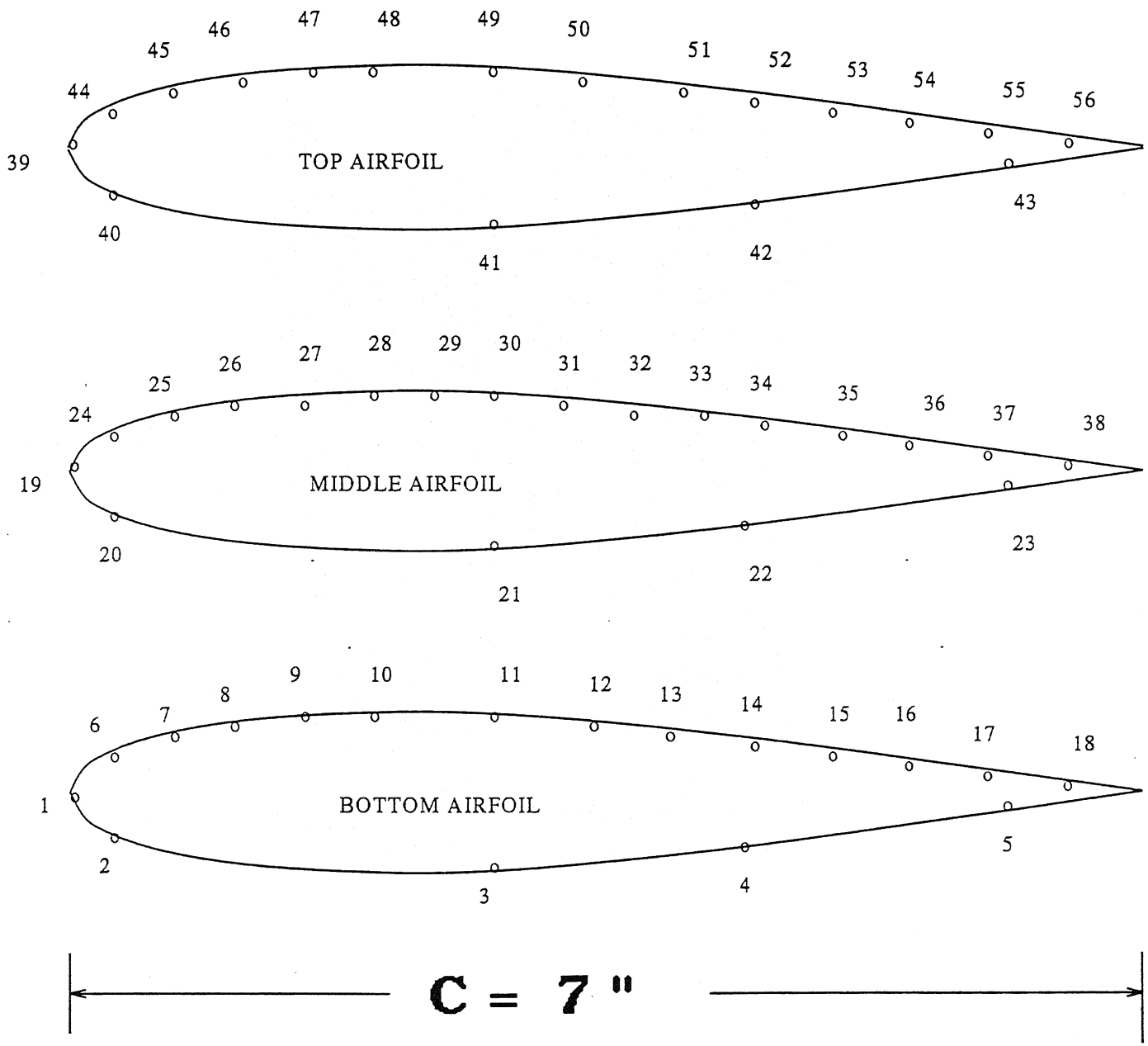

Figure 3.1: Loaction of Pressure Tubes

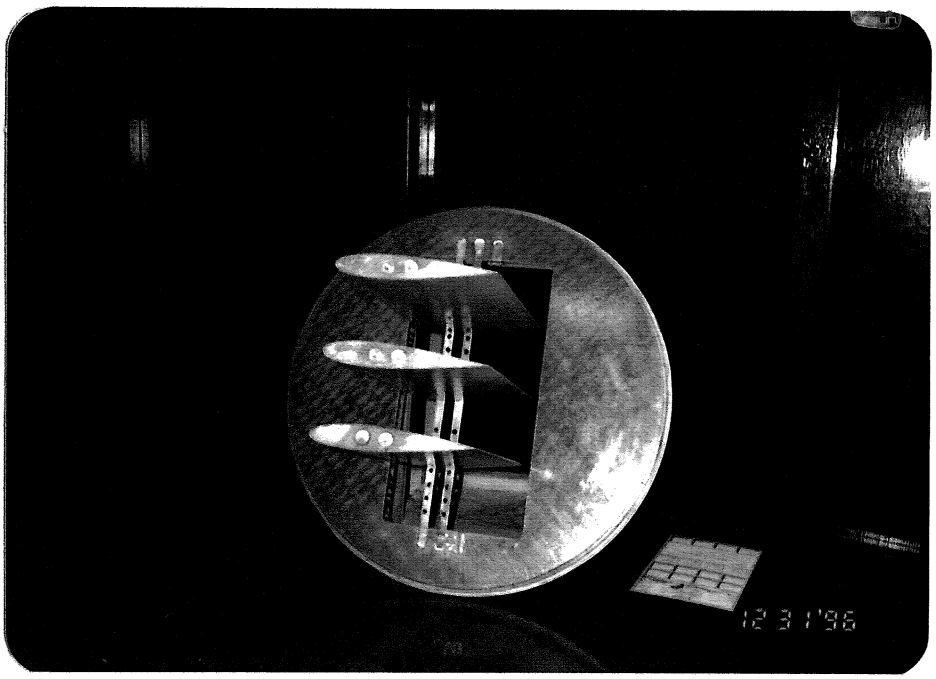

Figure 3.2: The Model with Base Disc before mounting in the Test Section

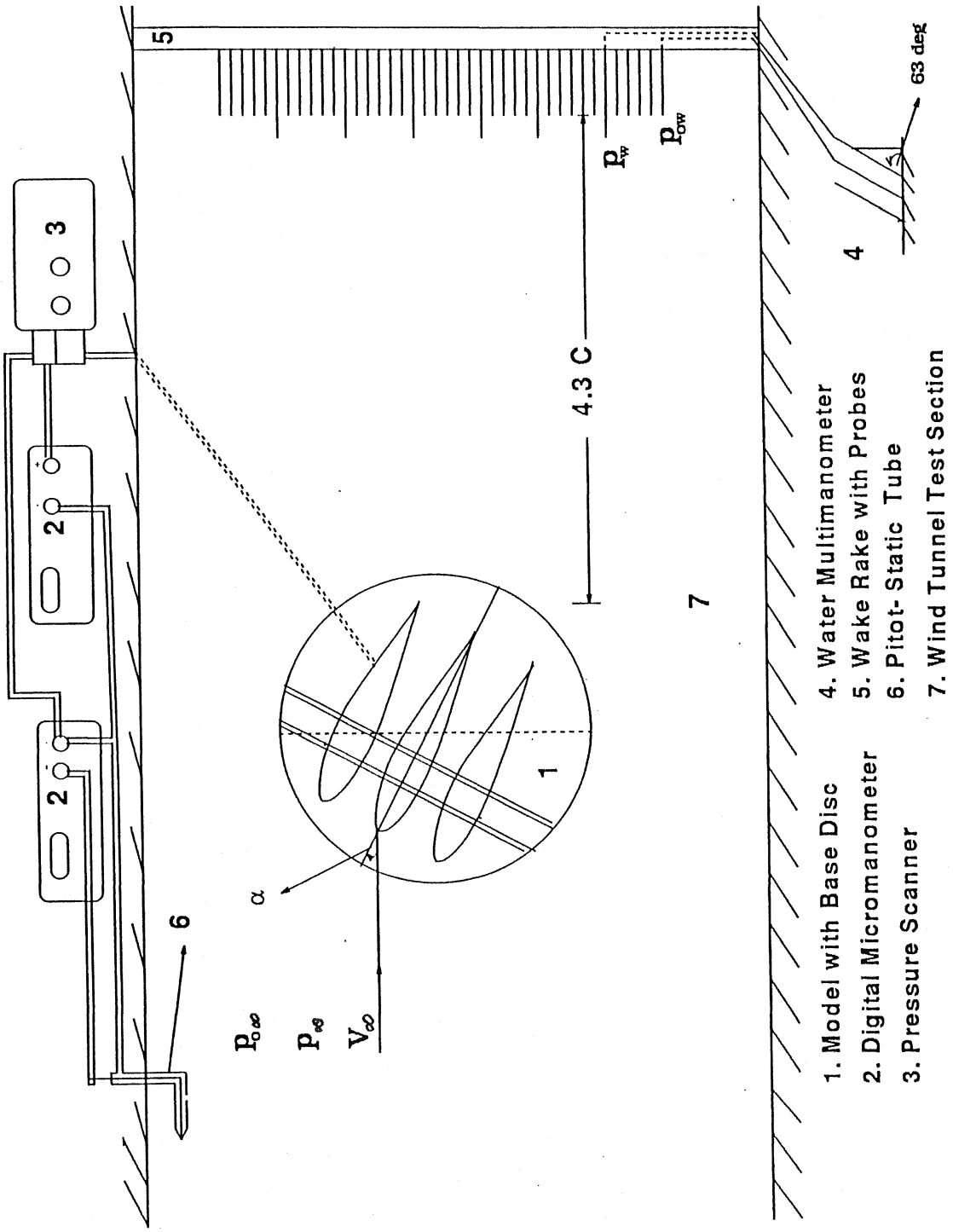

Figure 3.3: Experimental Set Up

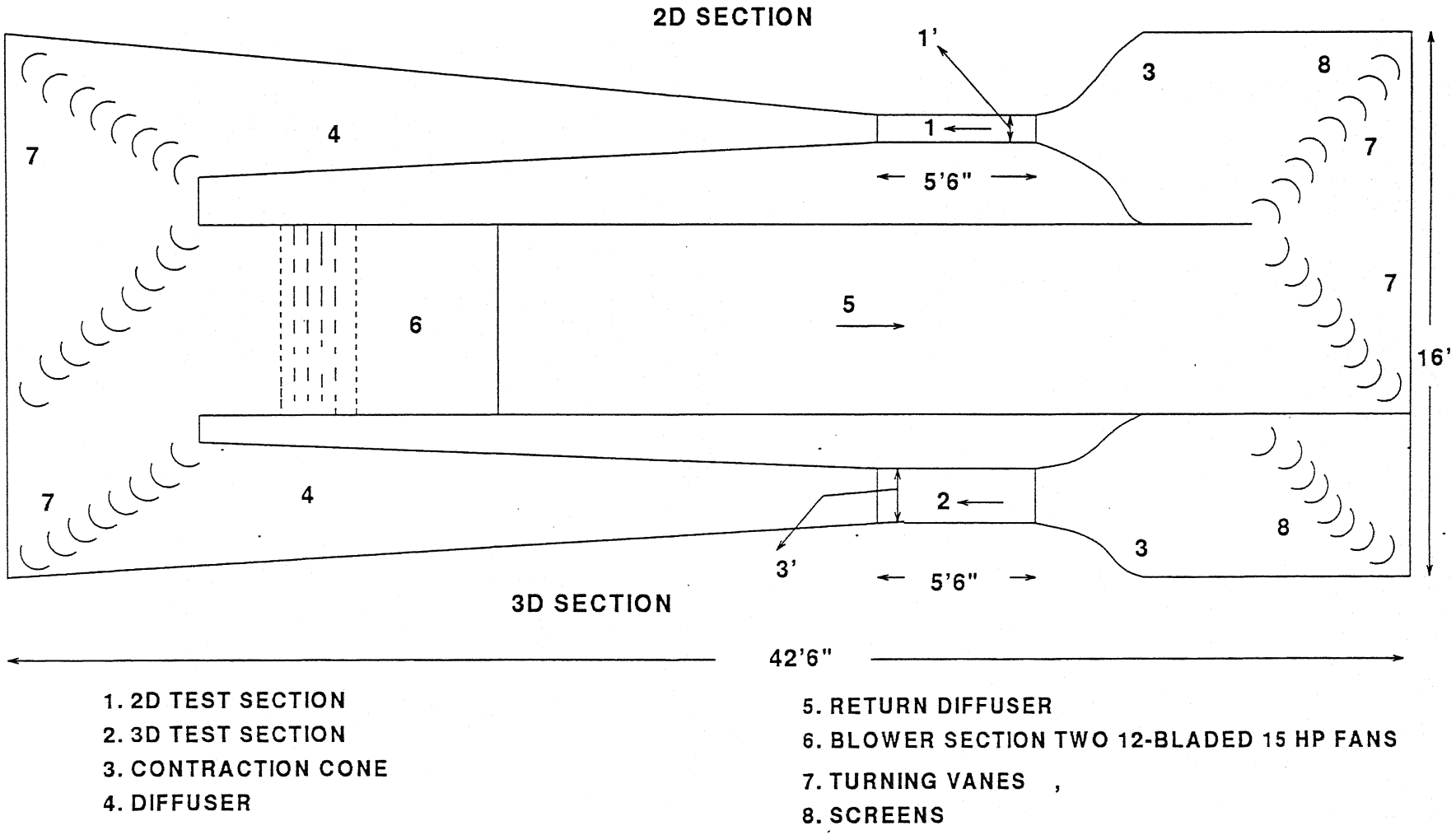

Figure 3.4: Schematic Diagram of 5D Wind Tunnel

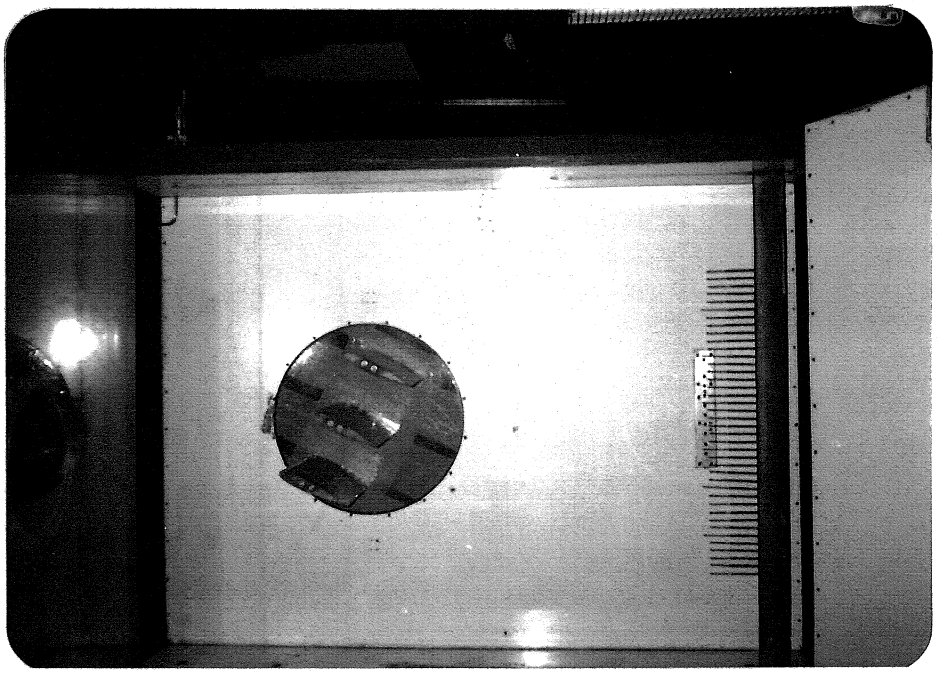

Figure 3.5: Wake rake in the Wind Tunnel Test Section

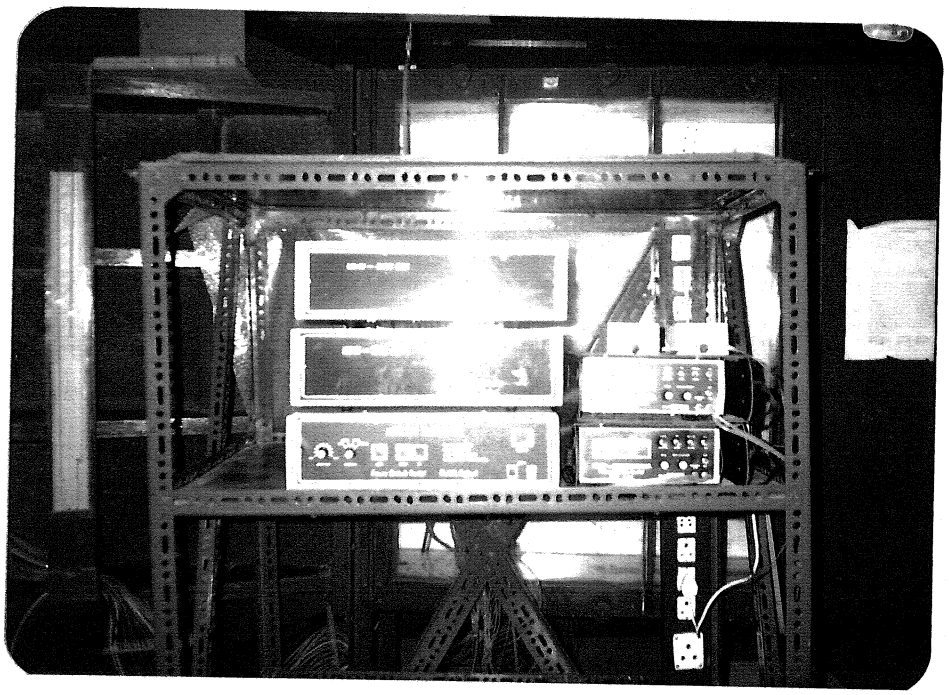

Figure 3.6: Digital Micromanometer with Pressure Scanner

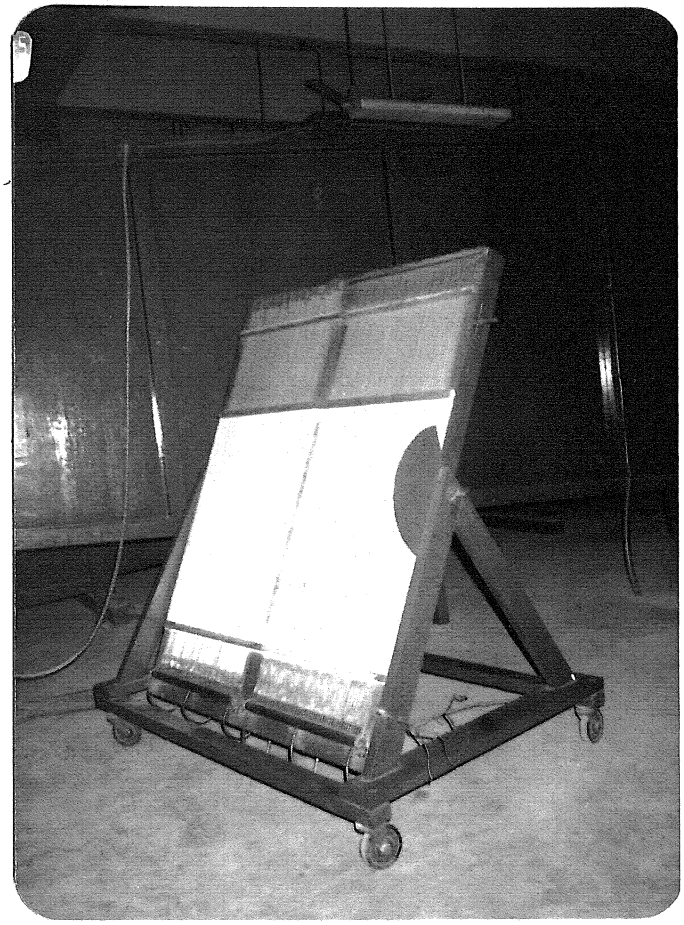

Figure 3.7: Water Multimanometer

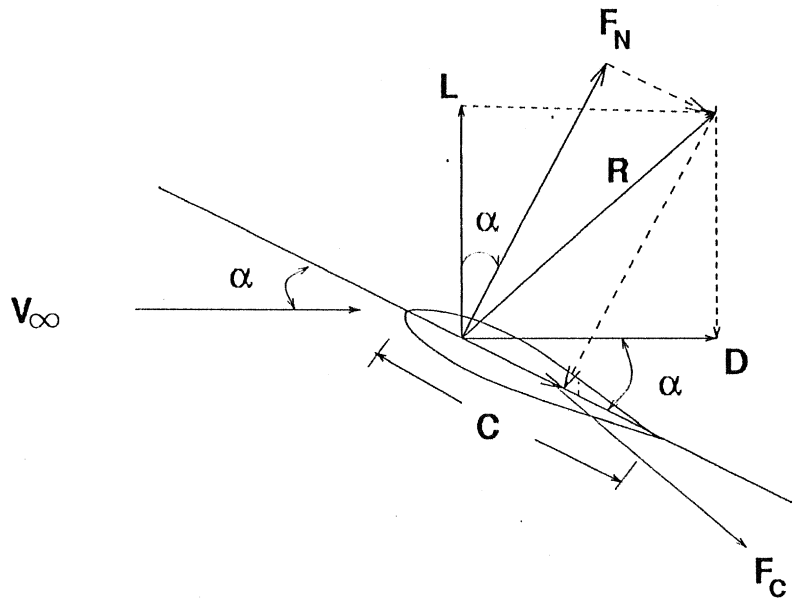

Figure 3.8: Resultant Aerodynamic Force and Components

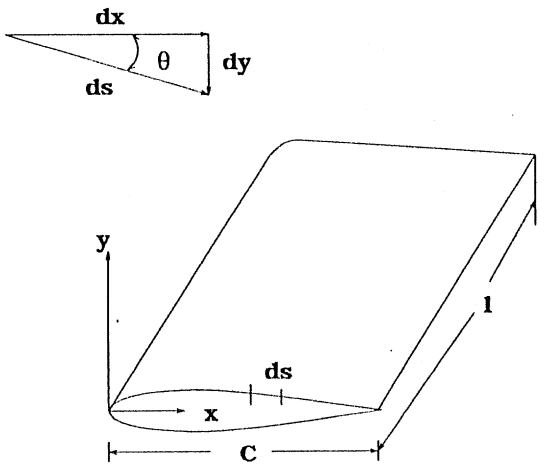

Figure 3.9: Geometry of the Wing

Tube No	X/C	Tube No	X/C	Tube No	X/C
1	0	19	0	39	0
2	0.00714	20	0.00714	40	0.00714
3	.37	21	0.375	41	0.375
4	0.643	22	0.643	42	0.643
5	0.821	23	0.821	43	0.821
6	0.005.4	24	0.0054	44	0.0054
7	0.107	25	0.107	45	0.107
8	0.161	26	0.161	46	0.161
9	0.214	27	0.214	47	0.214
10	0.259	28	0.259	48	0.259
11	0.375	29	0.304	49	0.375
12	0.5	30	0.375	50	0.5
13	0.571	31	0.446	51	0.571
14	0.643	32	0.5	52	0.643
15	0.714	33	0.574	53	0.714
16	0.786	34	0.643	54	0.786
17	0.857	35	0.714	55	0.857
18	0.929	36	0.786	56	0.929
		37	0.857		
		38	0.929		

Table 3.1: Location of Pressure Tubes

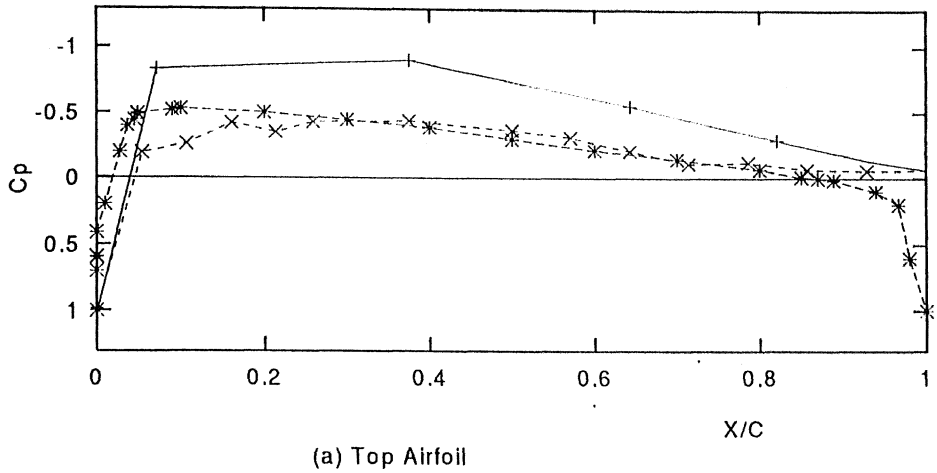

(a) Top Airfoil

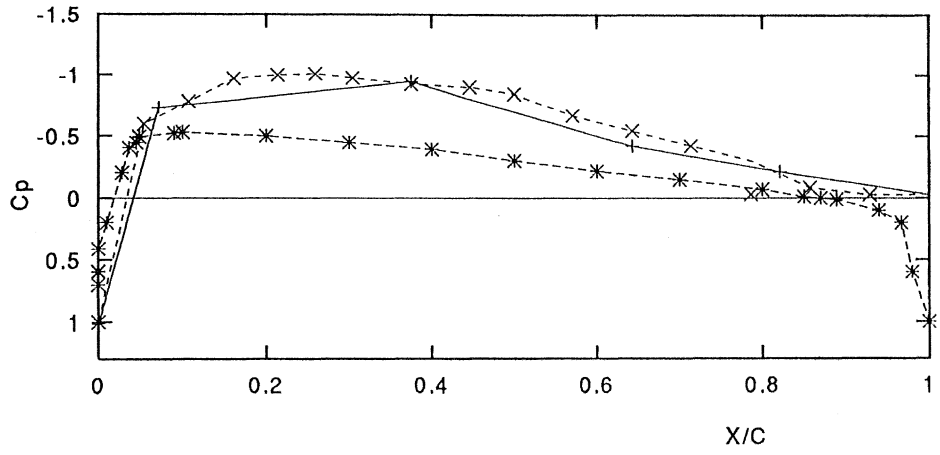

(b) Middle Airfoil

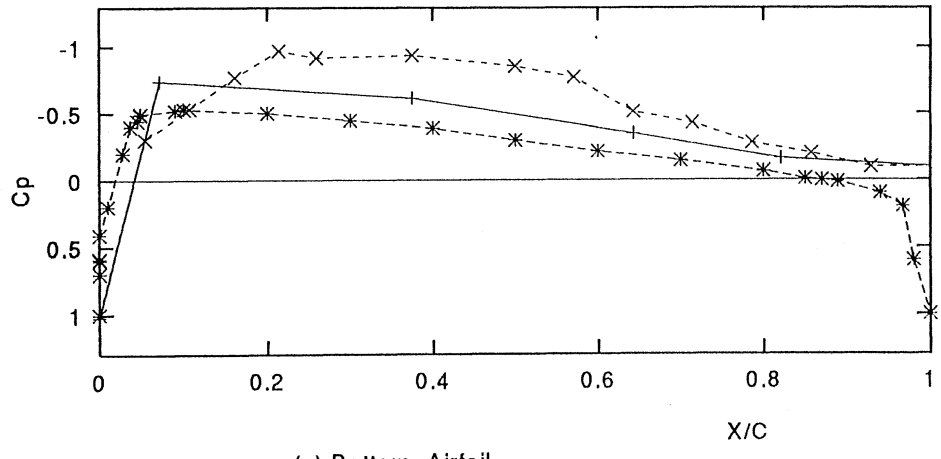

(c) Bottom Airfoil

Figure 4.1: Pressure Distribution of Airfoil; S/C = 0.5, $\alpha = 0^o$, $V_\infty = 25$ m/s, $*$ Abbott et al (1959), + Lower Surface, $\times$ Upper Surface.

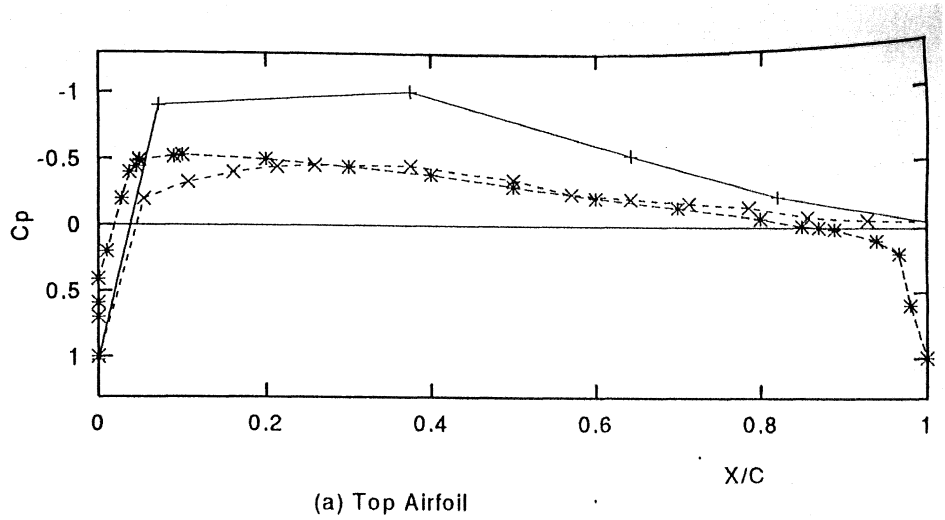

(a) Top Airfoil

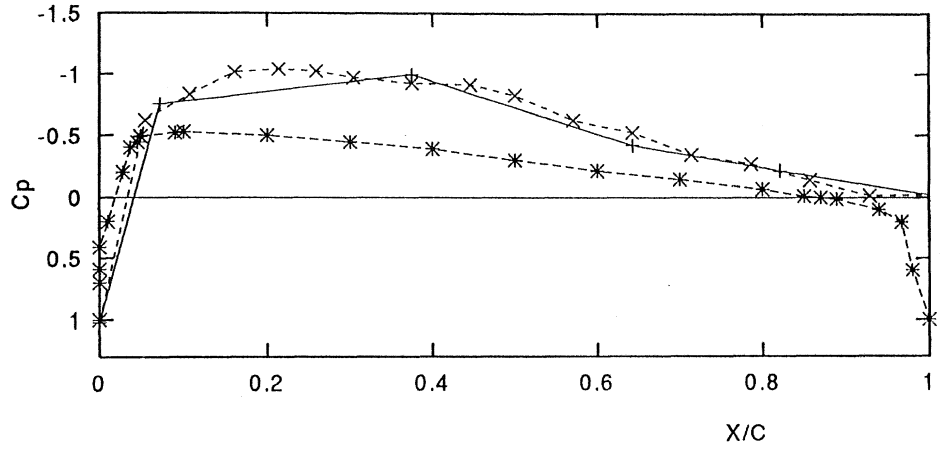

(b) Middle Airfoil

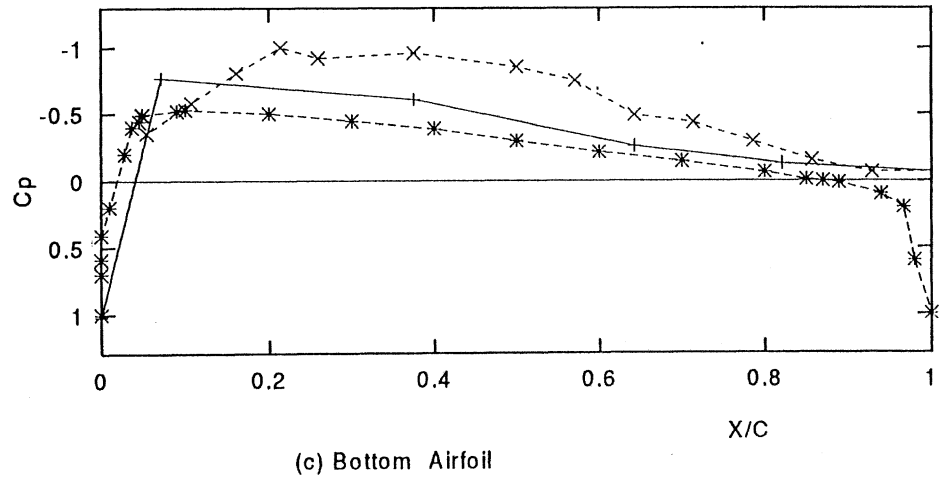

(c) Bottom Airfoil

Figure 4.2: Pressure Distribution of Airfoil; S/C = 0.5, $\alpha = 0^o$, $V_\infty = 35$ m/s, $*$ Abbott et al (1959), + Lower Surface, $\times$ Upper Surface.

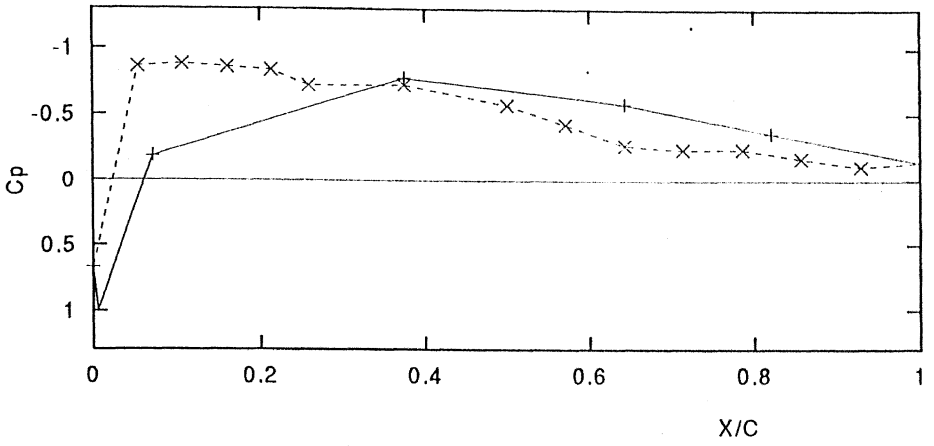

(a) Top Airfoil

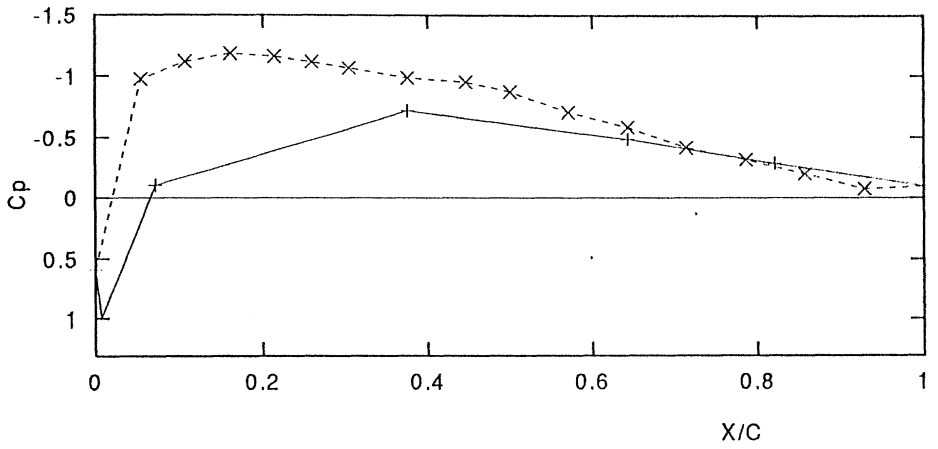

(b) Middle Airfoil

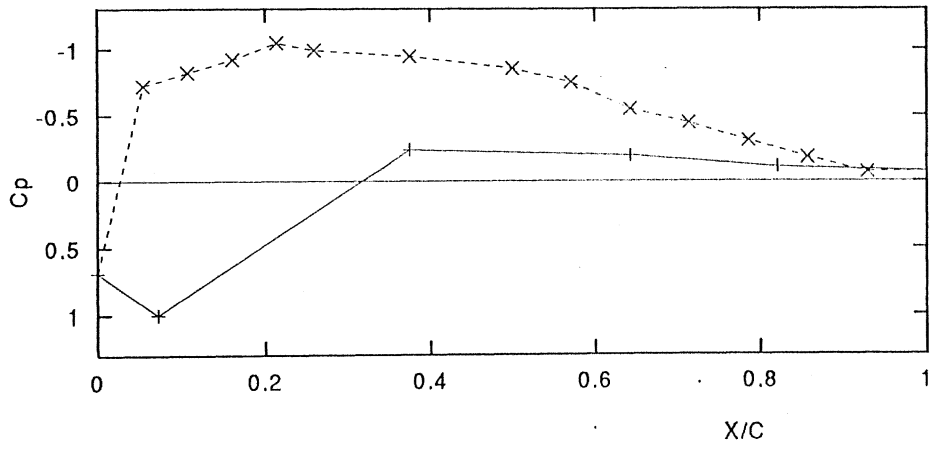

(c) Bottom Airfoil

Figure 4.3: Pressure Distribution of Airfoil; S/C = 0.5, $\alpha = 5^o$, $V_\infty = 25$ m/s, + Lower Surface, × Upper Surface.

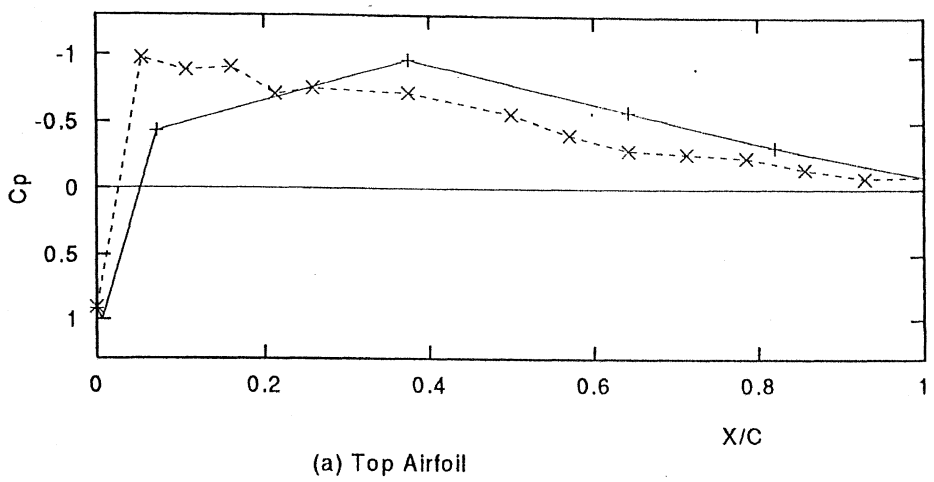

(a) Top Airfoil

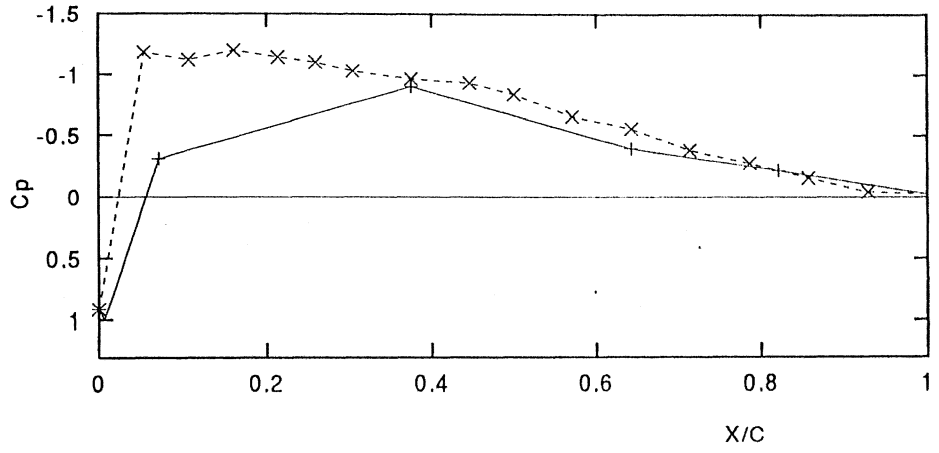

(b) Middle Airfoil

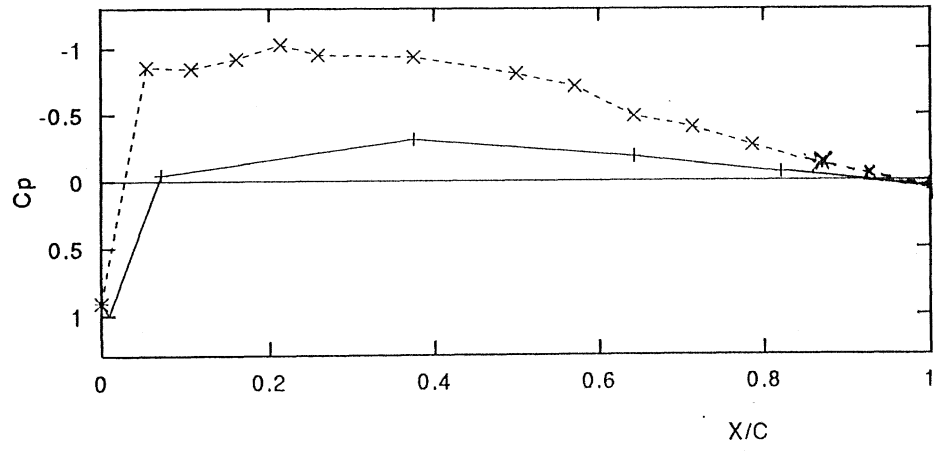

(c) Bottom Airfoil

Figure 4.4: Pressure Distribution of Airfoil; S/C = 0.5, $\alpha = 5^o$, $V_\infty = 35$ m/s, + Lower Surface, × Upper Surface.

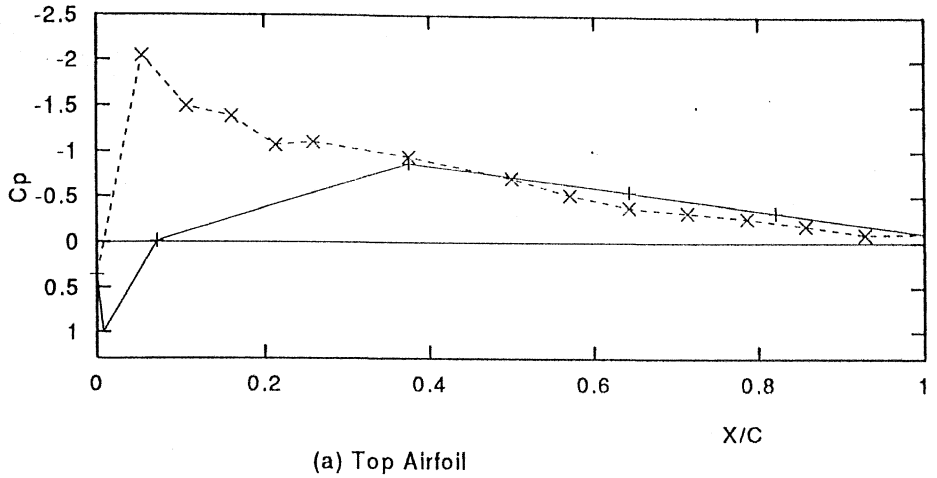

(a) Top Airfoil

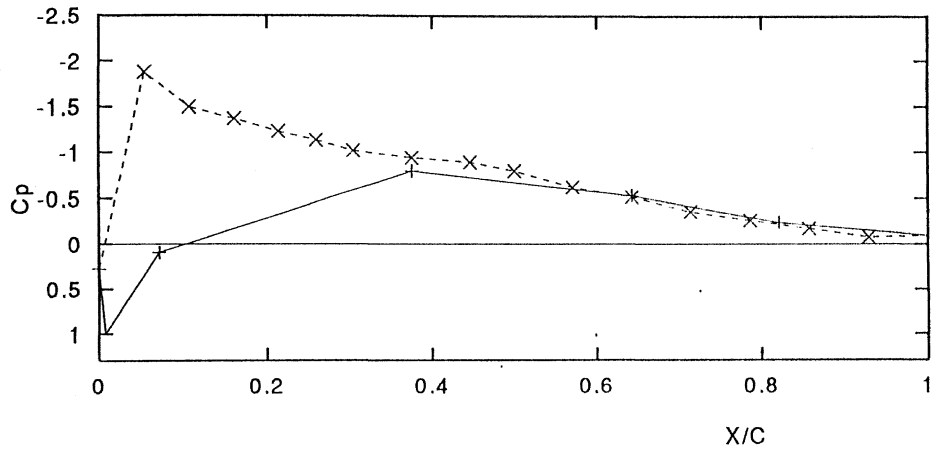

(b) Middle Airfoil

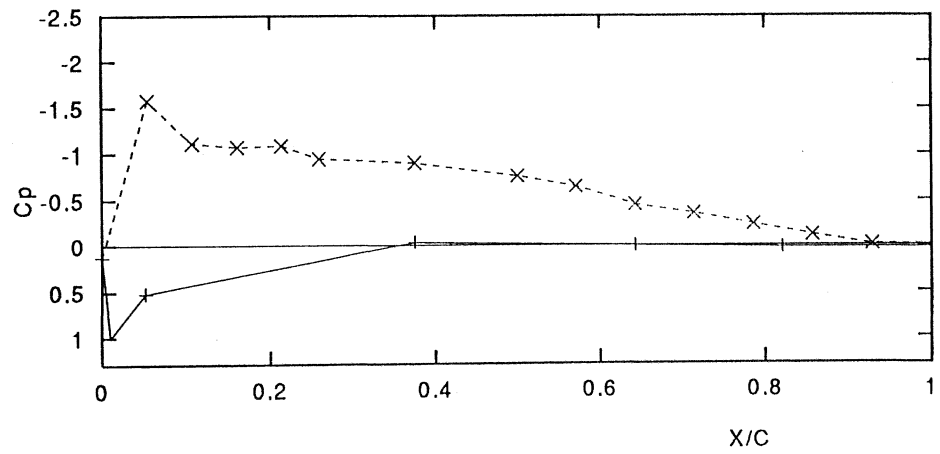

(c) Bottom Airfoil

Figure 4.5: Pressure Distribution of Airfoil; S/C = 0.5, $\alpha = 10^o$, $V_\infty = 25$ m/s, + Lower Surface, × Upper Surface.

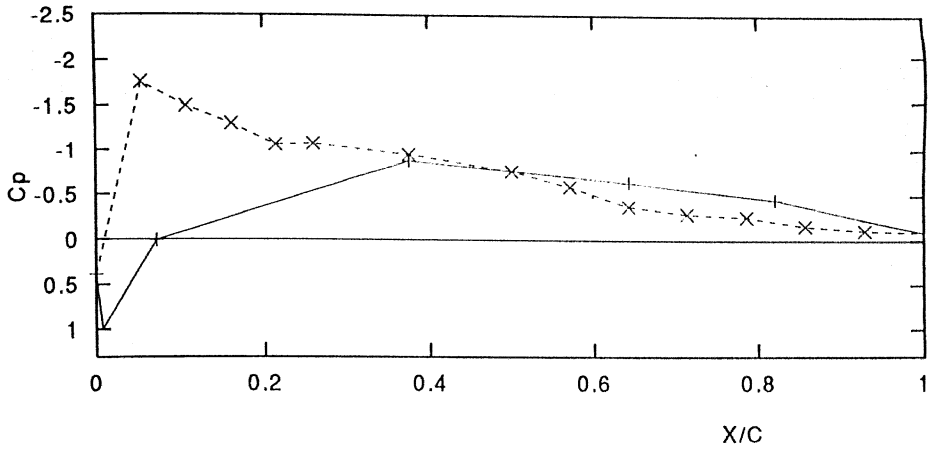

(a) Top Airfoil

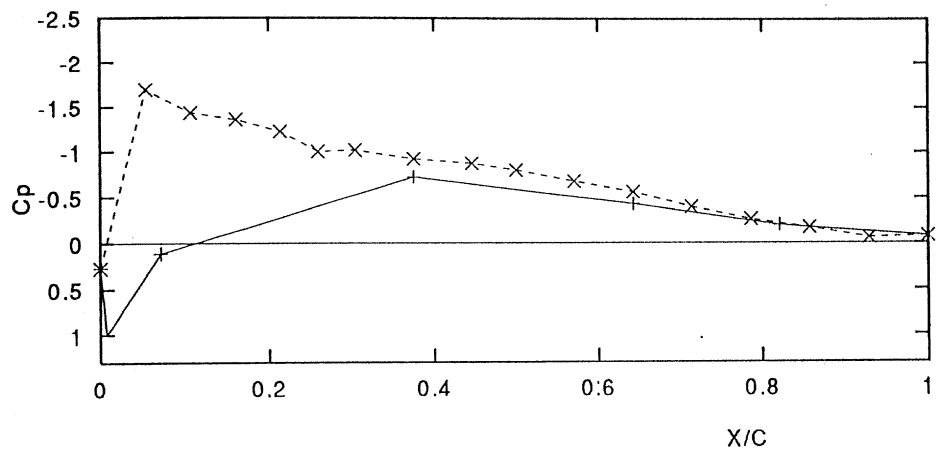

(b) Middle Airfoil

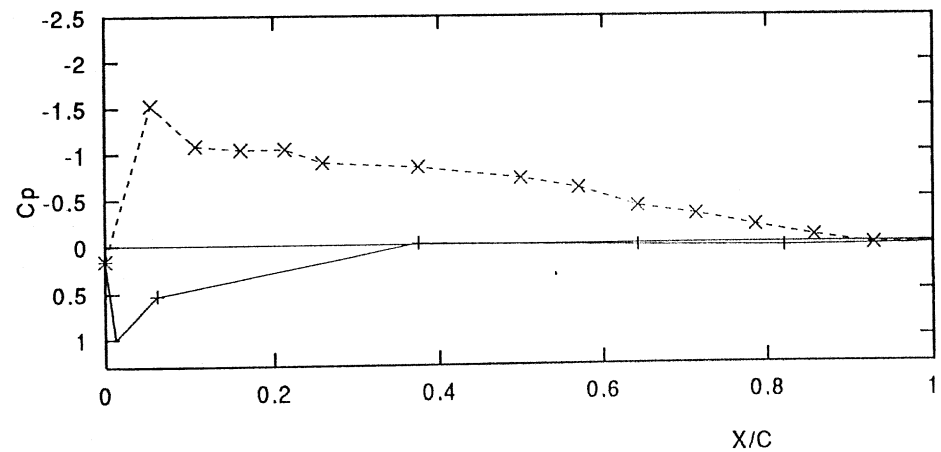

(c) Bottom Airfoil

Figure 4.6: Pressure Distribution of Airfoil; S/C = 0.5, $\alpha = 10^o$, $V_\infty = 35$ m/s, + Lower Surface, × Upper Surface.

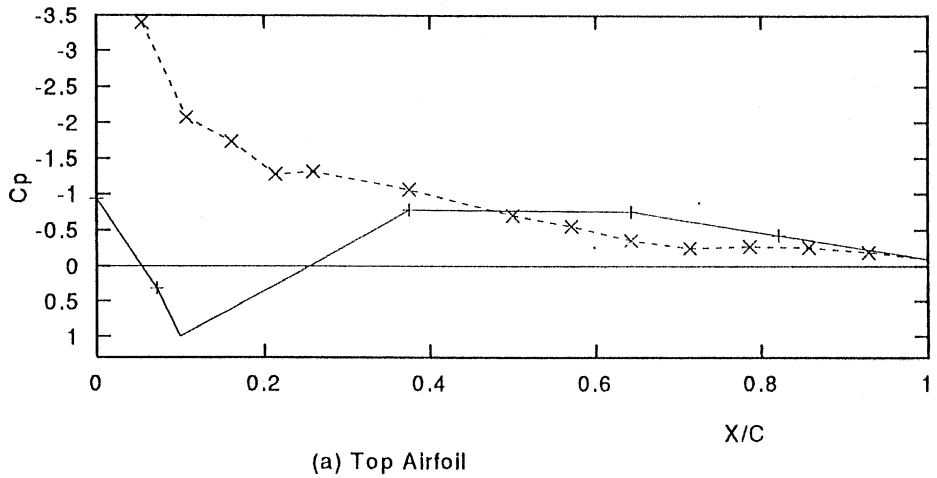

(a) Top Airfoil

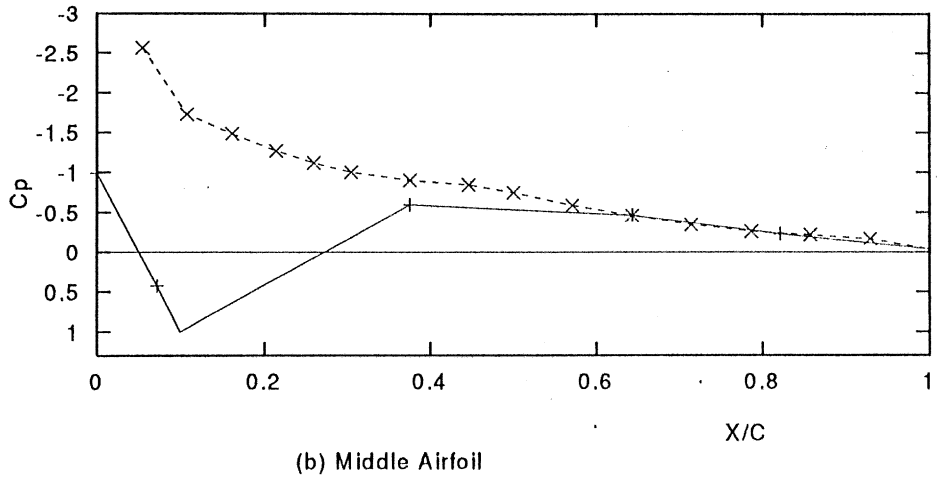

(b) Middle Airfoil

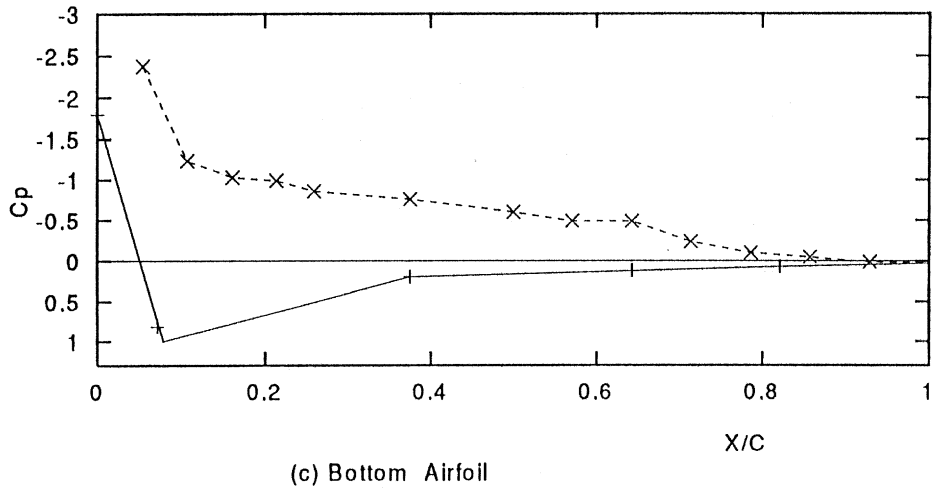

(c) Bottom Airfoil

Figure 4.7: Pressure Distribution of Airfoil; S/C = 0.5, $\alpha = 15^o$, $V_\infty = 25$ m/s, + Lower Surface, × Upper Surface.

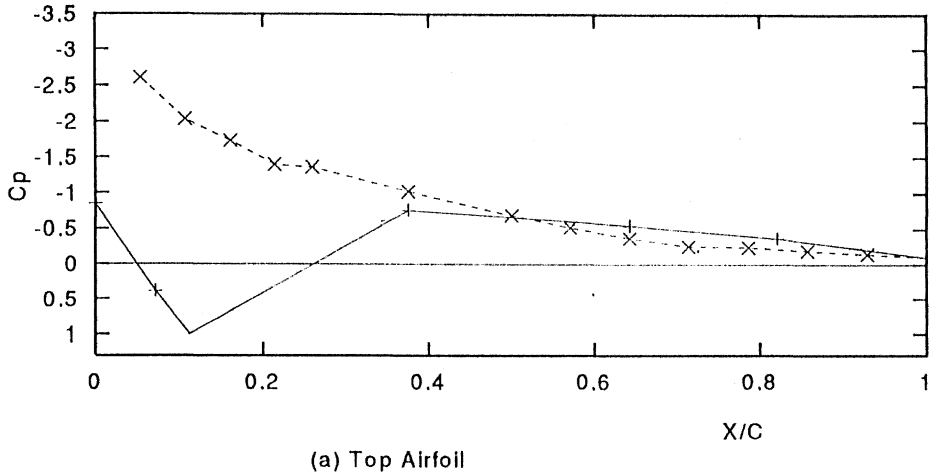

(a) Top Airfoil

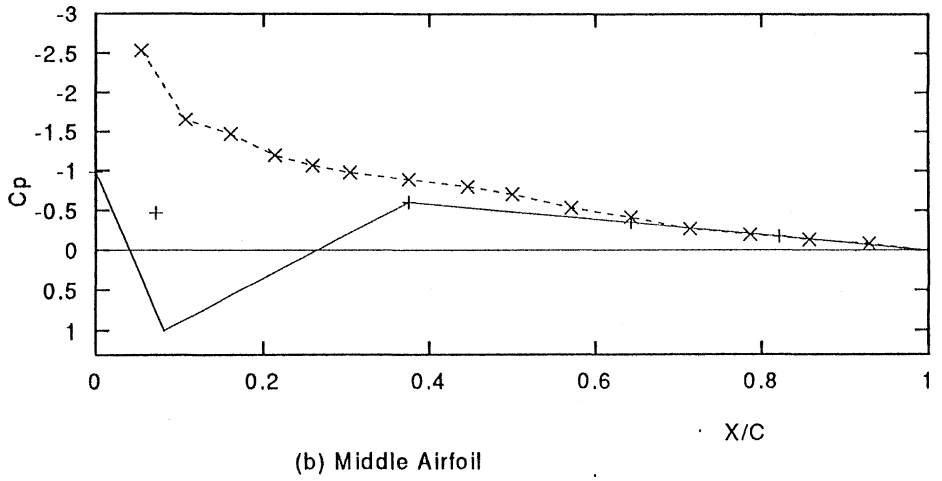

(b) Middle Airfoil

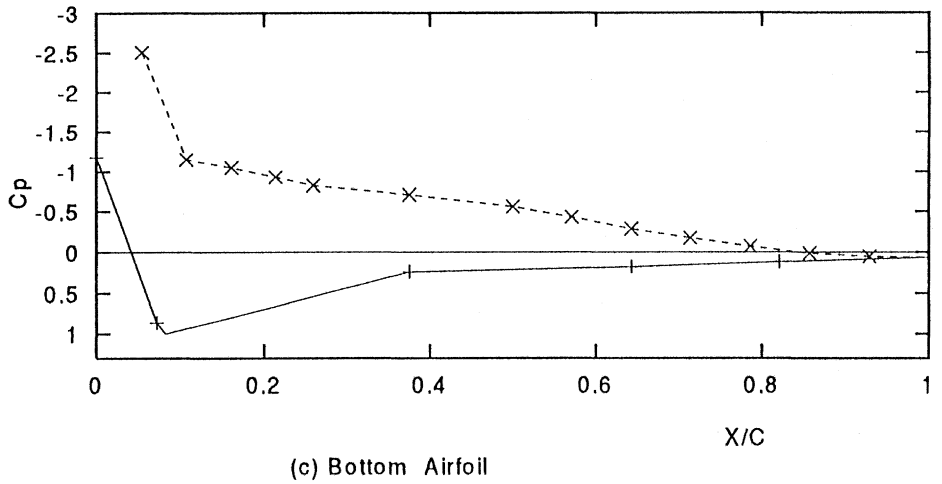

(c) Bottom Airfoil

Figure 4.8: Pressure Distribution of Airfoil; S/C = 0.5, $\alpha = 15°$, $V_\infty = 35$ m/s, + Lower Surface, × Upper Surface.

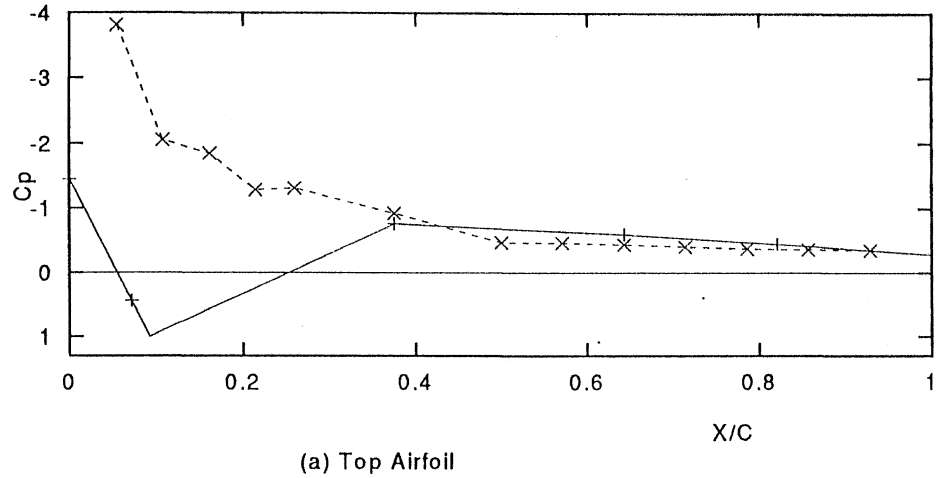

(a) Top Airfoil

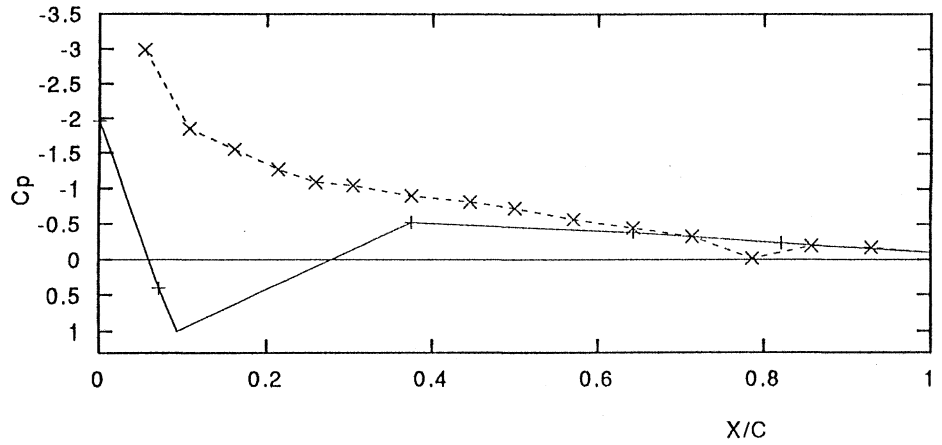

(b) Middle Airfoil

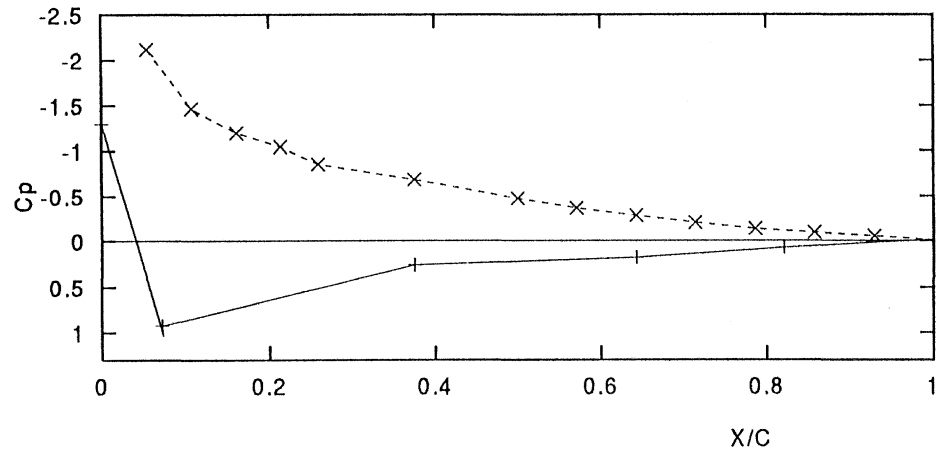

(c) Bottom Airfoil

Figure 4.9: Pressure Distribution of Airfoil; S/C = 0.5, $\alpha = 17.5$, $V_\infty = 25$ m/s, + Lower Surface, × Upper Surface.

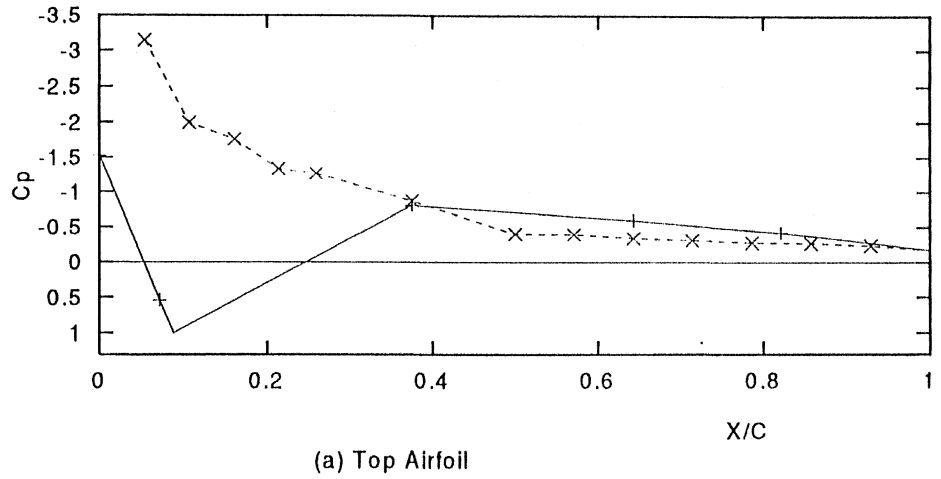

(a) Top Airfoil

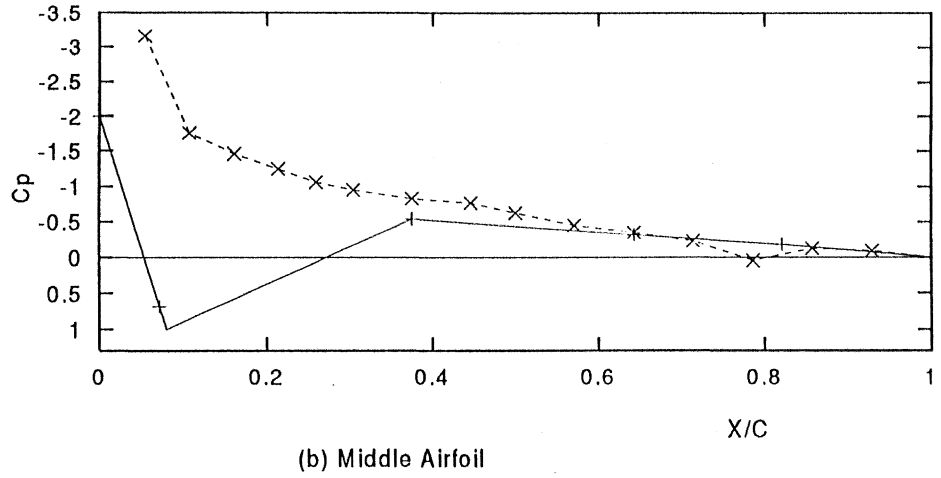

(b) Middle Airfoil

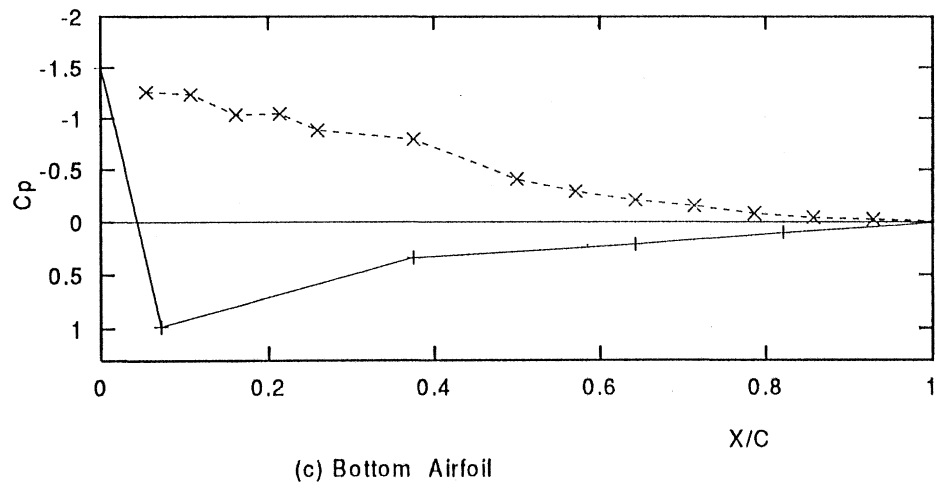

(c) Bottom Airfoil

Figure 4.10: Pressure Distribution of Airfoil; S/C = 0.5, $\alpha = 17.5$, $V_\infty = 35$ m/s. + Lower Surface, × Upper Surface.

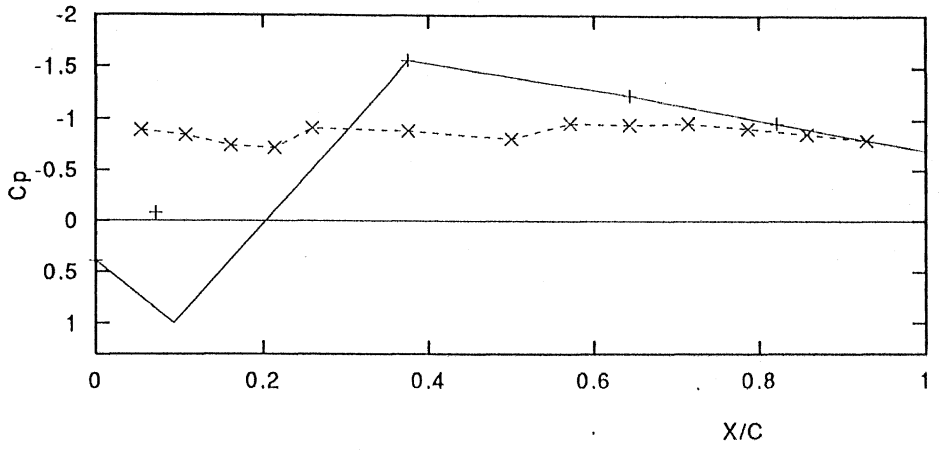

(a) Top Airfoil

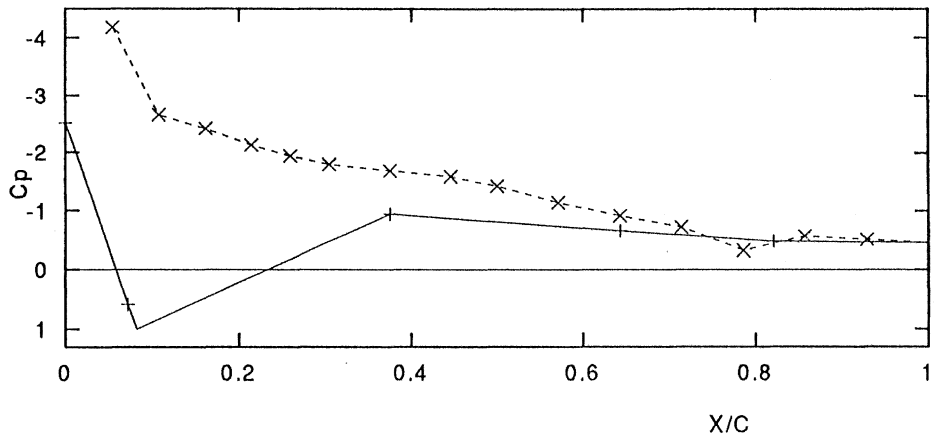

(b) Middle Airfoil

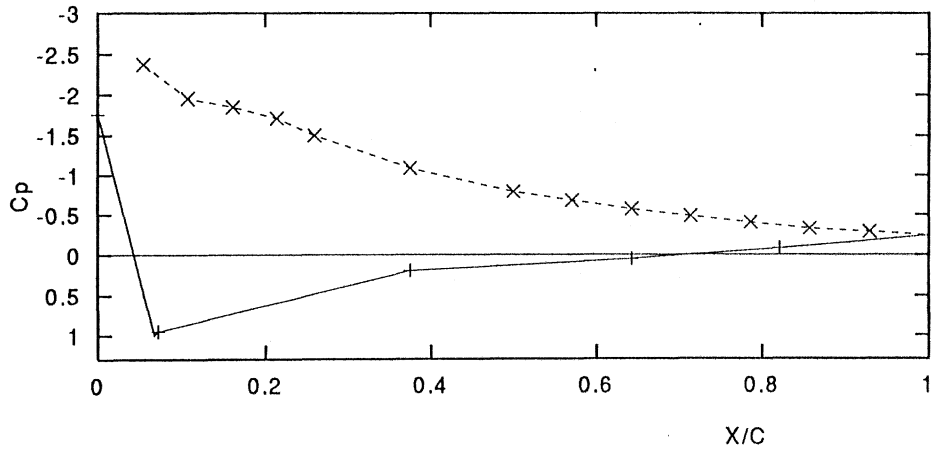

(c) Bottom Airfoil

Figure 4.11: Pressure Distribution of Airfoil; S/C = 0.5, $\alpha = 20^o$, $V_\infty = 25$ m/s, + Lower Surface, × Upper Surface.

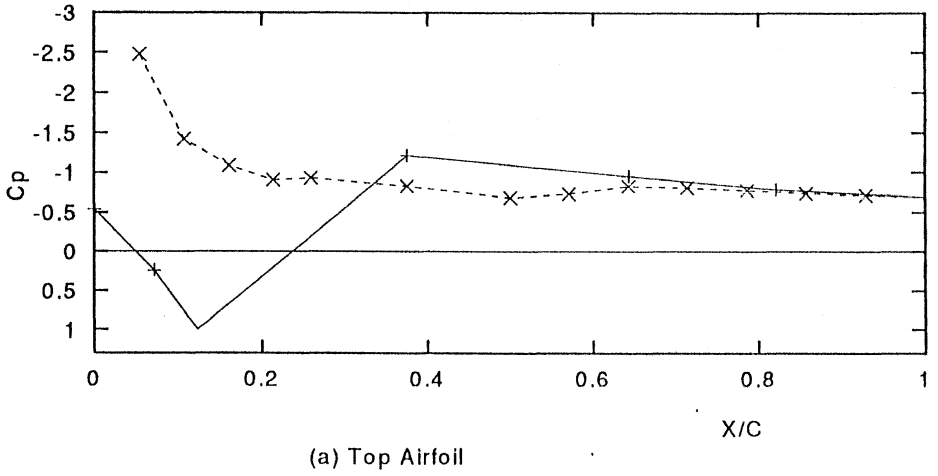

(a) Top Airfoil

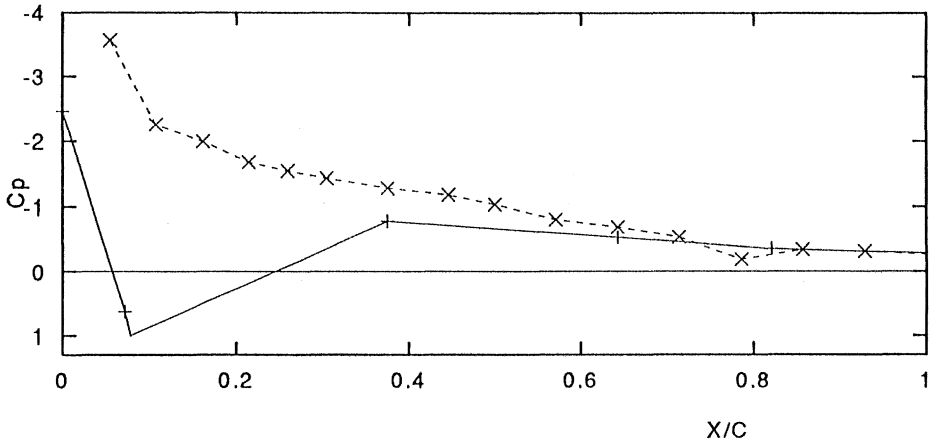

(b) Middle Airfoil

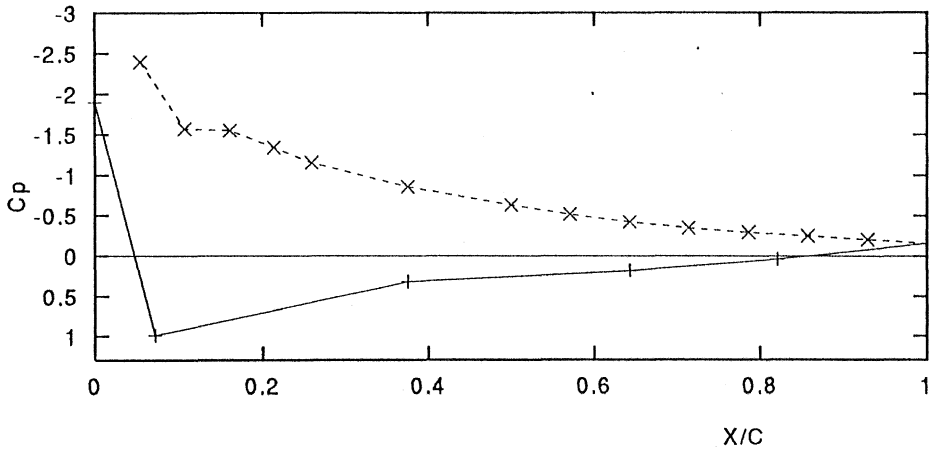

(c) Bottom Airfoil

Figure 4.12: Pressure Distribution of Airfoil; S/C = 0.5, $\alpha = 20^o$, $V_\infty = 35$ m/s, + Lower Surface, × Upper Surface.

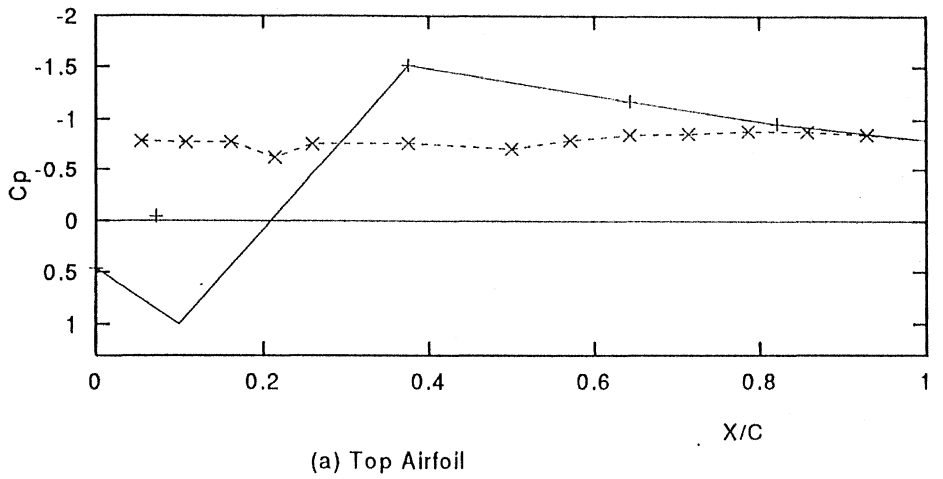

(a) Top Airfoil

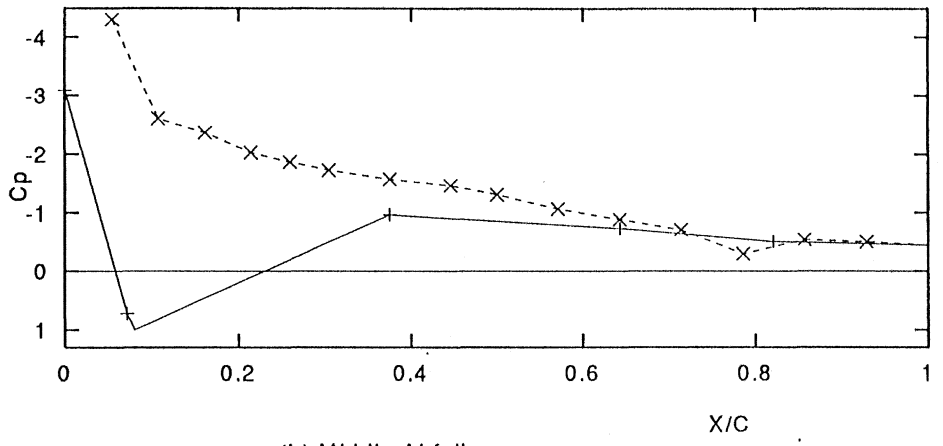

(b) Middle Airfoil

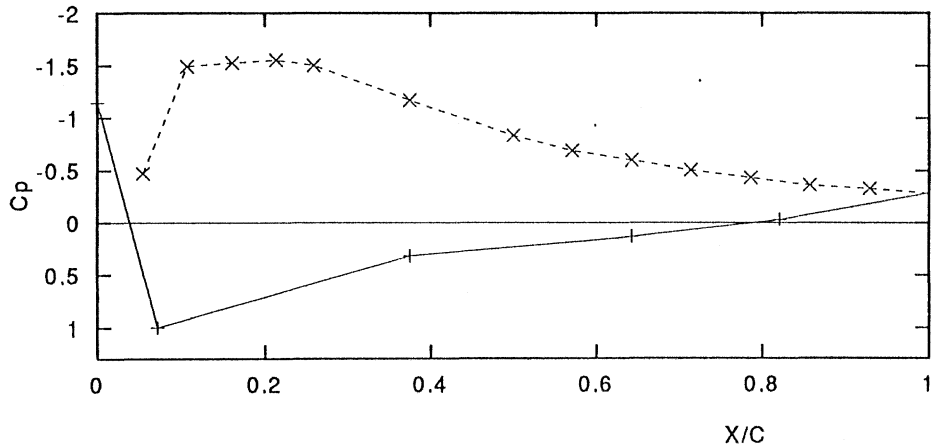

(c) Bottom Airfoil

Figure 4.13: Pressure Distribution of Airfoil; S/C = 0.5, $\alpha = 22.5^o$, $V_\infty = 25$ m/s. + Lower Surface,× Upper Surface.

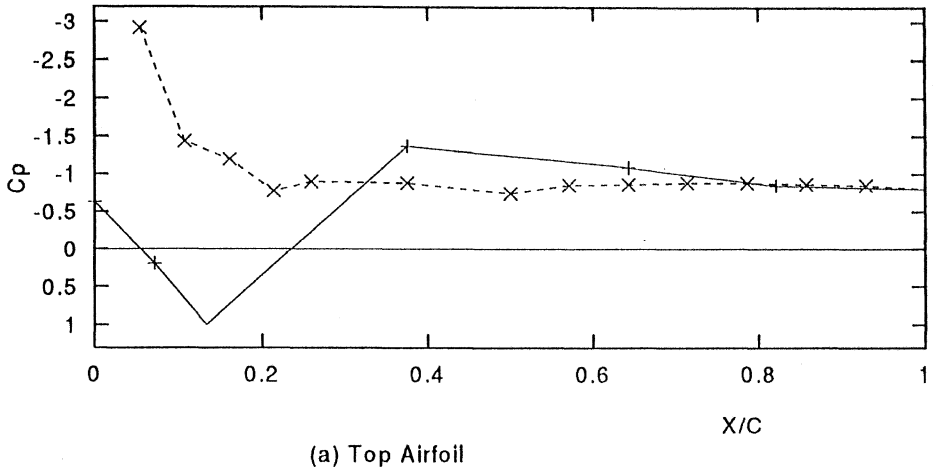

(a) Top Airfoil

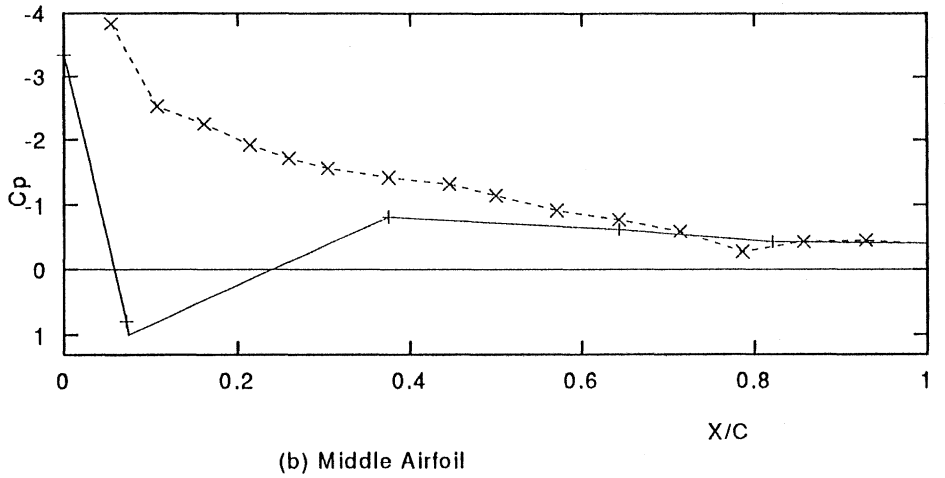

(b) Middle Airfoil

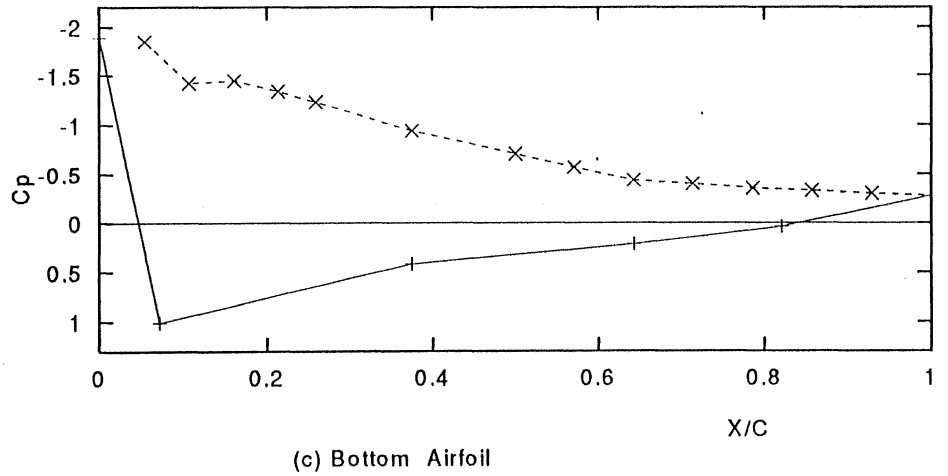

(c) Bottom Airfoil

Figure 4.14: Pressure Distribution of Airfoil; S/C = 0.5, $\alpha = 22.5^o$, $V_\infty = 35$ m/s, + Lower Surface, × Upper Surface.

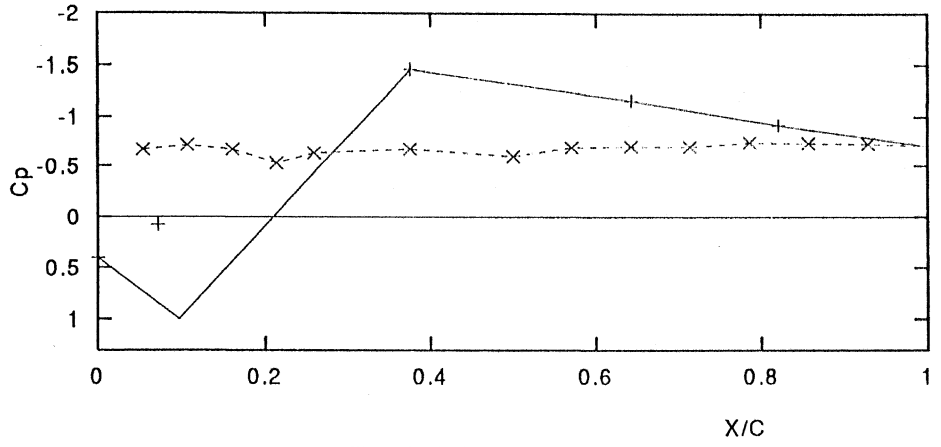

(a) Top Airfoil

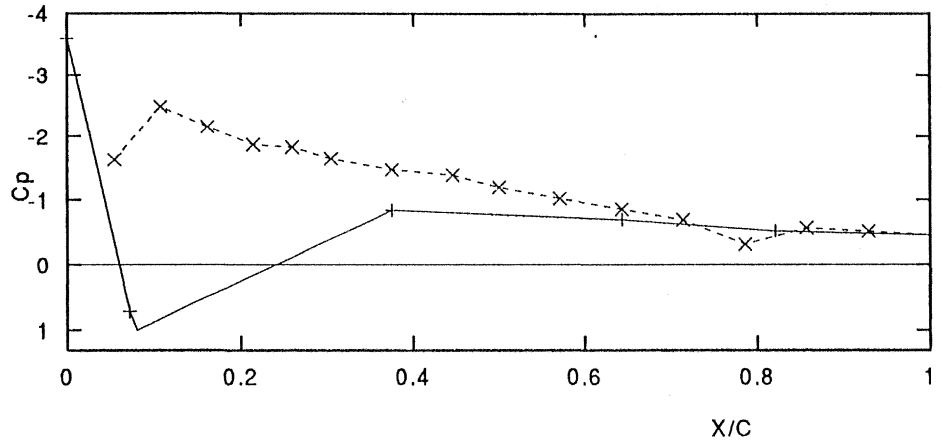

(b) Middle Airfoil

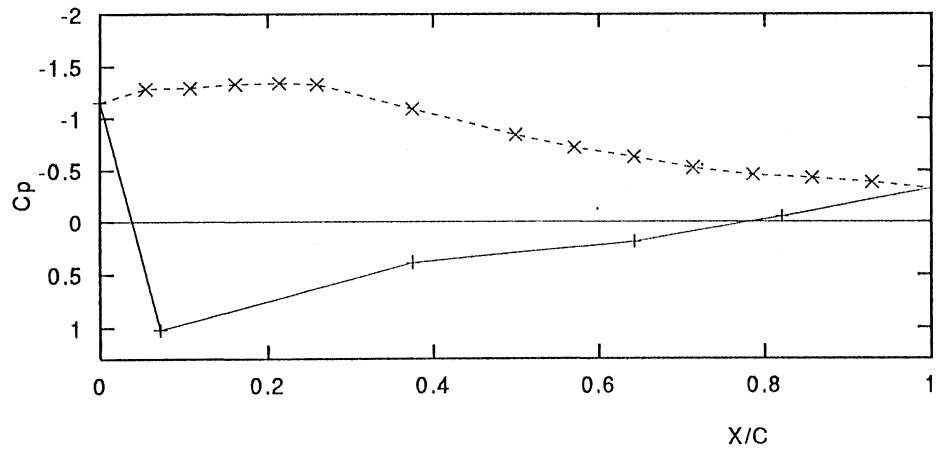

(c) Bottom Airfoil

Figure 4.15: Pressure Distribution of Airfoil; S/C = 0.5, $\alpha = 25^o$, $V_\infty = 25$ m/s, + Lower Surface, × Upper Surface.

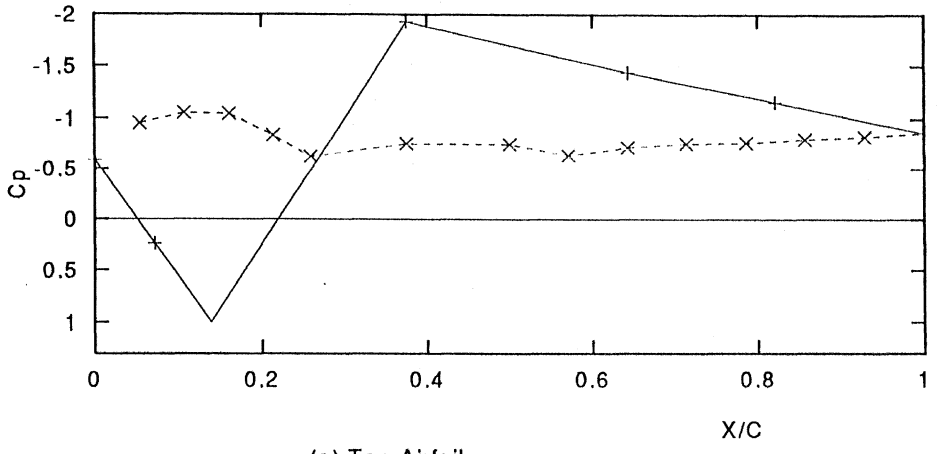

(a) Top Airfoil

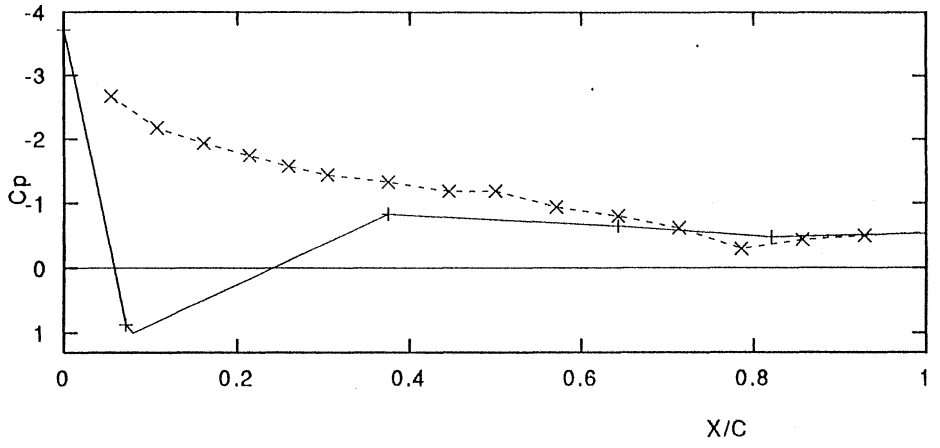

(b) Middle Airfoil

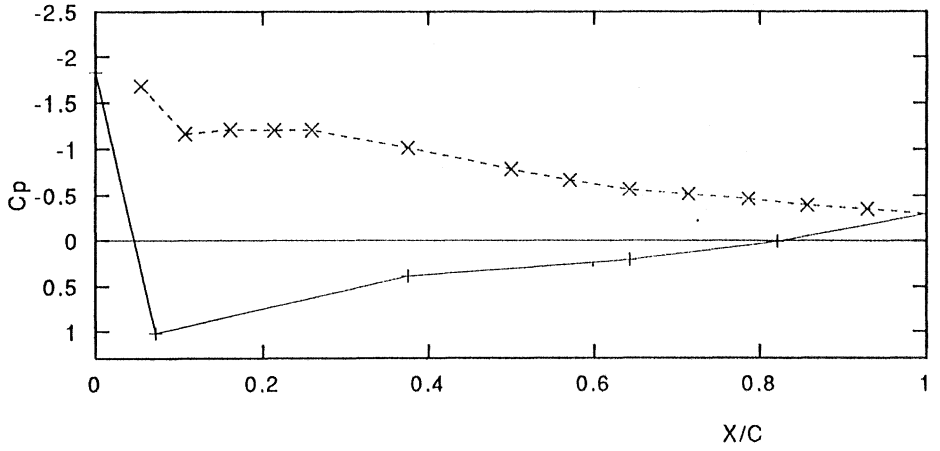

(c) Bottom Airfoil

Figure 4.16: Pressure Distribution of Airfoil; S/C = 0.5, $\alpha = 25^o$, $V_\infty = 35$ m/s, + Lower Surface, × Upper Surface.

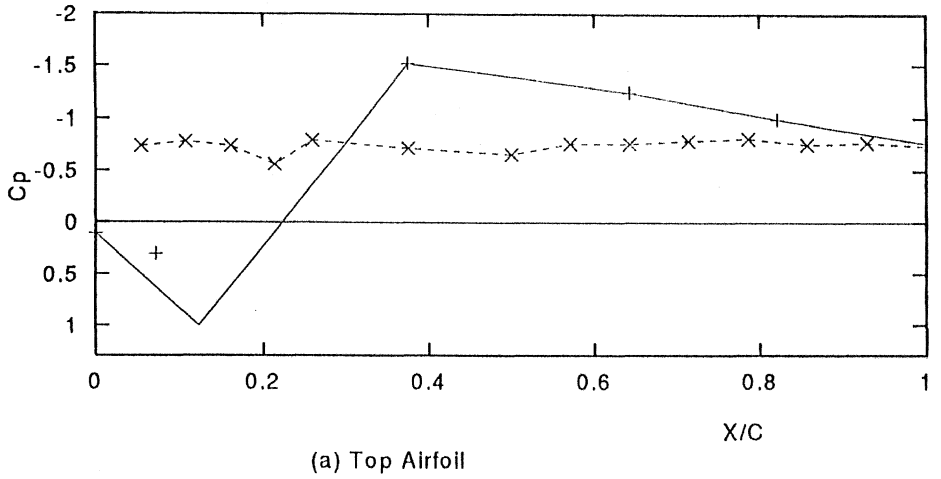

(a) Top Airfoil

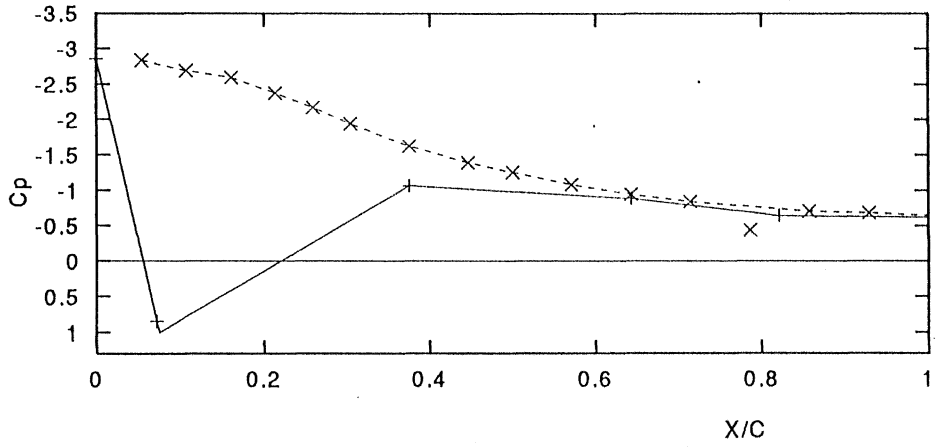

(b) Middle Airfoil

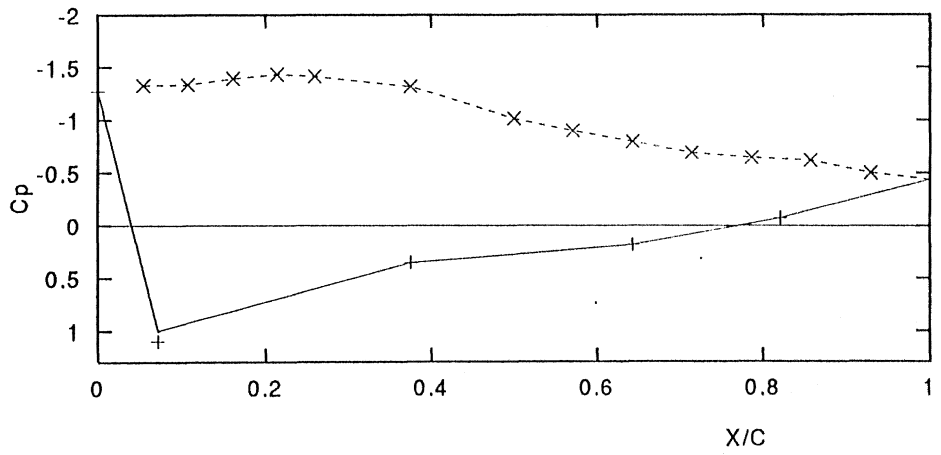

(c) Bottom Airfoil

Figure 4.17: Pressure Distribution of Airfoil; S/C = 0.5, $\alpha = 27.5^o$, $V_\infty = 25$ m/s, + Lower Surface, × Upper Surface.

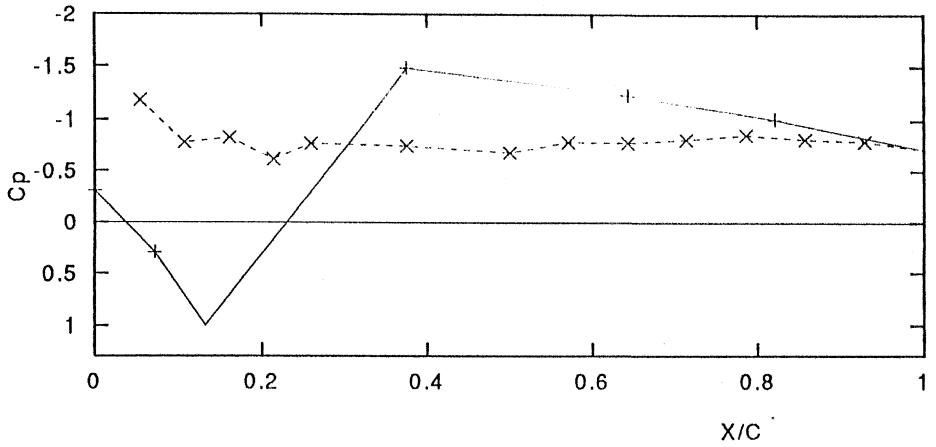

(a) Top Airfoil

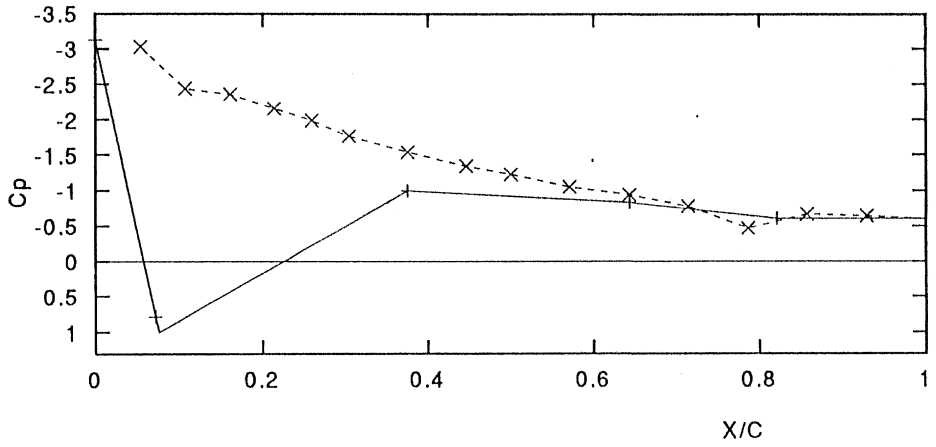

(b) Middle Airfoil

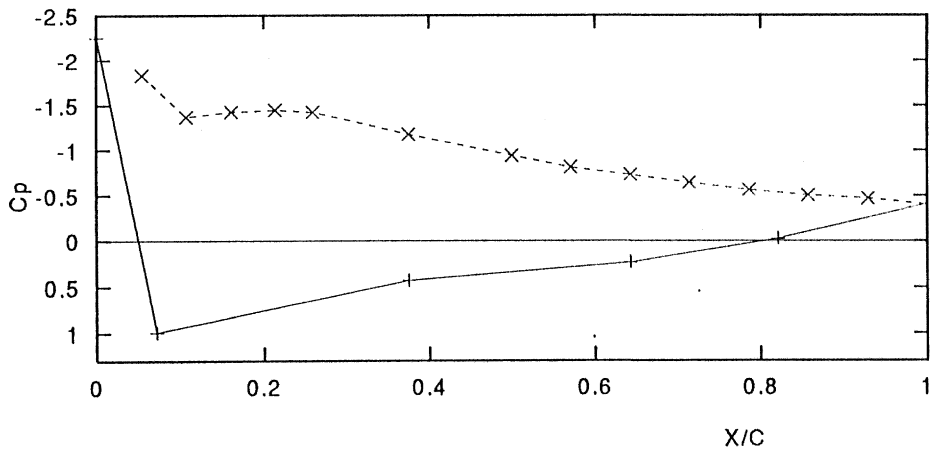

(c) Bottom Airfoil

Figure 4.18: Pressure Distribution of Airfoil; S/C = 0.5, $\alpha = 27.5^o$, $V_\infty = 35$ m/s, + Lower Surface, × Upper Surface.

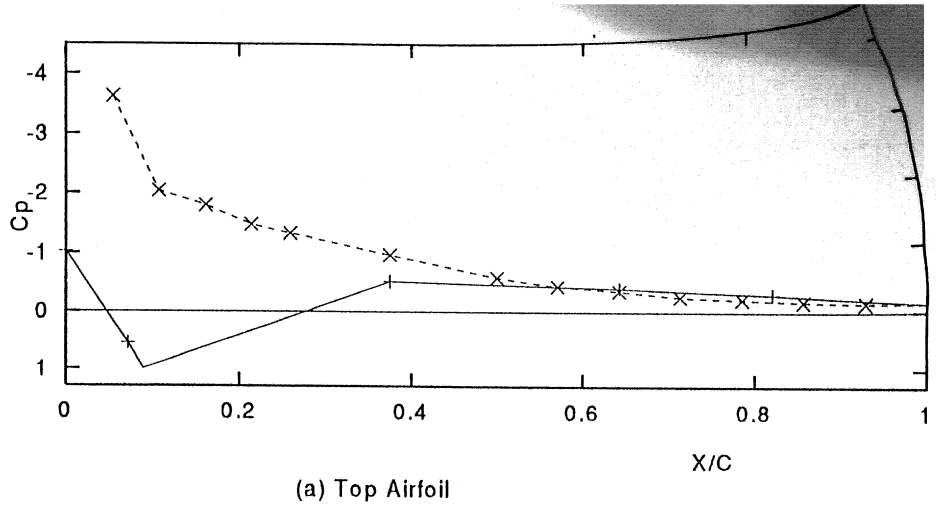

(a) Top Airfoil

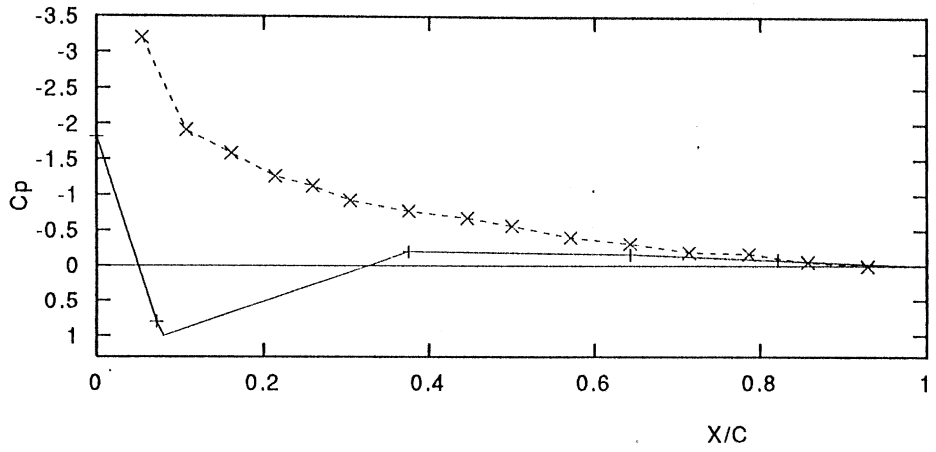

(b) Middle Airfoil

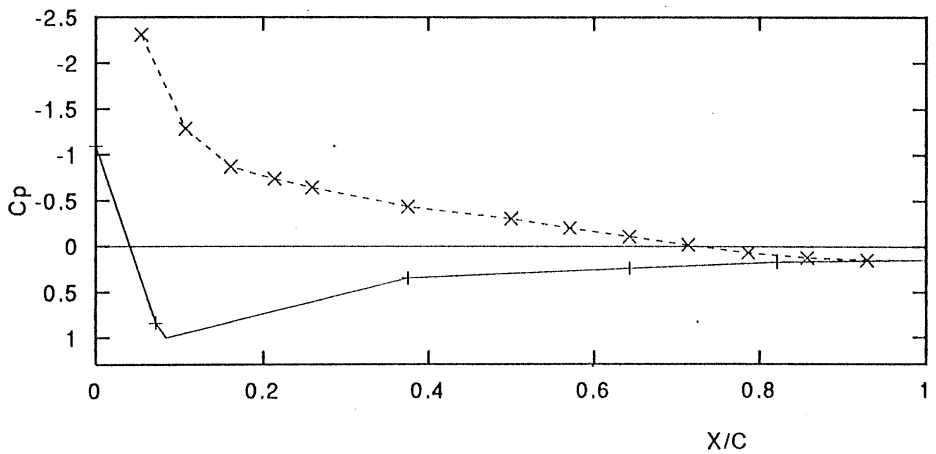

(c) Bottom Airfoil

Figure 4.19: Pressure Distribution of Airfoil; S/C = 0.7, $\alpha = 15^o$, $V_\infty = 25$ m/s, + Lower Surface, × Upper Surface.

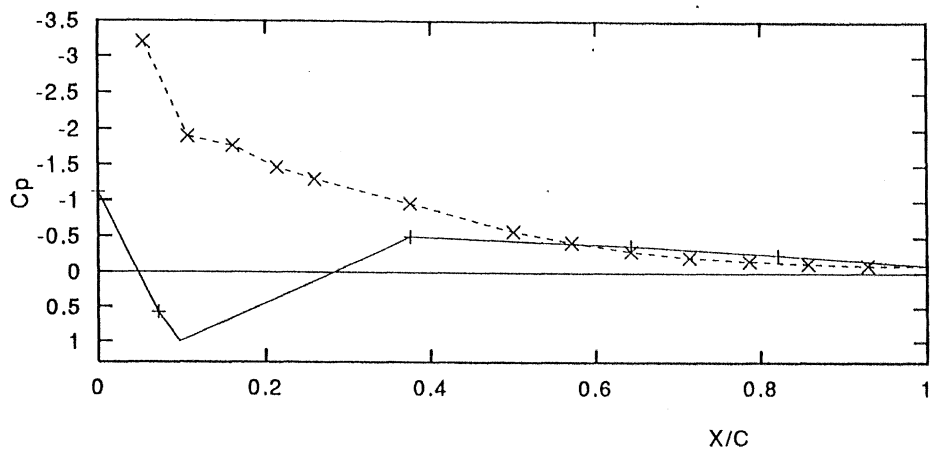

(a) Top Airfoil

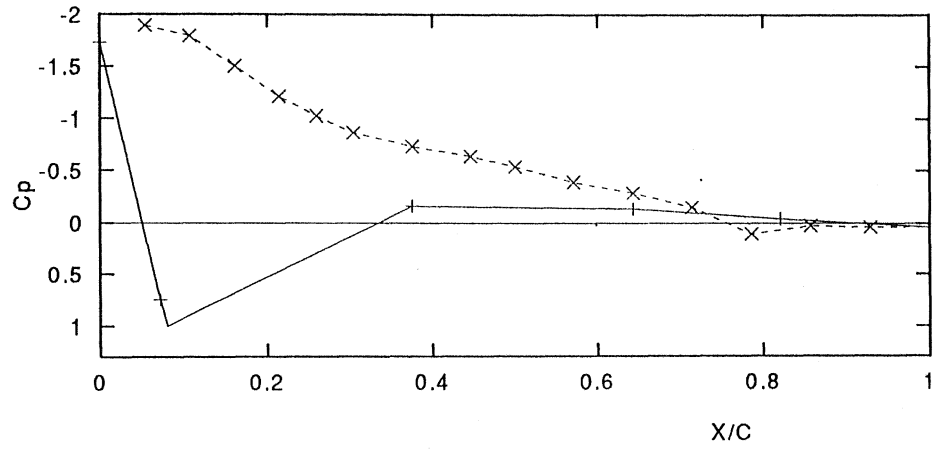

(b) Middle Airfoil

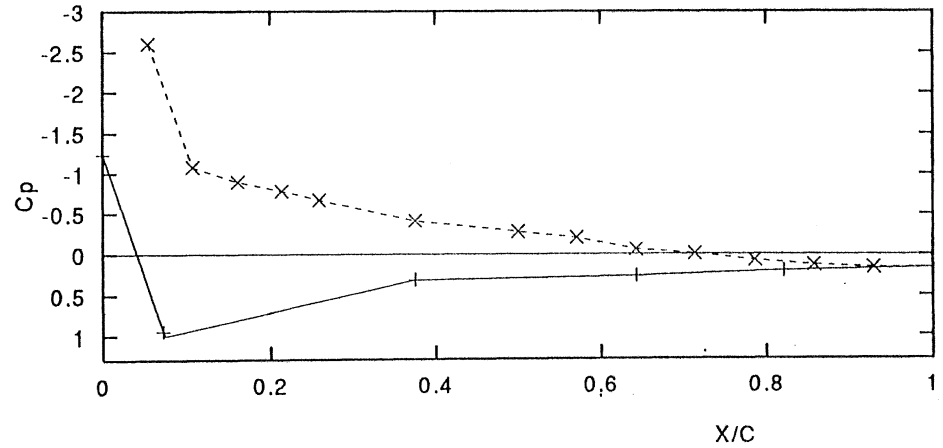

(c) Bottom Airfoil

Figure 4.20: Pressure Distribution of Airfoil; S/C = 0.7, $\alpha = 15^o$, $V_\infty = 35$ m/s, + Lower Surface, × Upper Surface.

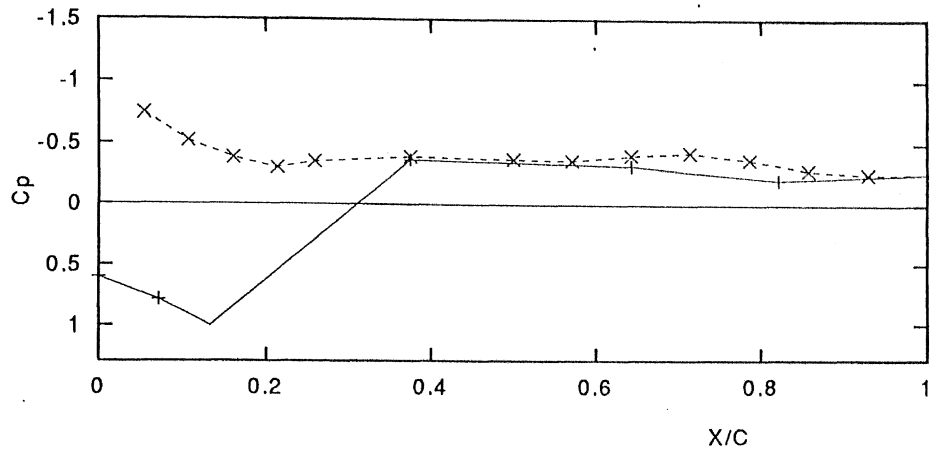

(a) Top Airfoil

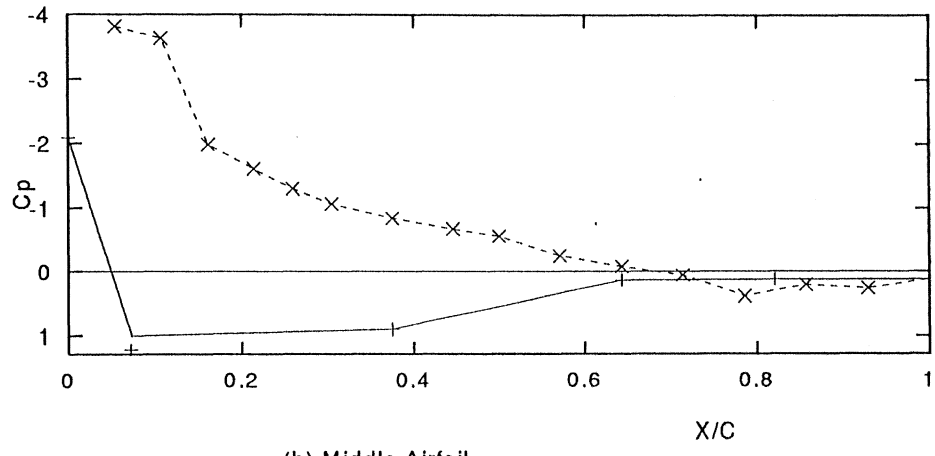

(b) Middle Airfoil

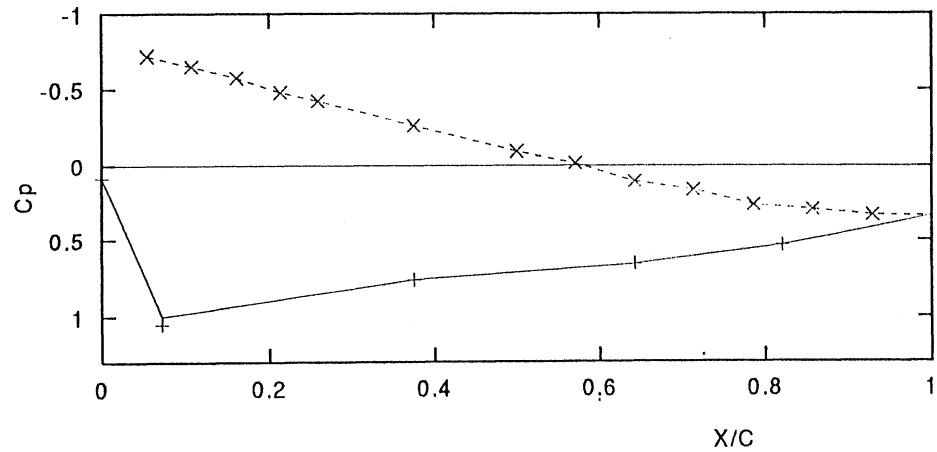

(c) Bottom Airfoil

Figure 4.21: Pressure Distribution of Airfoil; S/C = 0.7, $\alpha = 17.5$, $V_\infty = 25$ m/s, + Lower Surface, × Upper Surface.

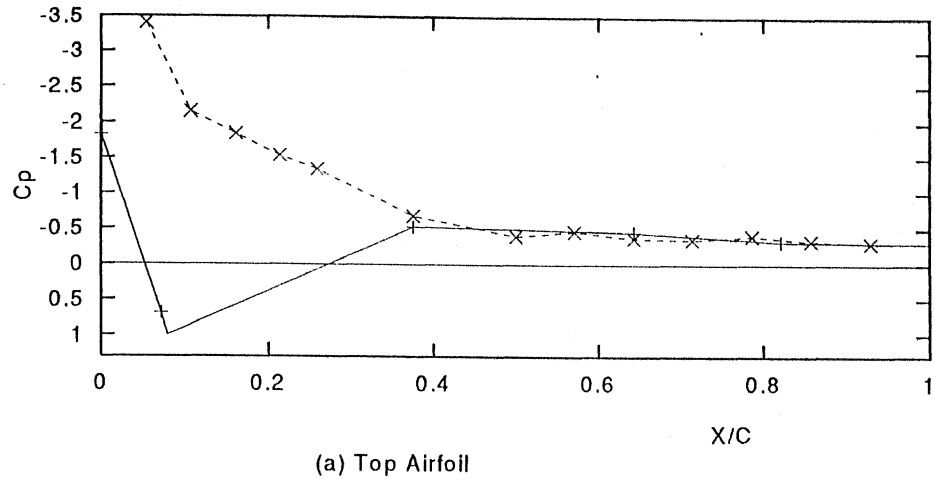

(a) Top Airfoil

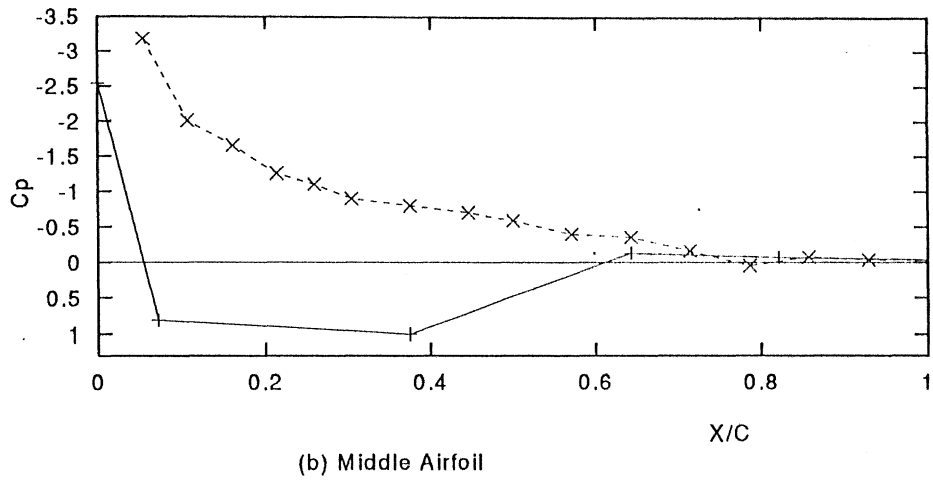

(b) Middle Airfoil

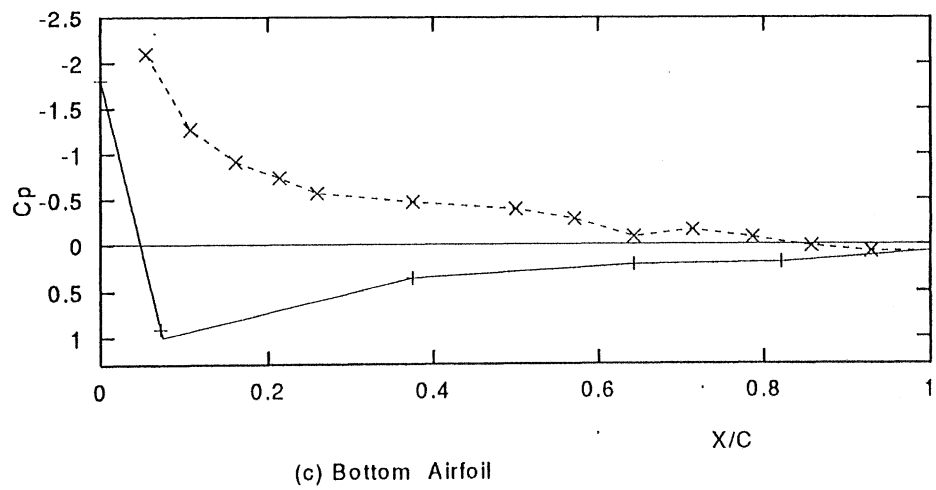

(c) Bottom Airfoil

Figure 4.22: Pressure Distribution of Airfoil; S/C = 0.7, $\alpha = 17.5^o$, $V_\infty = 35$ m/s, + Lower Surface, × Upper Surface.

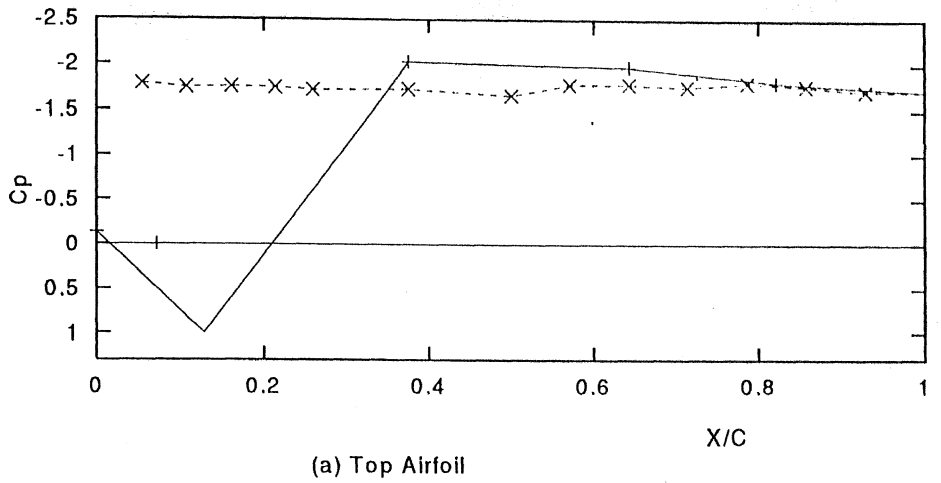

(a) Top Airfoil

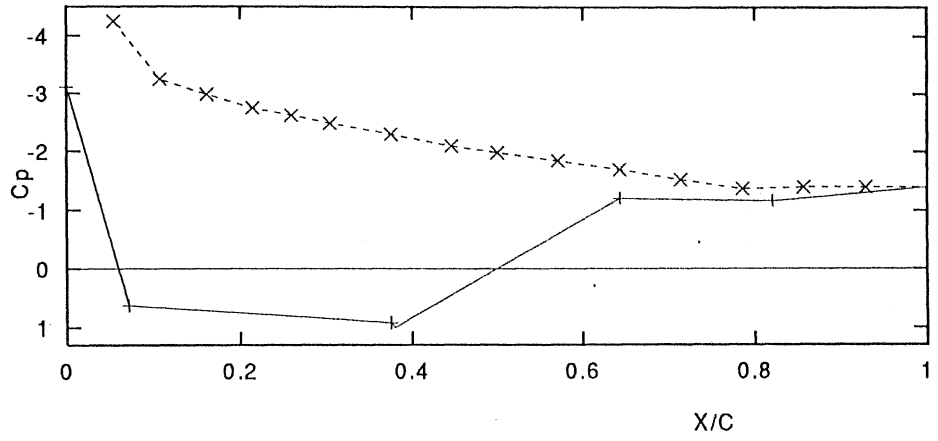

(b) Middle Airfoil

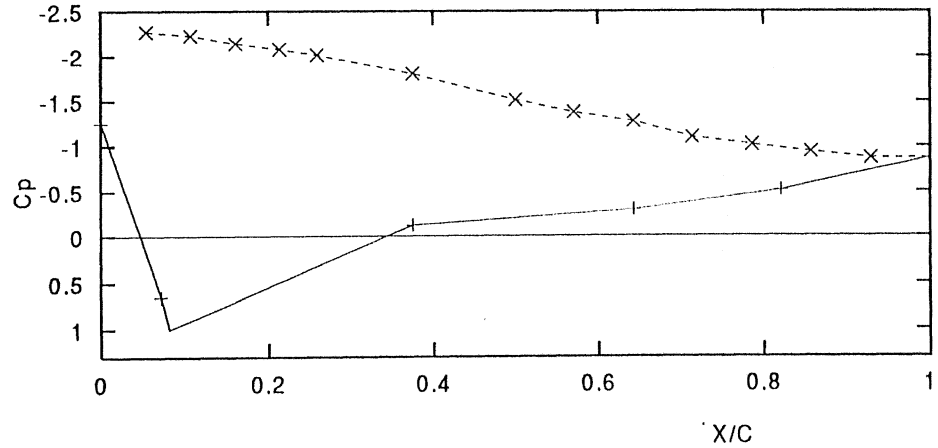

(c) Bottom Airfoil

Figure 4.23: Pressure Distribution of Airfoil; S/C = 0.7, $\alpha = 20^o$, $V_\infty = 25$ m/s, + Lower Surface, × Upper Surface.

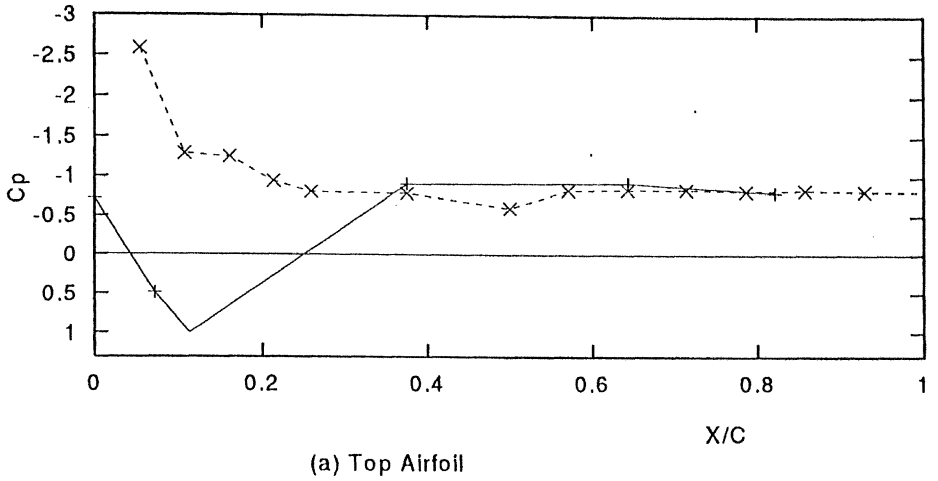

(a) Top Airfoil

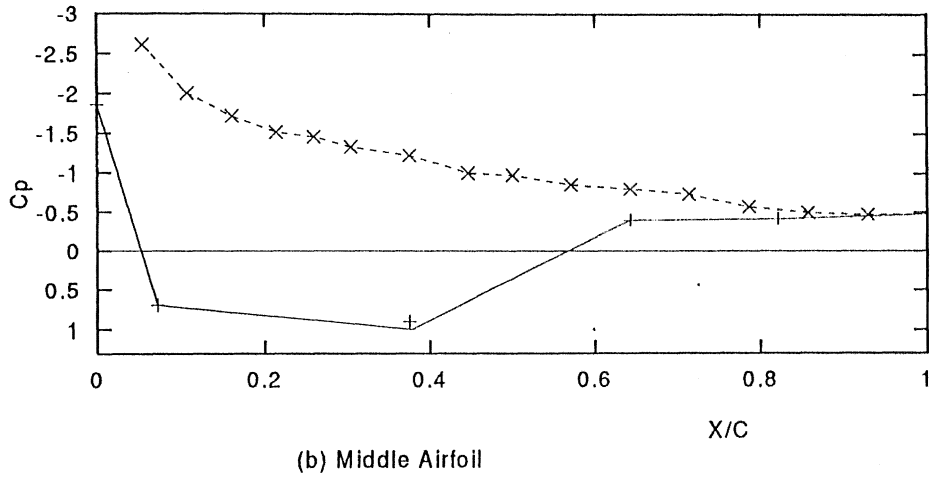

(b) Middle Airfoil

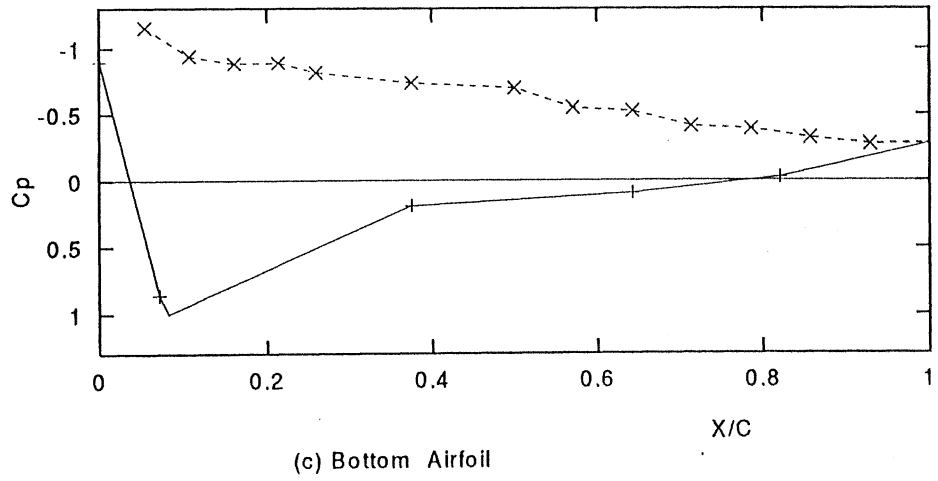

(c) Bottom Airfoil

Figure 4.24: Pressure Distribution of Airfoil; S/C = 0.7, $\alpha = 20^o$, $V_\infty = 35$ m/s, + Lower Surface, × Upper Surface.

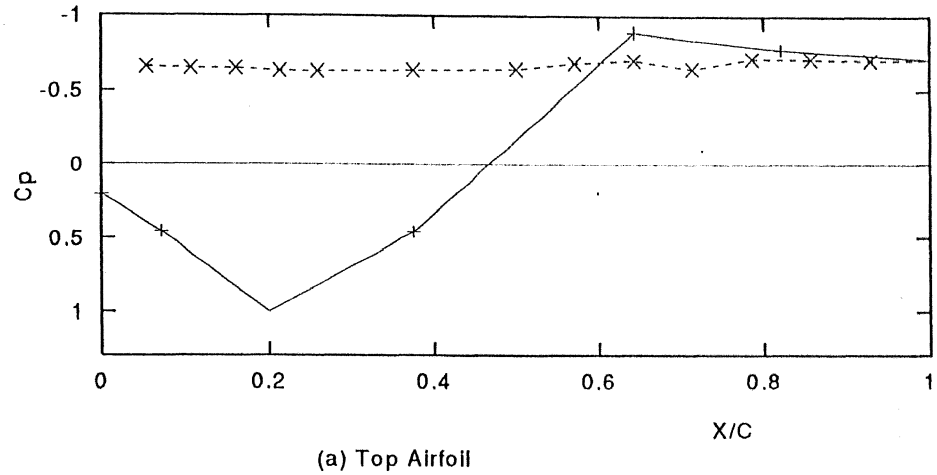

(a) Top Airfoil

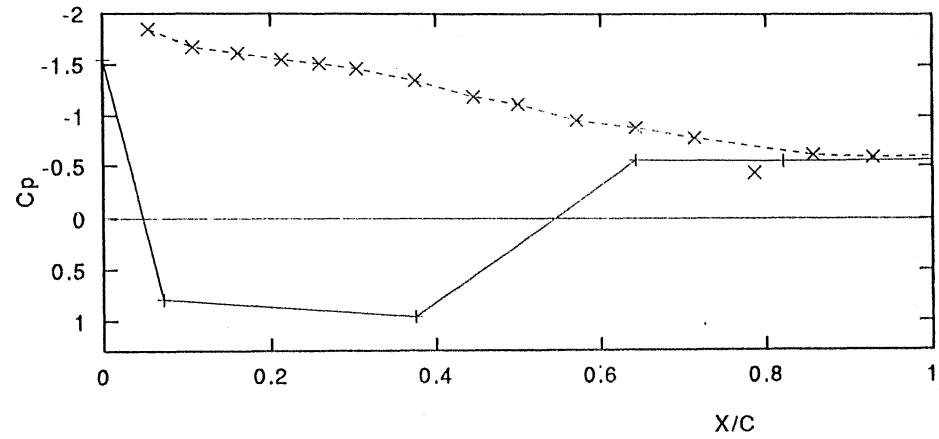

(b) Middle Airfoil

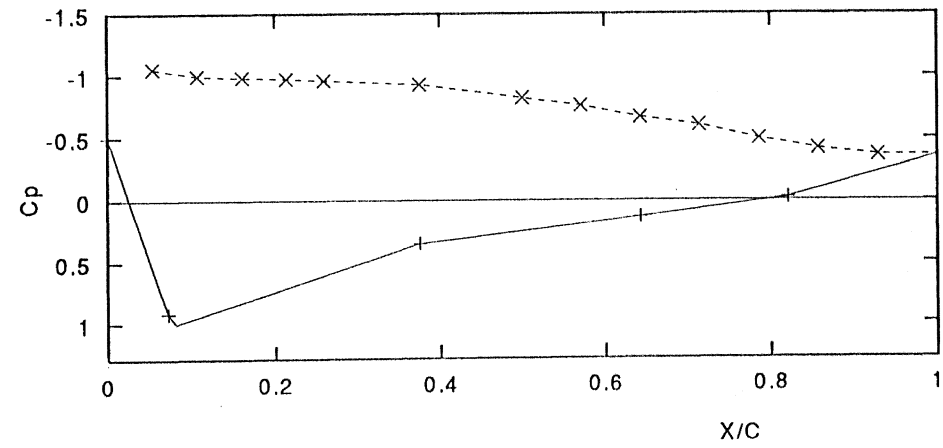

(c) Bottom Airfoil

Figure 4.25: Pressure Distribution of Airfoil; S/C = 0.7, $\alpha = 22.5^o$, $V_\infty = 25$ m/s, + Lower Surface, × Upper Surface.

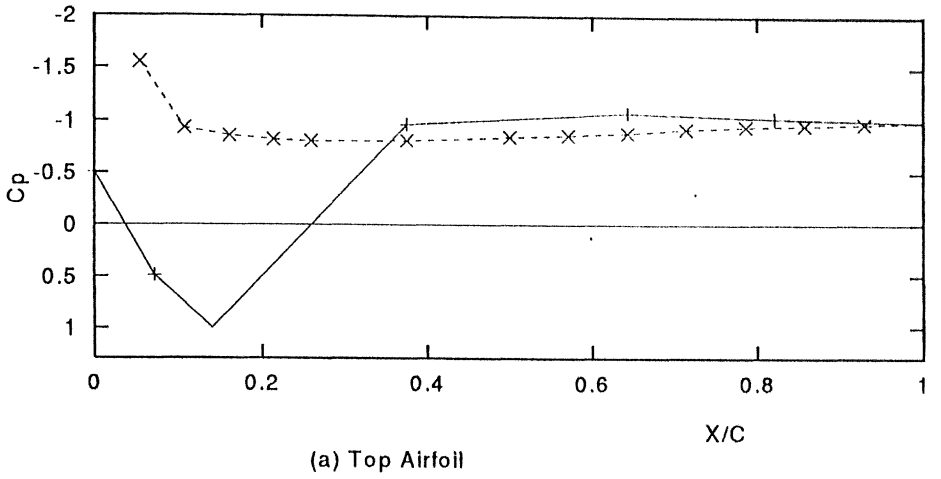

(a) Top Airfoil

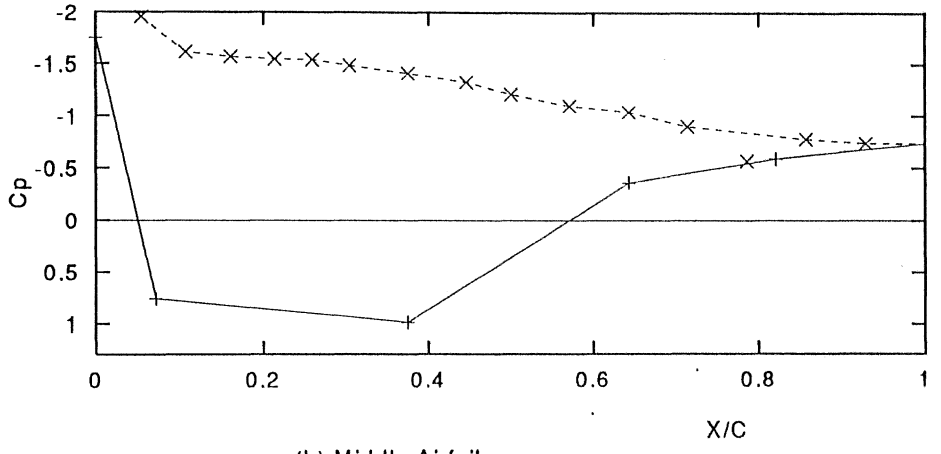

(b) Middle Airfoil

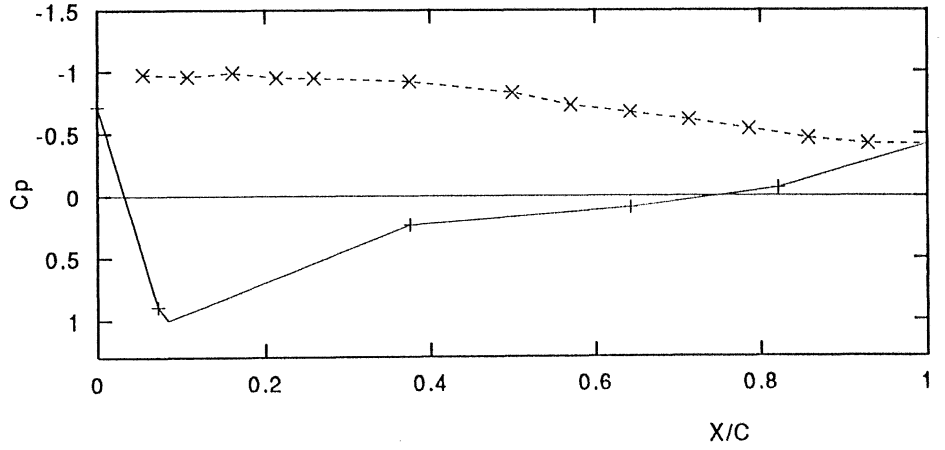

(c) Bottom Airfoil

Figure 4.26: Pressure Distribution of Airfoil; S/C = 0.7, $\alpha = 22.5^o$, $V_\infty = 35$ m/s, + Lower Surface, × Upper Surface.

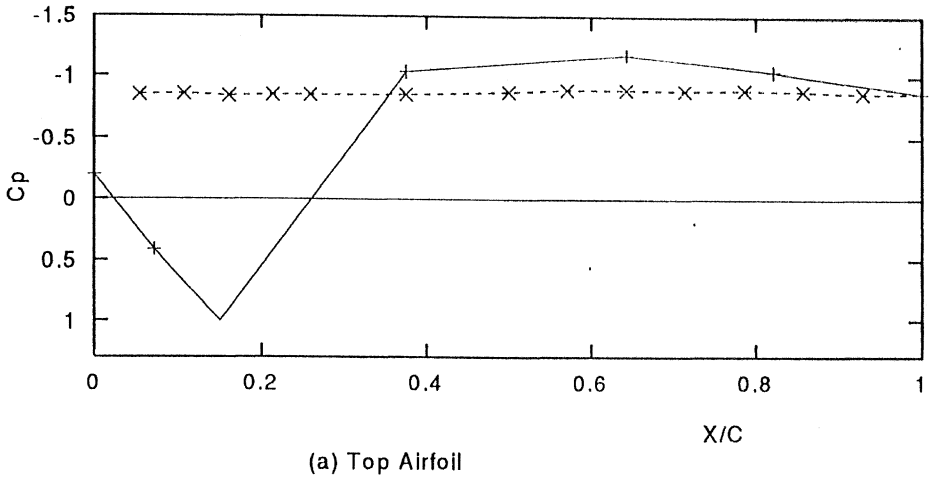

(a) Top Airfoil

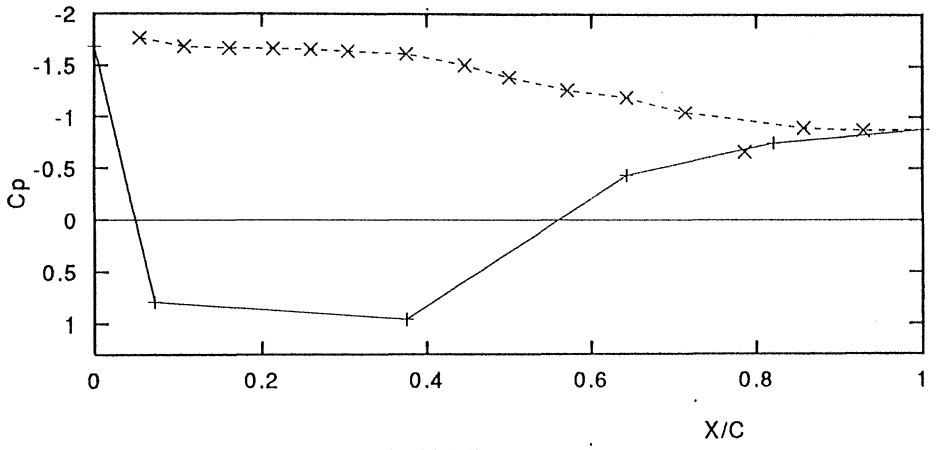

(b) Middle Airfoil

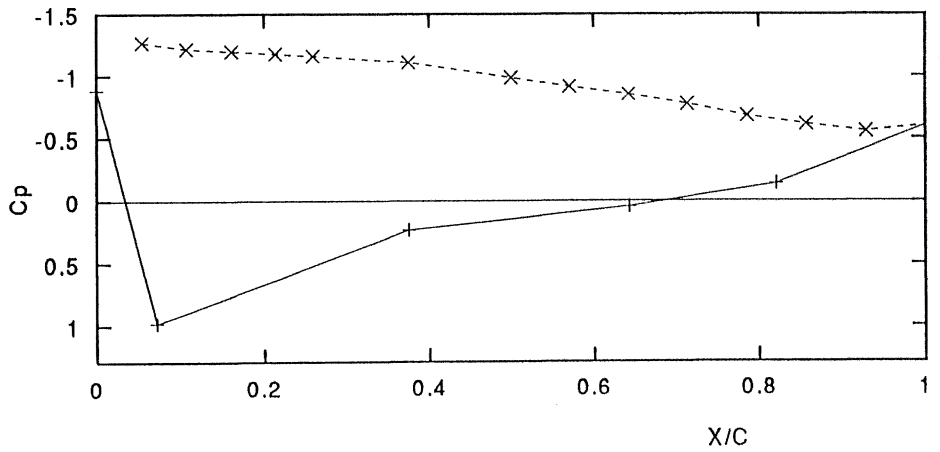

(c) Bottom Airfoil

Figure 4.27: Pressure Distribution of Airfoil; S/C = 0.7, $\alpha = 25^o$, $V_\infty = 25$ m/s, + Lower Surface, × Upper Surface.

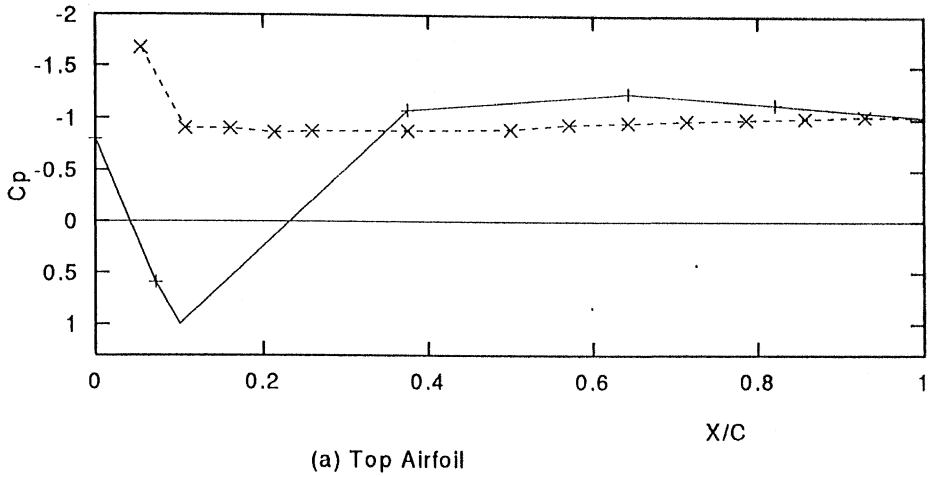

(a) Top Airfoil

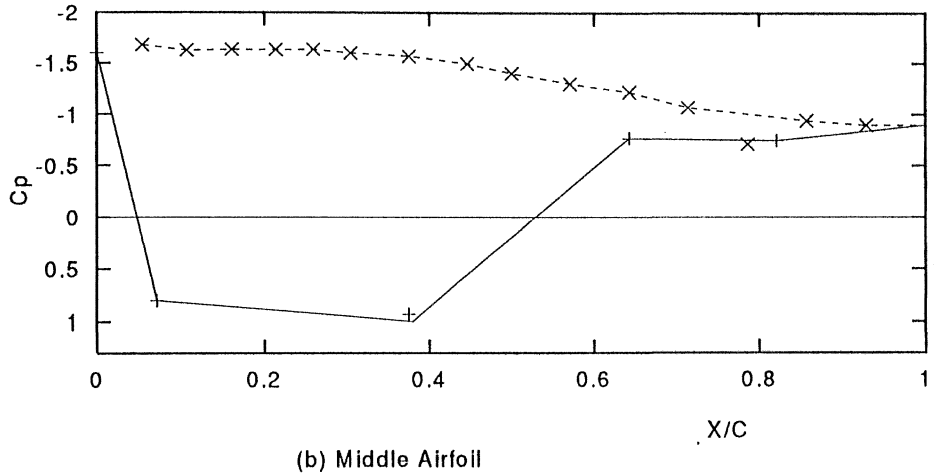

(b) Middle Airfoil

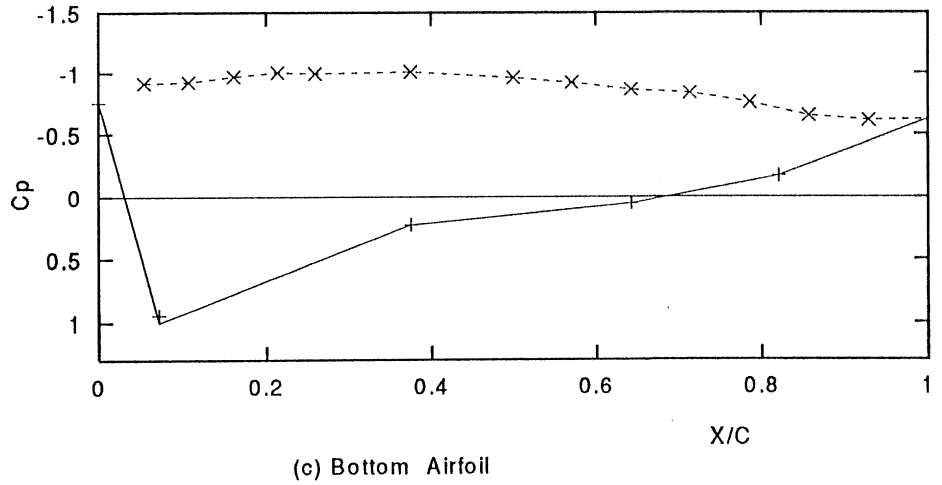

(c) Bottom Airfoil

Figure 4.28: Pressure Distribution of Airfoil; S/C = 0.7, $\alpha = 25^o$, $V_\infty = 35$ m/s, + Lower Surface, × Upper Surface.

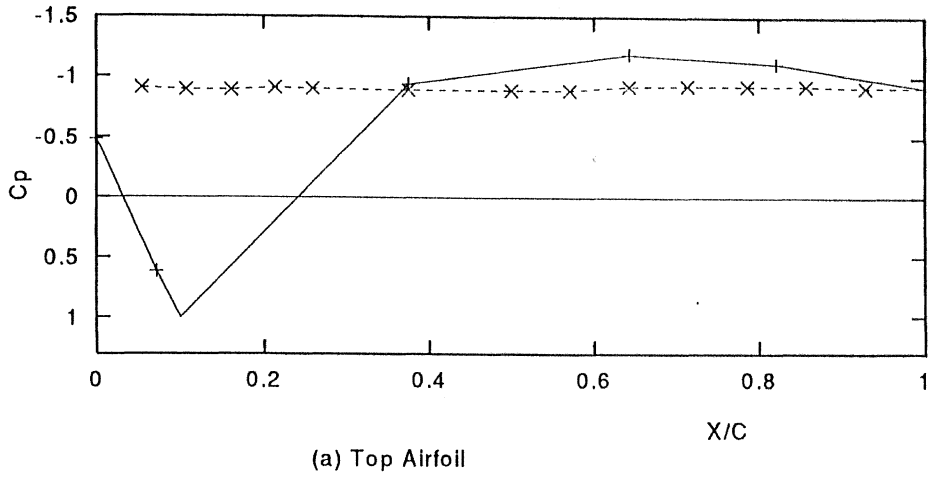

(a) Top Airfoil

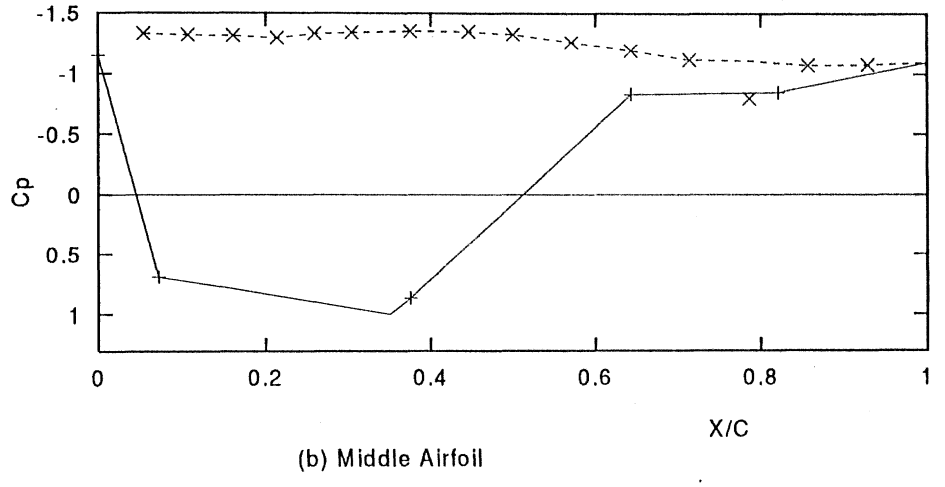

(b) Middle Airfoil

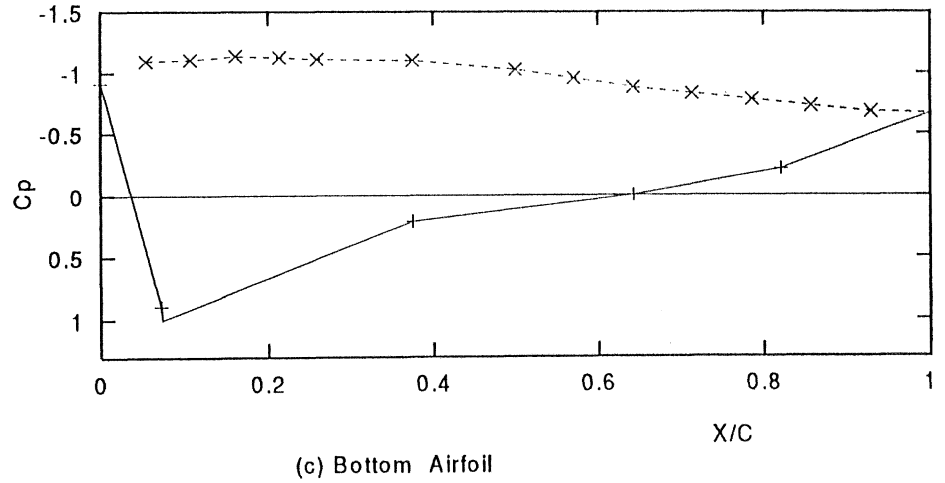

(c) Bottom Airfoil

Figure 4.29: Pressure Distribution of Airfoil; S/C = 0.7, $\alpha = 27.5^o$, $V_\infty = 25$ m/s, + Lower Surface, × Upper Surface.

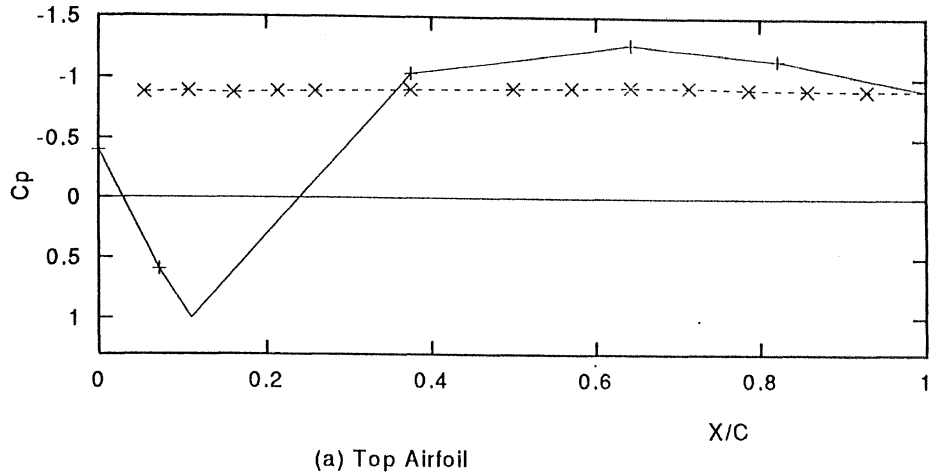

(a) Top Airfoil

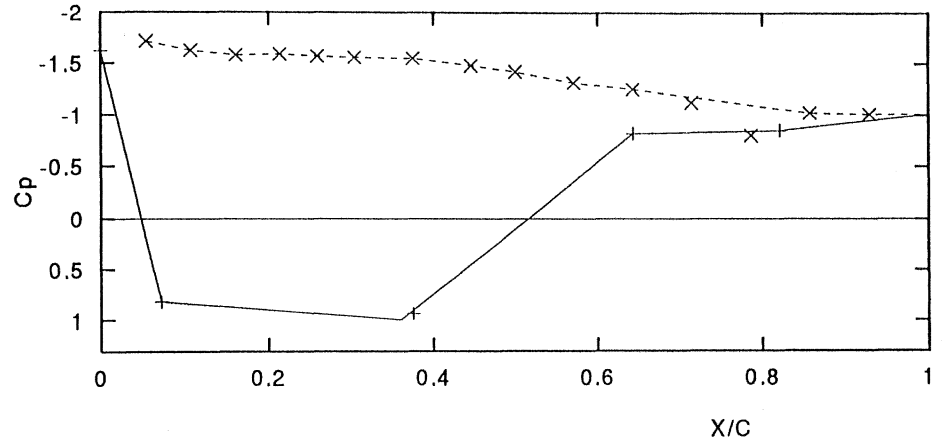

(b) Middle Airfoil

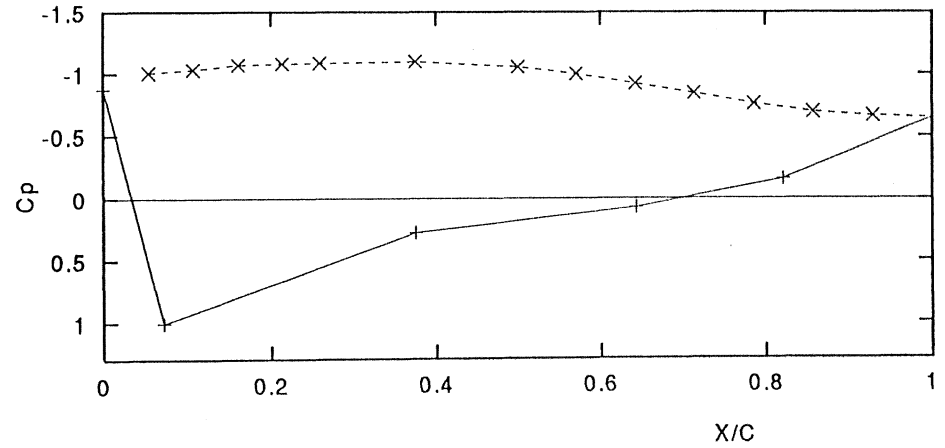

(c) Bottom Airfoil

Figure 4.30: Pressure Distribution of Airfoil; S/C = 0.7, $\alpha = 27.5^o$, $V_\infty = 35$ m/s, + Lower Surface, × Upper Surface.

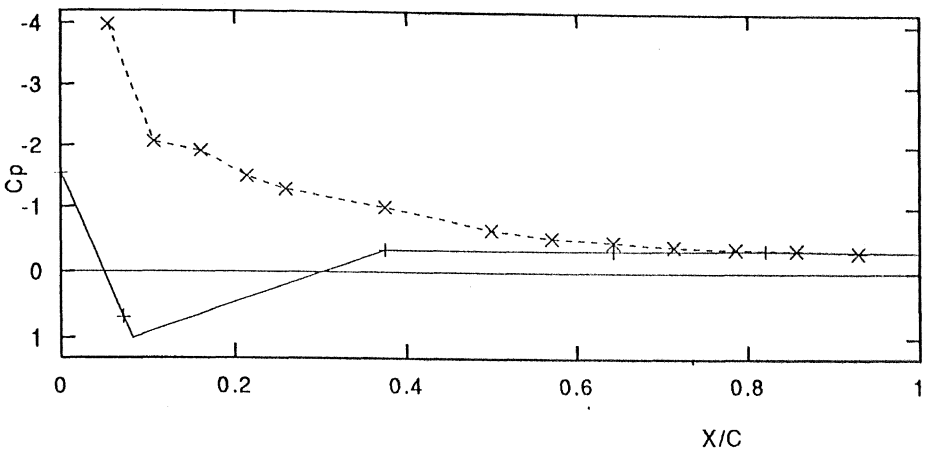

(a) Top Airfoil

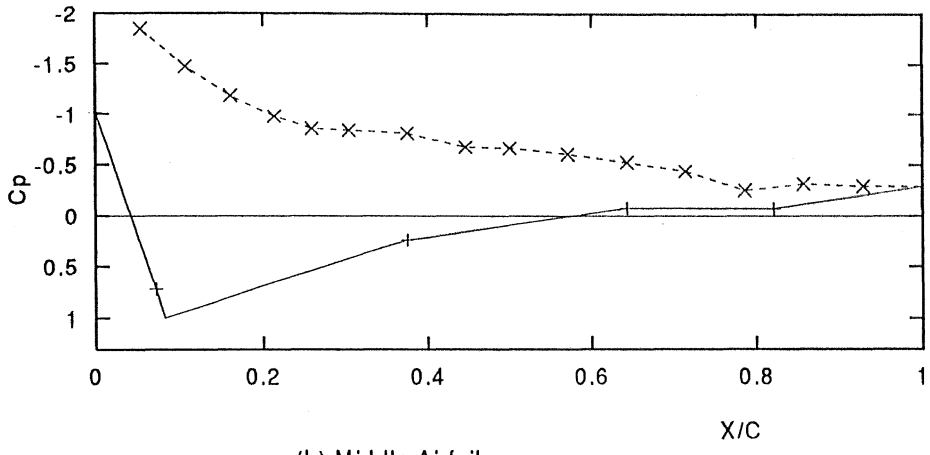

(b) Middle Airfoil

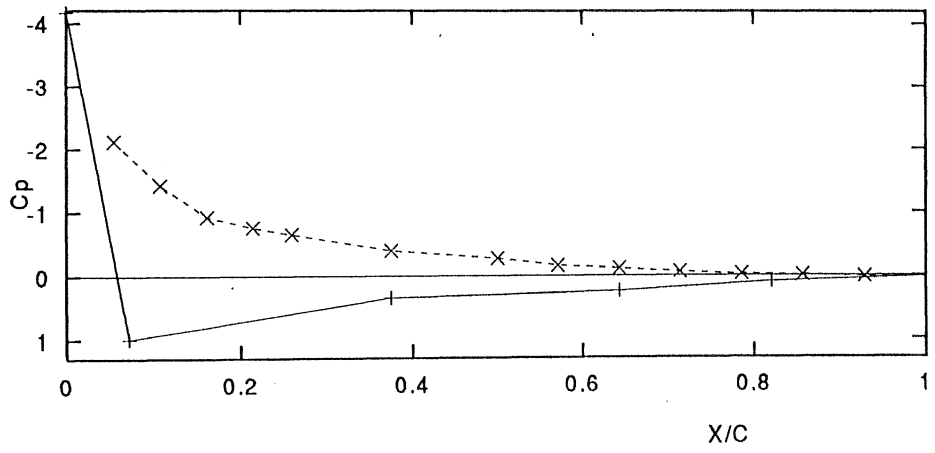

(c) Bottom Airfoil

Figure 4.31: Pressure Distribution of Airfoil; S/C = 0.9, $\alpha = 15^o$, $V_\infty = 25$ m/s, + Lower Surface, × Upper Surface.

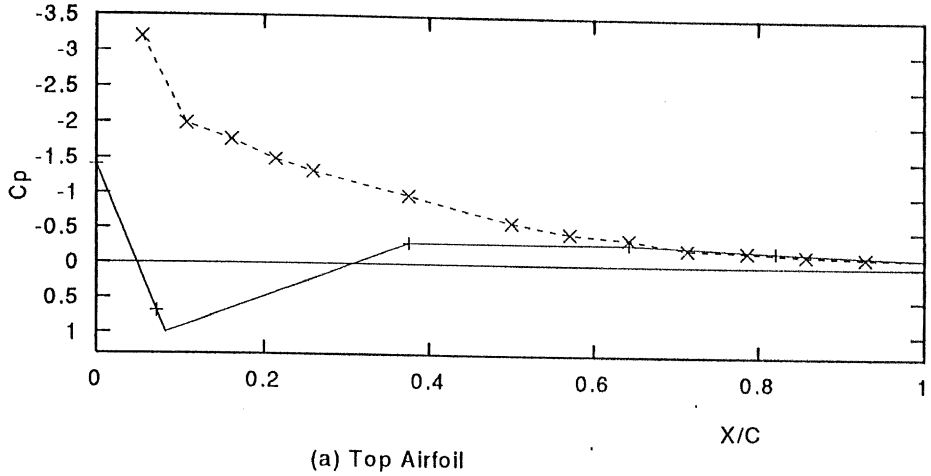

(a) Top Airfoil

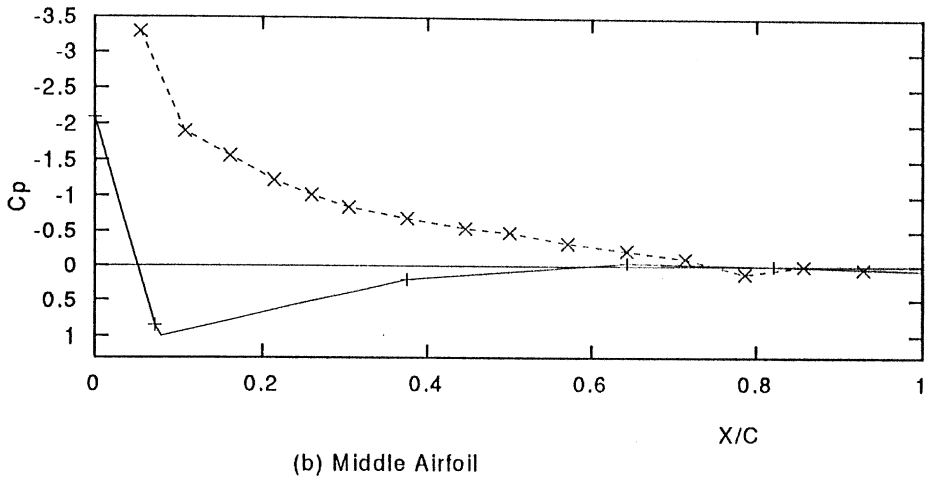

(b) Middle Airfoil

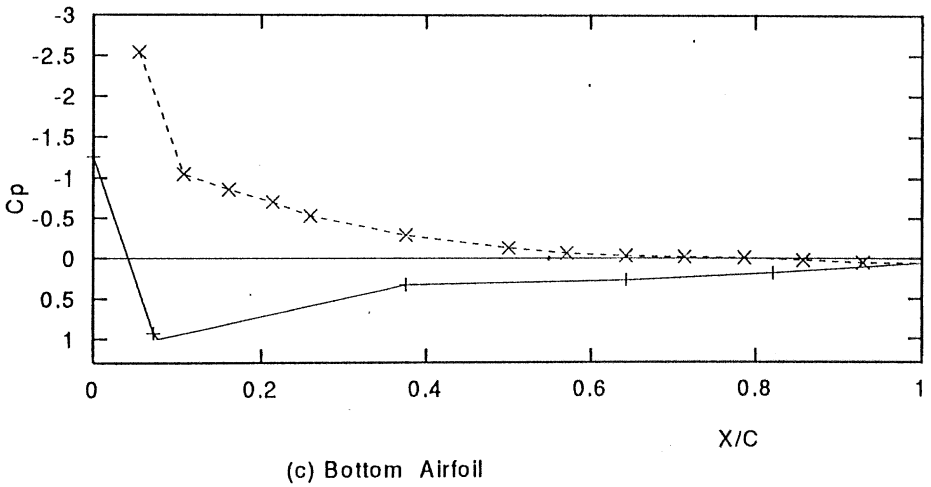

(c) Bottom Airfoil

Figure 4.32: Pressure Distribution of Airfoil; S/C = 0.9, $\alpha = 15^o$, $V_\infty = 35$ m/s, + Lower Surface, × Upper Surface.

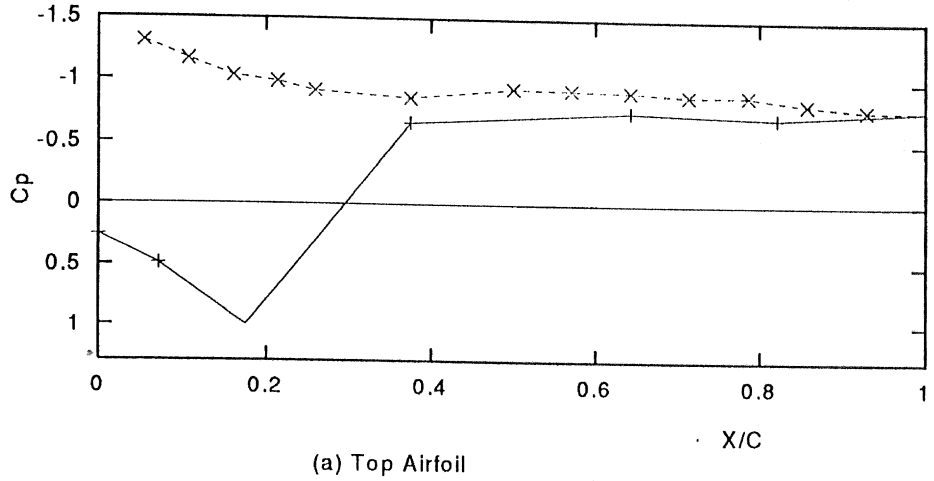

(a) Top Airfoil

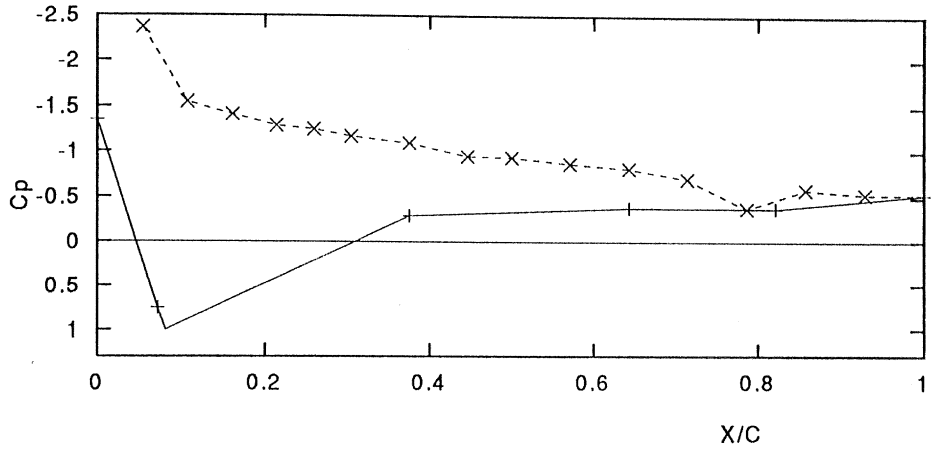

(b) Middle Airfoil

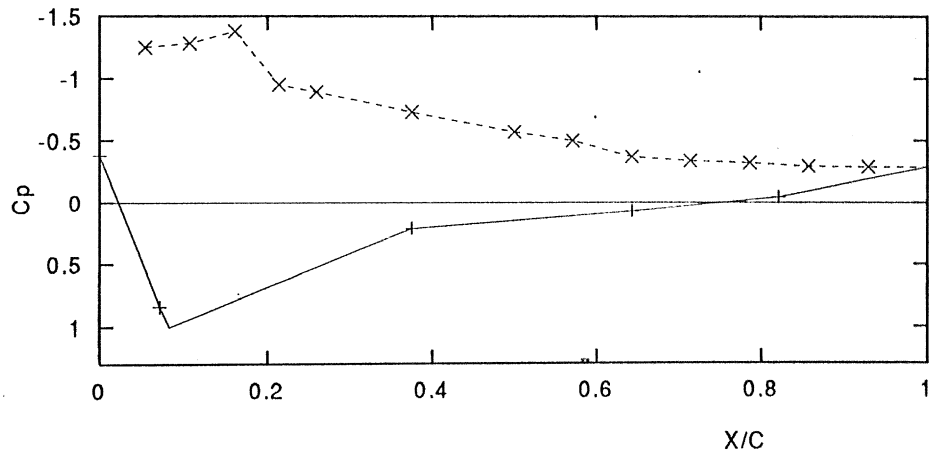

(c) Bottom Airfoil

Figure 4.33: Pressure Distribution of Airfoil; S/C = 0.9, $\alpha = 17.5°$, $V_\infty = 25$ m/s, + Lower Surface, × Upper Surface.

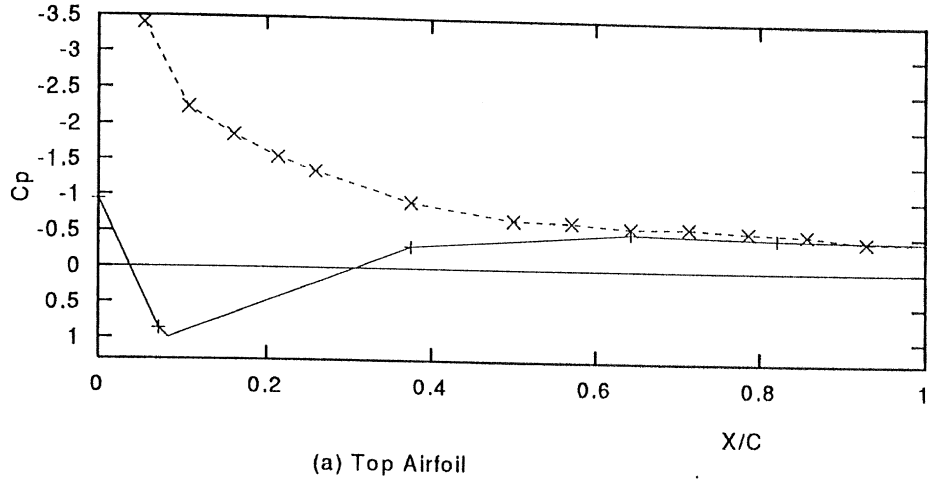

(a) Top Airfoil

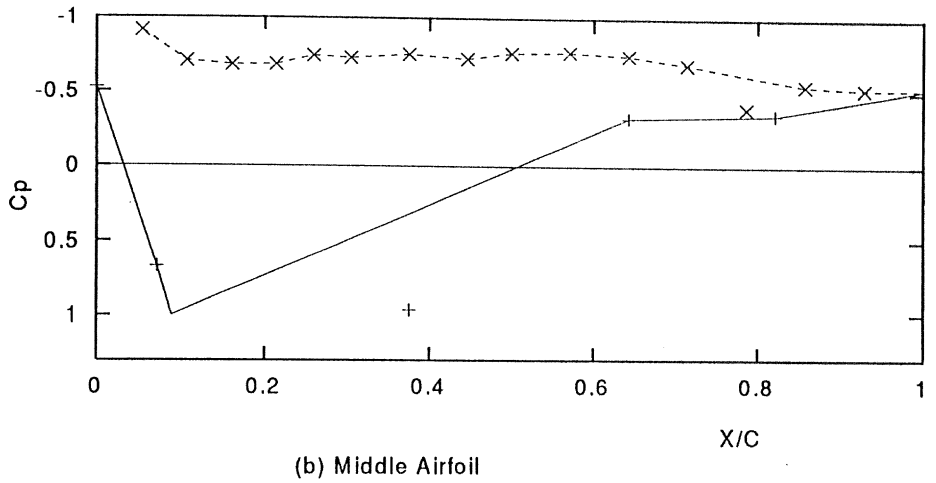

(b) Middle Airfoil

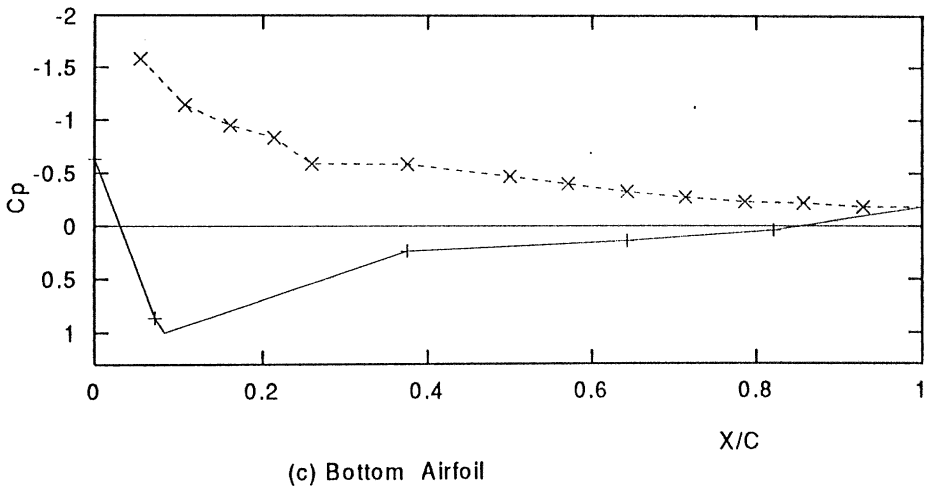

(c) Bottom Airfoil

Figure 4.34: Pressure Distribution of Airfoil; S/C = 0.9, $\alpha = 17.5^o$, $V_\infty = 35$ m/s, + Lower Surface, × Upper Surface.

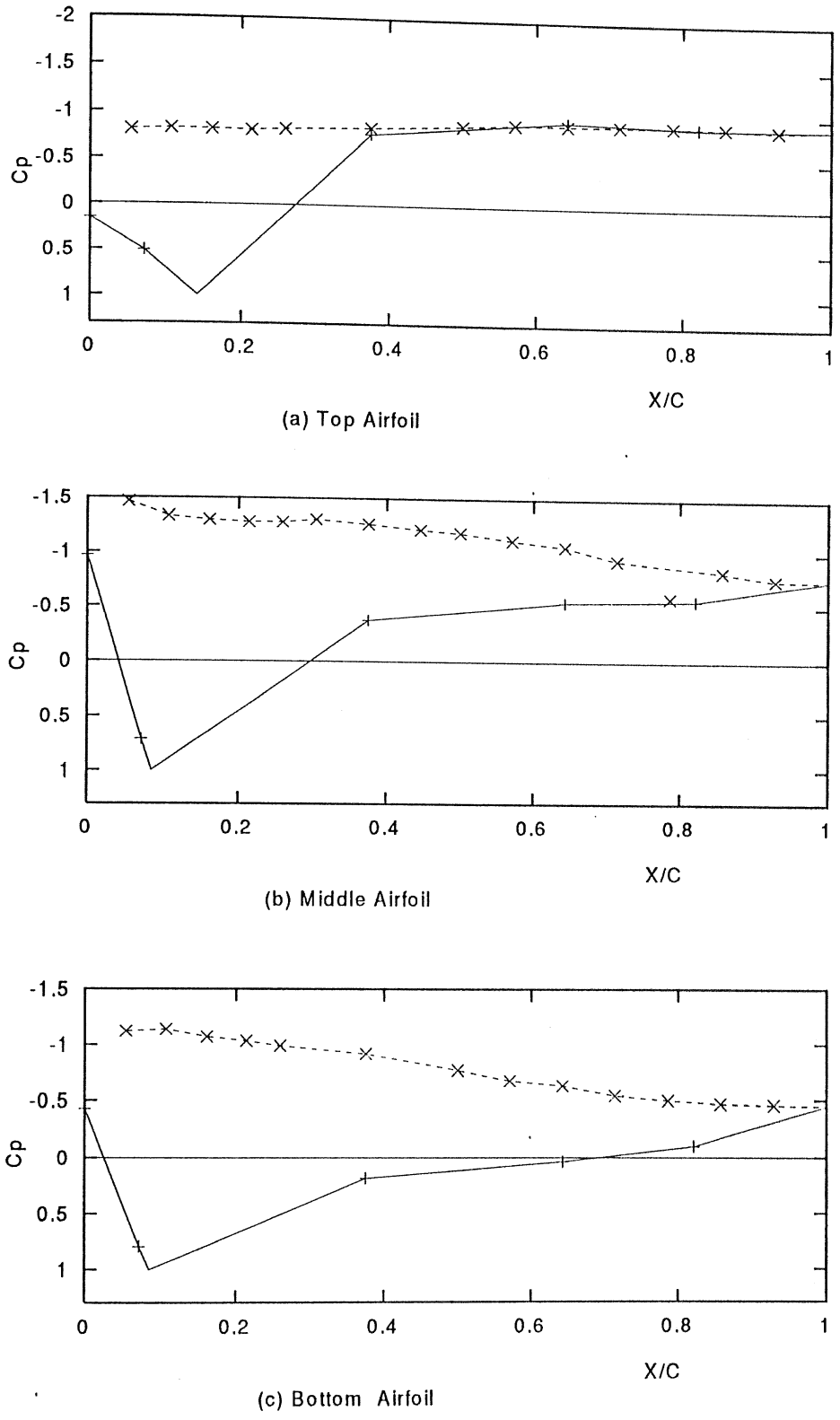

Figure 4.35: Pressure Distribution of Airfoil; S/C = 0.9, $\alpha = 20^o$, $V_\infty = 25$ m/s, + Lower Surface, × Upper Surface.

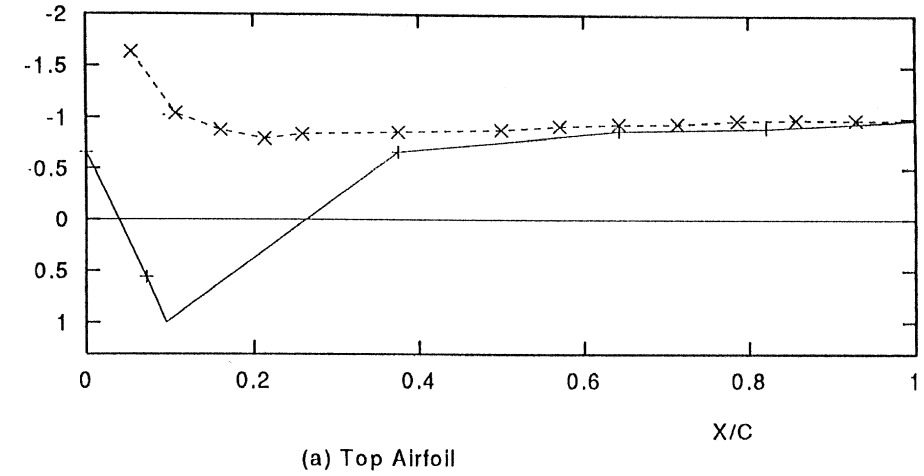

(a) Top Airfoil

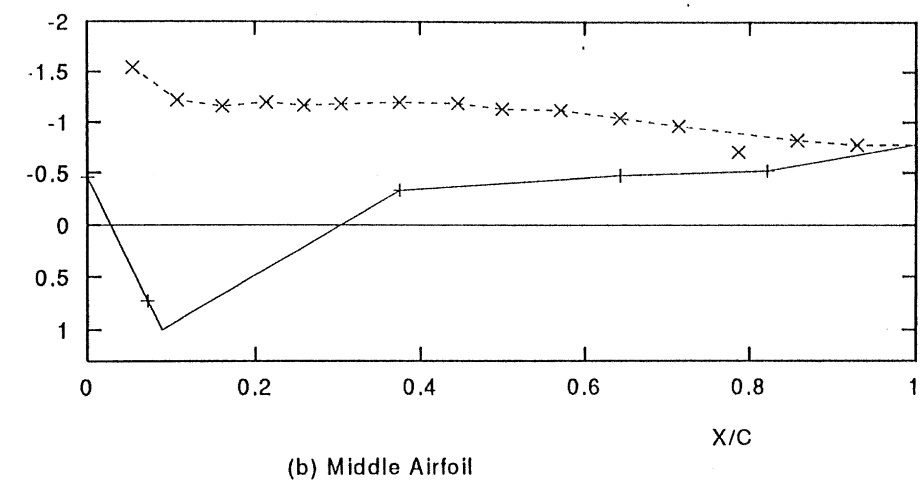

(b) Middle Airfoil

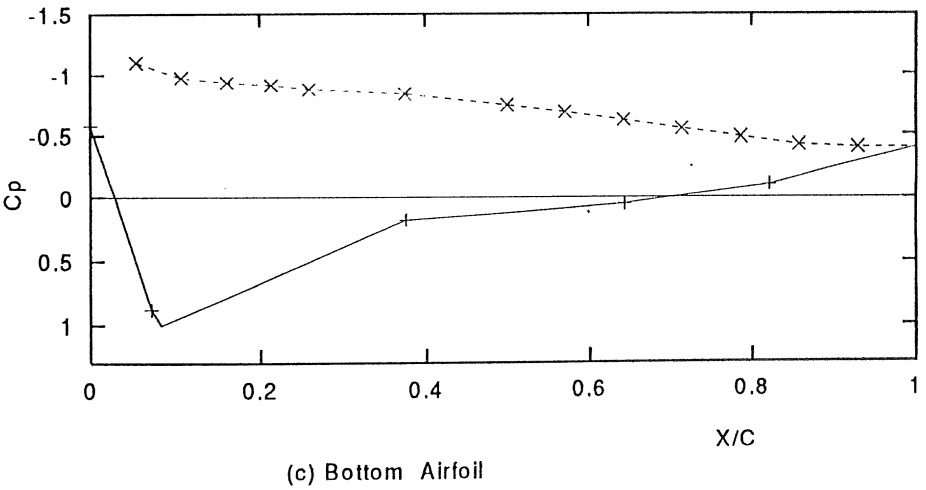

(c) Bottom Airfoil

Figure 4.36: Pressure Distribution of Airfoil; S/C = 0.9, $\alpha = 20^o$, $V_\infty = 35$ m/s, + Lower Surface, × Upper Surface.

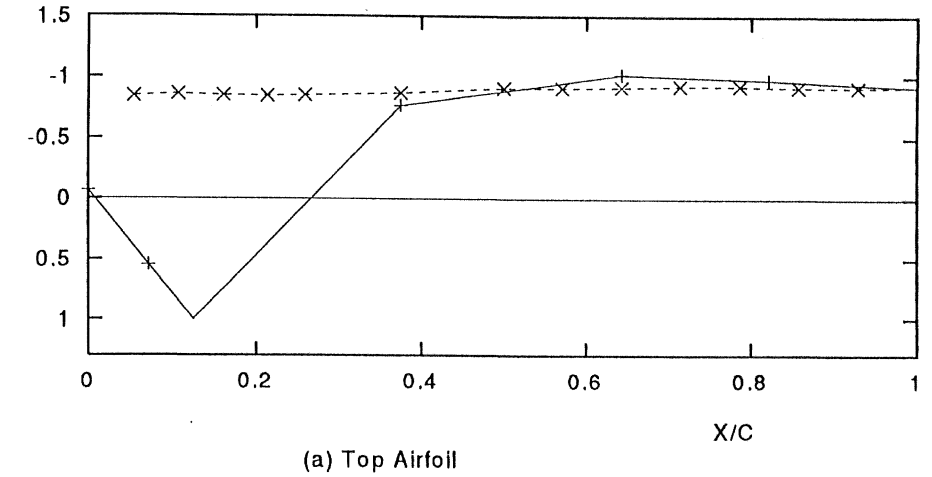

(a) Top Airfoil

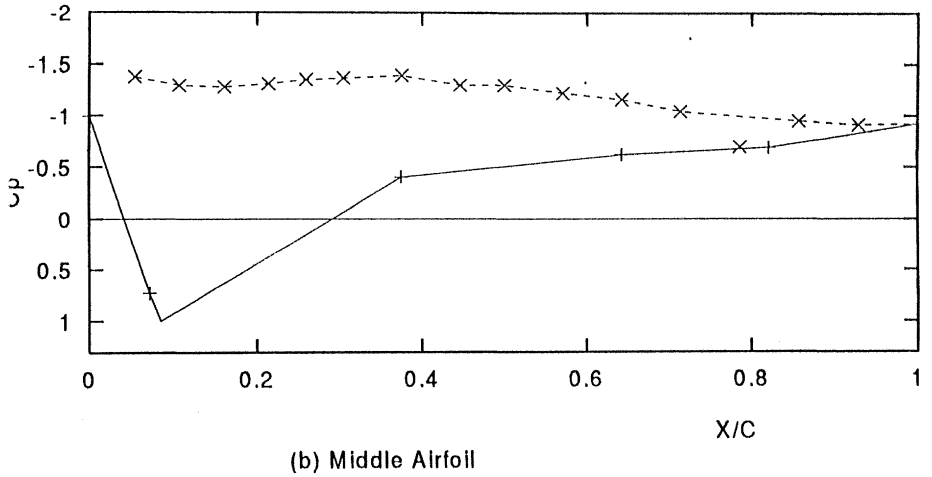

(b) Middle Airfoil

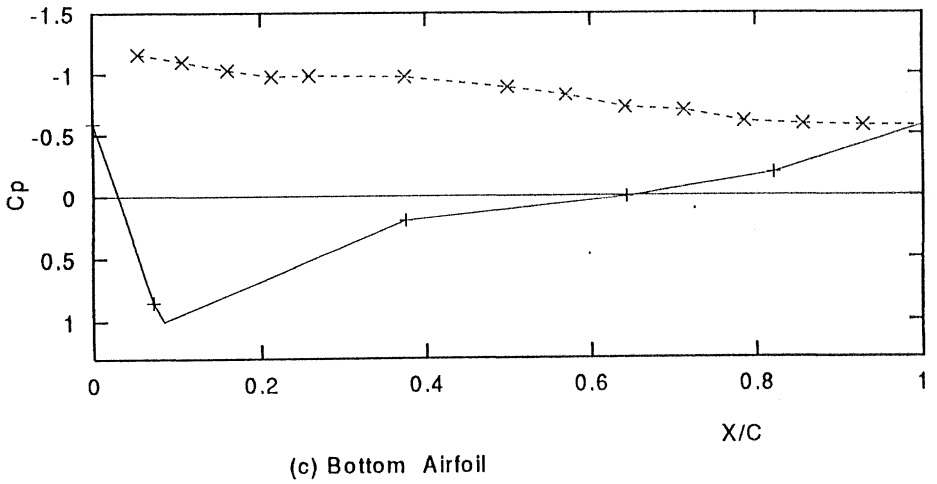

(c) Bottom Airfoil

igure 4.37: Pressure Distribution of Airfoil; S/C = 0.9, $\alpha = 22.5^o$, $V_\infty = 25$ m/s, + Lower Surface, × Upper Surface.

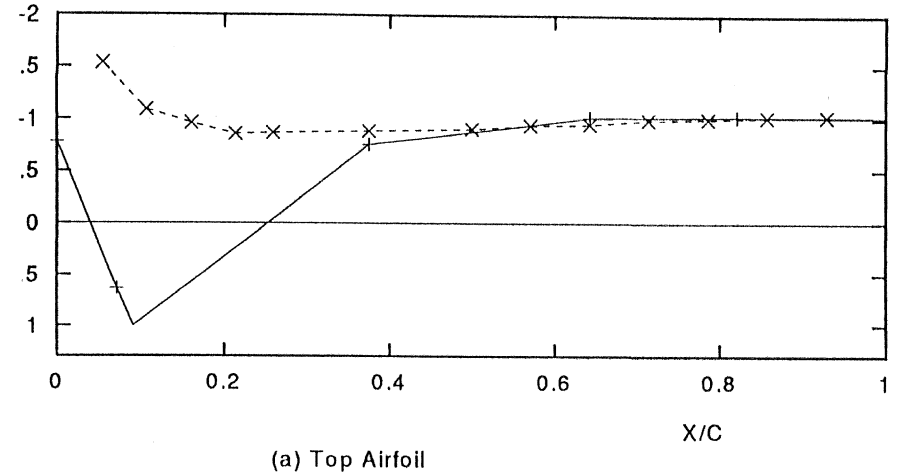

(a) Top Airfoil

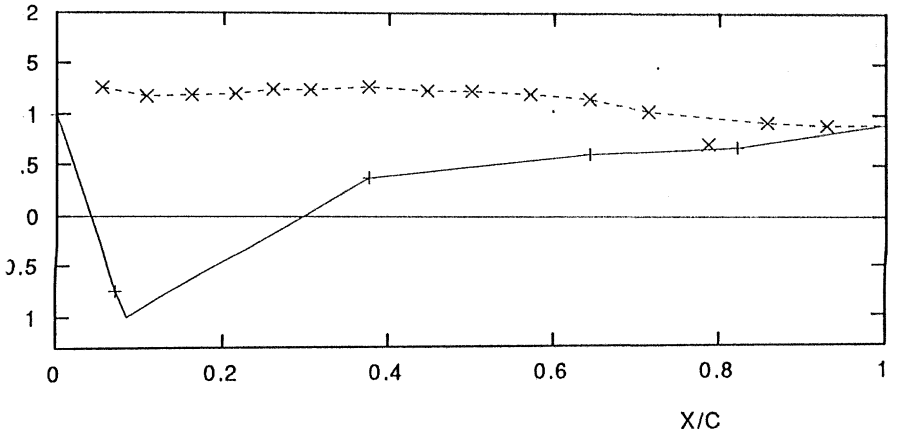

(b) Middle Airfoil

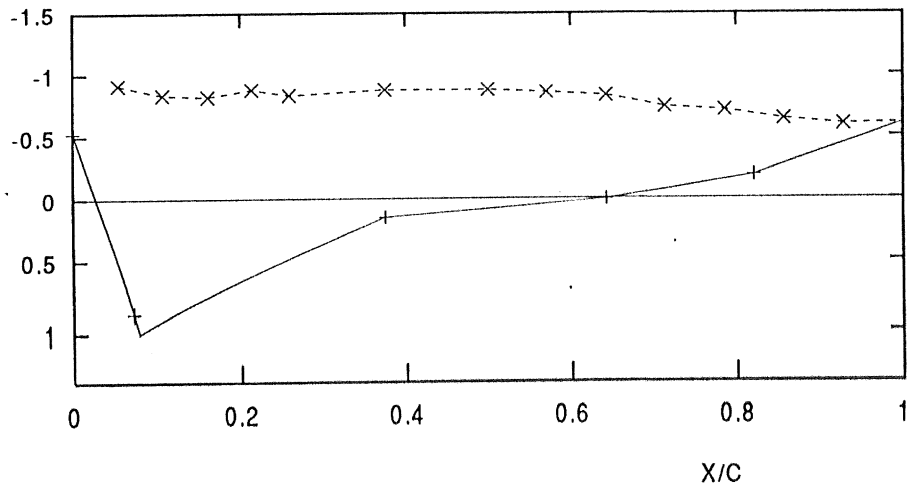

(c) Bottom Airfoil

;ure 4.38: Pressure Distribution of Airfoil; S/C = 0.9, $\alpha = 22.5°$, $V_\infty = 35$ m/s, + Lower Surface, × Upper Surface.

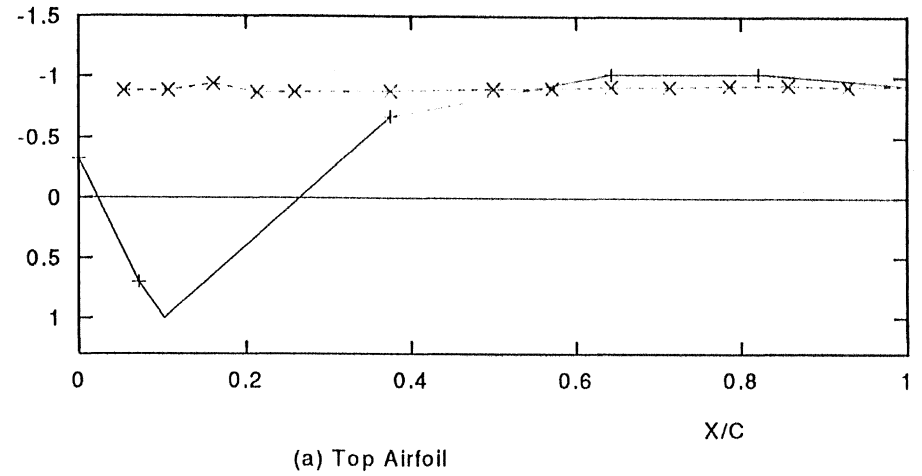

(a) Top Airfoil

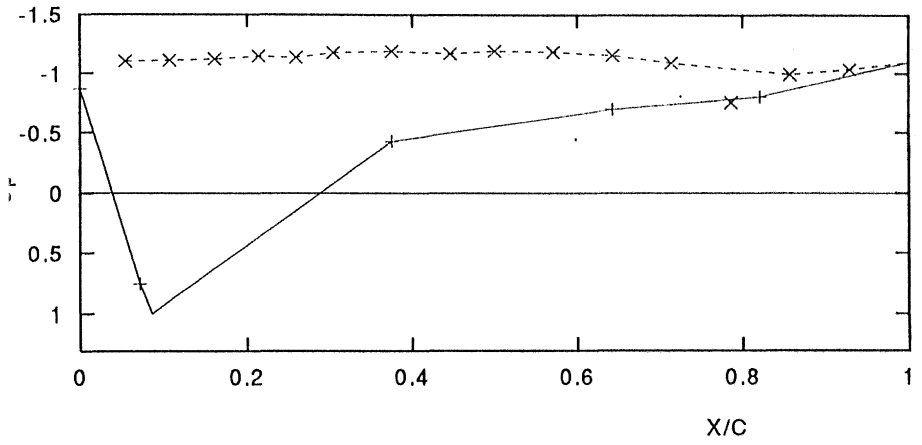

(b) Middle Airfoil

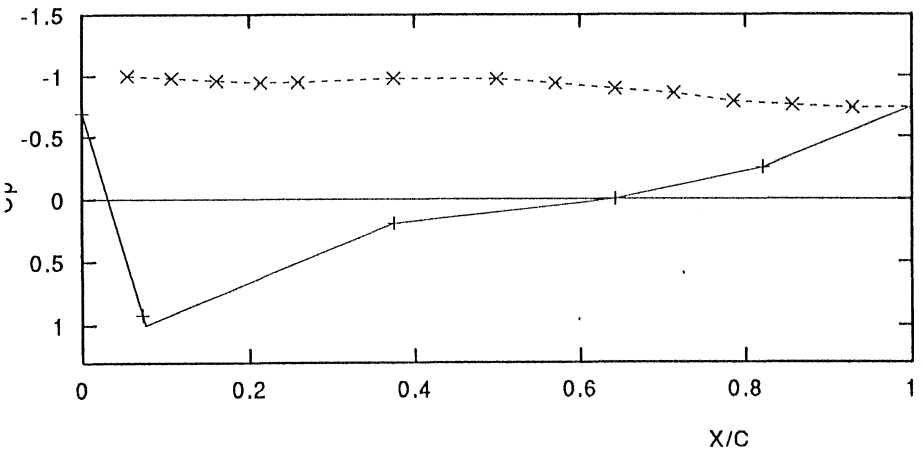

(c) Bottom Airfoil

igure 4.39: Pressure Distribution of Airfoil; S/C = 0.9, $\alpha = 25^o$, $V_\infty = 25$ m/s, -|- Lower Surface, × Upper Surface.

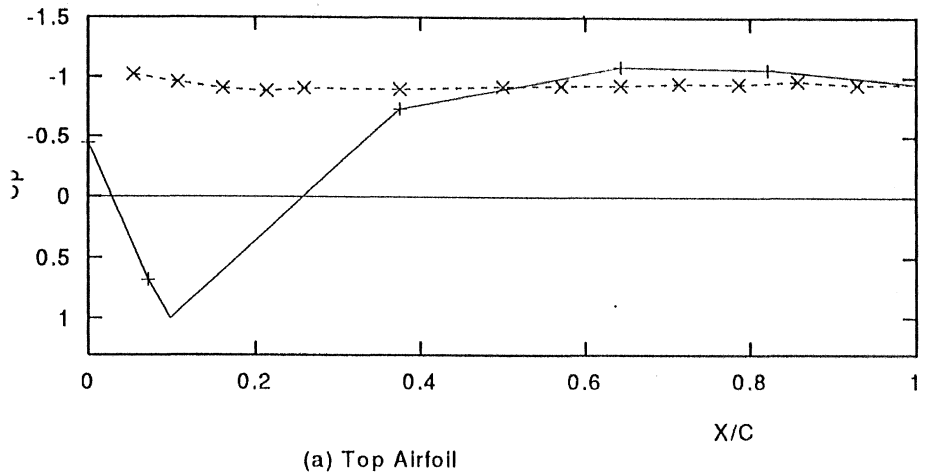

(a) Top Airfoil

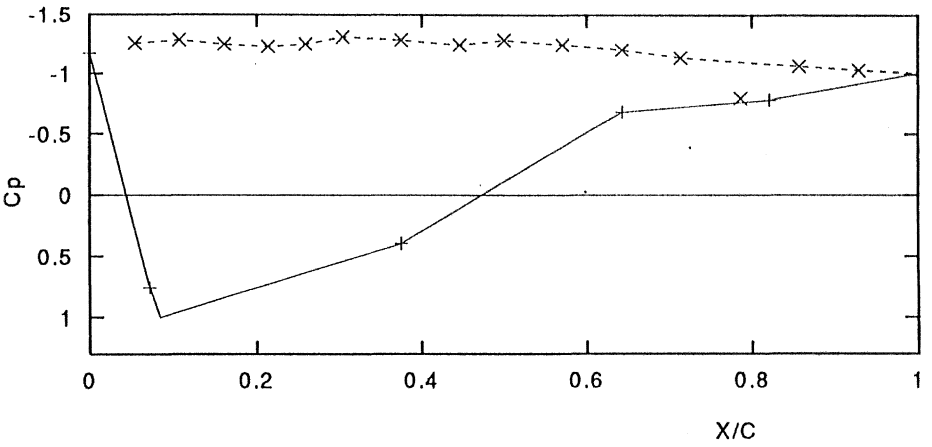

(b) Middle Airfoil

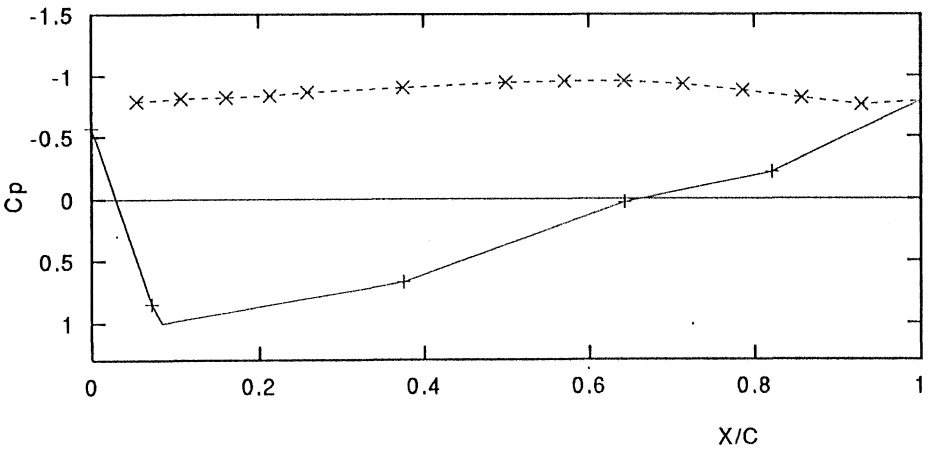

(c) Bottom Airfoil

Figure 4.40: Pressure Distribution of Airfoil; S/C = 0.9, $\alpha = 25^o$, $V_\infty = 35$ m/s, + Lower Surface, × Upper Surface.

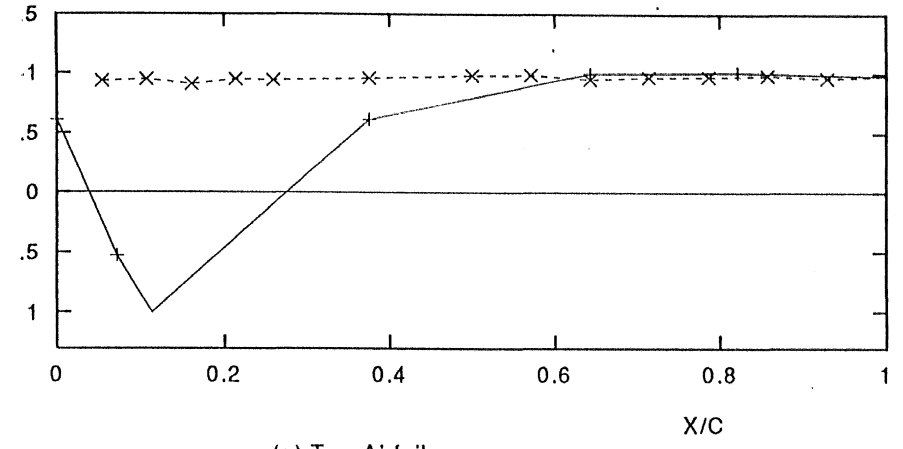

(a) Top Airfoil

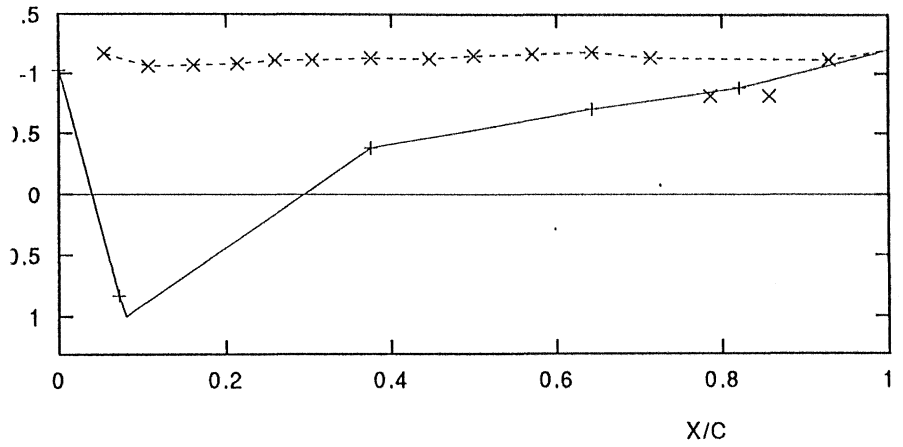

(b) Middle Airfoil

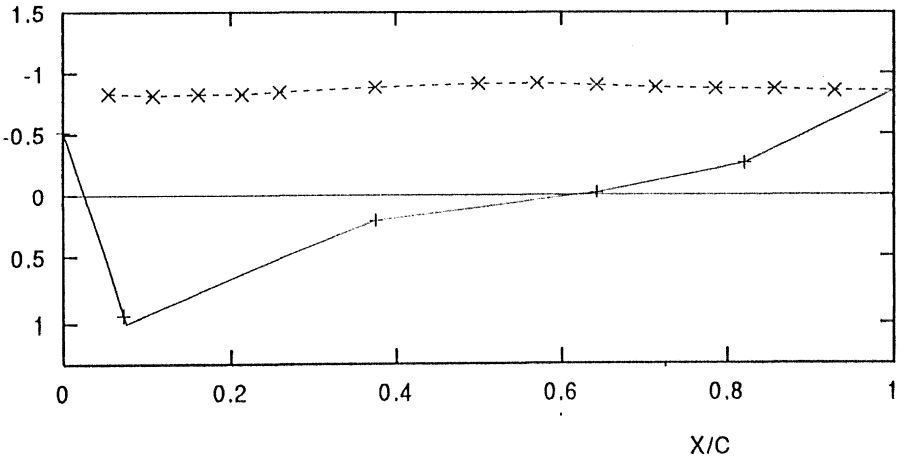

(c) Bottom Airfoil

ure 4.41: Pressure Distribution of Airfoil; S/C = 0.9, $\alpha = 27.5^o$, $V_\infty = 25$ m/s, + Lower Surface, × Upper Surface.

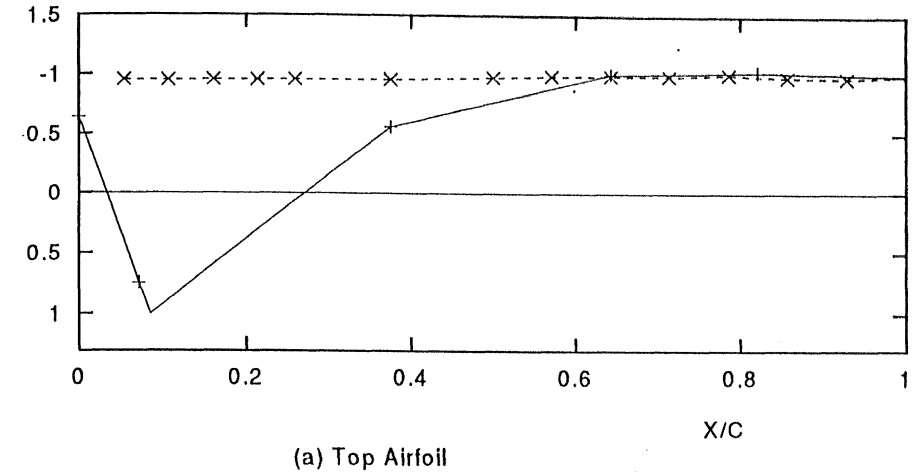

(a) Top Airfoil

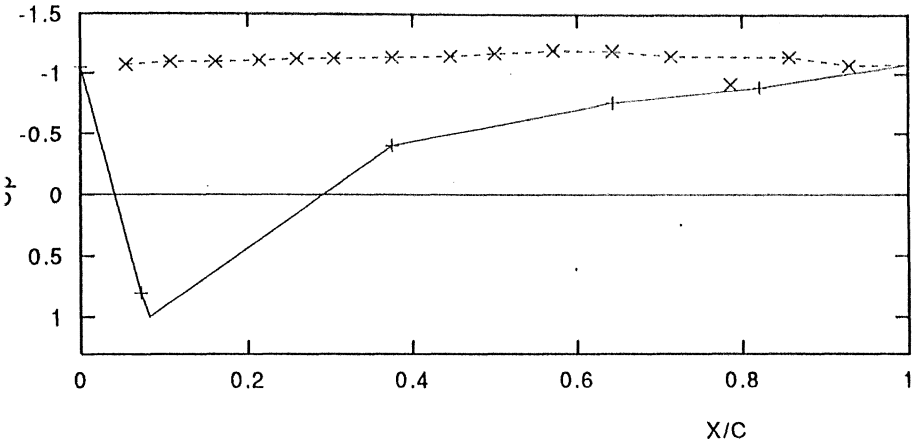

(b) Middle Airfoil

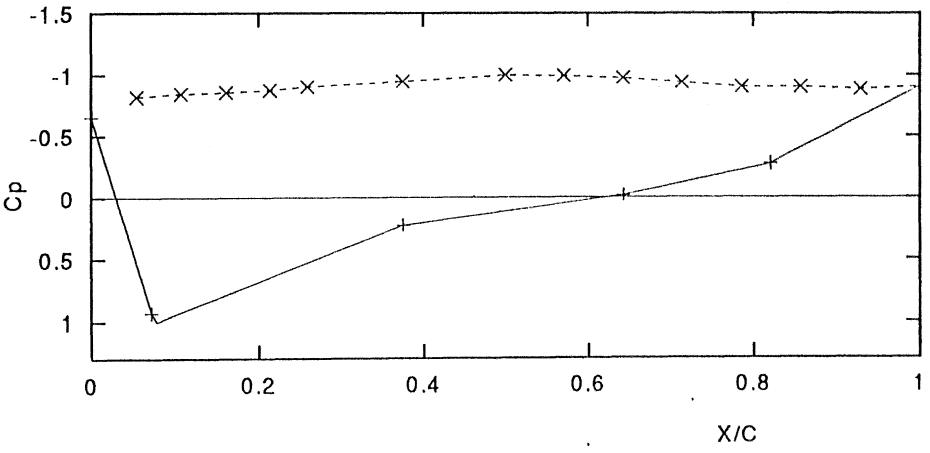

(c) Bottom Airfoil

'igure 4.42: Pressure Distribution of Airfoil; S/C = 0.9, $\alpha = 27.5^{o}$, $V_{\infty} = 35$ m/s, + Lower Surface, × Upper Surface.

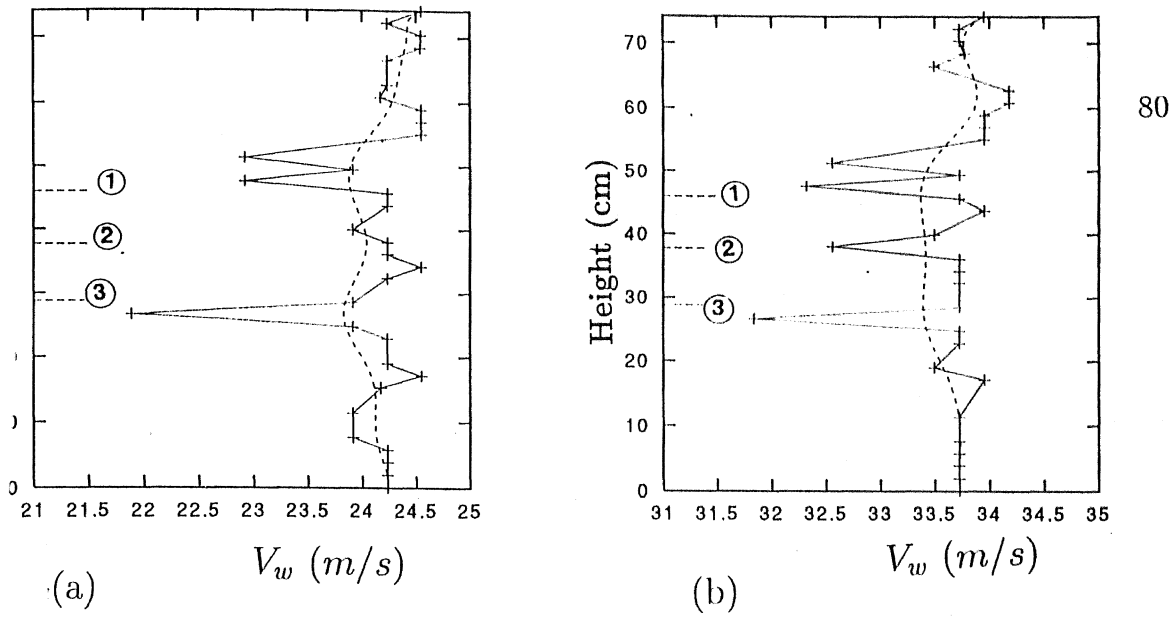

Figure 4.43 Velocity Profile from Wake Measurement; S/C = 0.5, $\alpha = 0^o$, $V_\infty = 25\ m/s$, (b). $V_\infty = 35\ m/s$, + Experimental, --- Bezier Apporoximation Curve, ①Location of Top Airfoil, ②Location of Middle Airfoil, ③ Location of Bottom Airfoil.

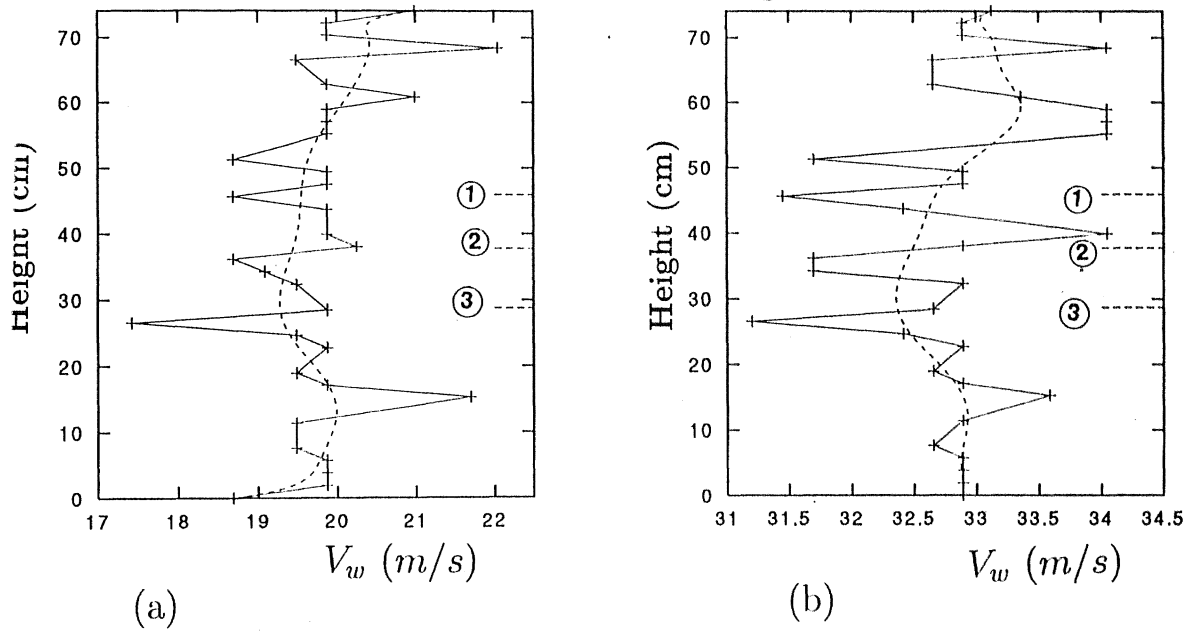

Figure 4.44 Velocity Profile from Wake Measurement; S/C = 0.5, $\alpha = 5^o$, $V_\infty = 25\ m/s$, (b). $V_\infty = 35\ m/s$, + Experimental, --- Bezier Apporoximation Curve, ①Location of Top Airfoil, ② Location of Middle Airfoil, ③ Location of Bottom Airfoil.

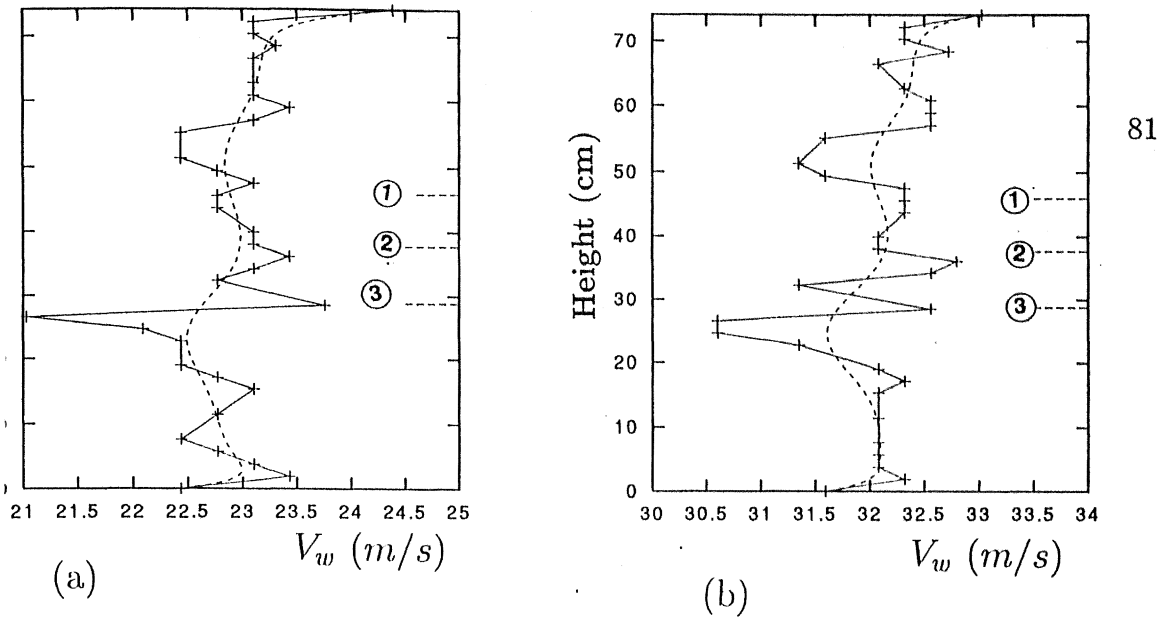

Figure 4.45 Velocity Profile from Wake Measurement; S/C = 0.5, $\alpha = 10^o$, $_\infty = 25\ m/s$, (b). $V_\infty = 35\ m/s$, + Experimental, --- Bezier Apporoximation Curve, cation of Top Airfoil, ② Location of Middle Airfoil, ③ Location of Bottom Airfoil.

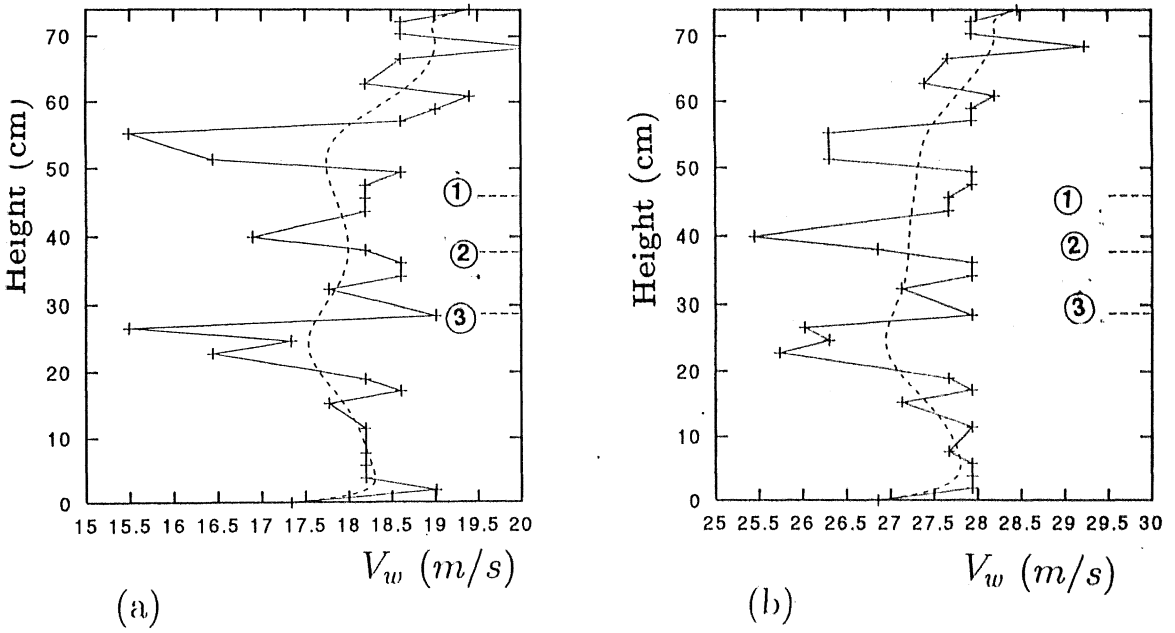

Figure 4.46 Velocity Profile from Wake Measurement; S/C = 0.5, $\alpha = 15^o$, $V_\infty = 25\ m/s$, (b). $V_\infty = 35\ m/s$, + Experimental, --- Bezier Apporoximation Curve, ocation of Top Airfoil, ② Location of Middle Airfoil, ③ Location of Bottom Airfoil.

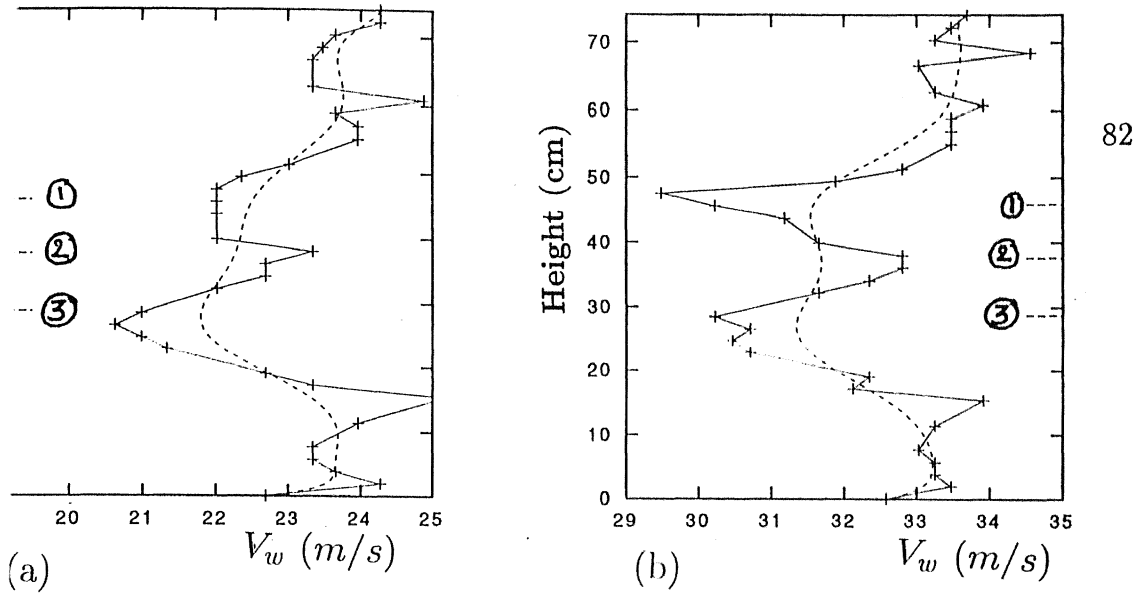

gure 4.47 Velocity Profile from Wake Measurement; S/C = 0.5, $\alpha = 17.5^o$,
= 25 m/s, (b). $V_\infty = 35$ m/s, + Experimental, ... Bezier Apporoximation Curve,
tion of Top Airfoil, ② Location of Middle Airfoil, ③ Location of Bottom Airfoil.

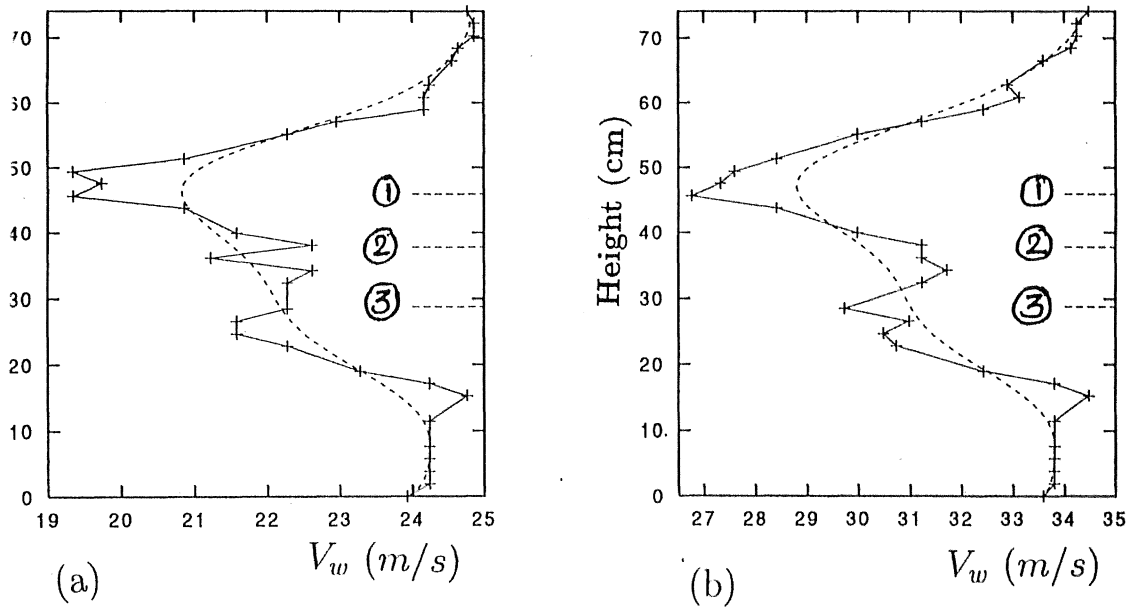

Figure 4. 48 Velocity Profile from Wake Measurement; S/C = 0.5, $\alpha = 20^o$,
= 25 m/s, (b). $V_\infty = 35$ m/s, + Experimental, ... Bezier Apporoximation Curve,
ation of Top Airfoil, ② Location of Middle Airfoil, ③ Location of Bottom Airfoil.

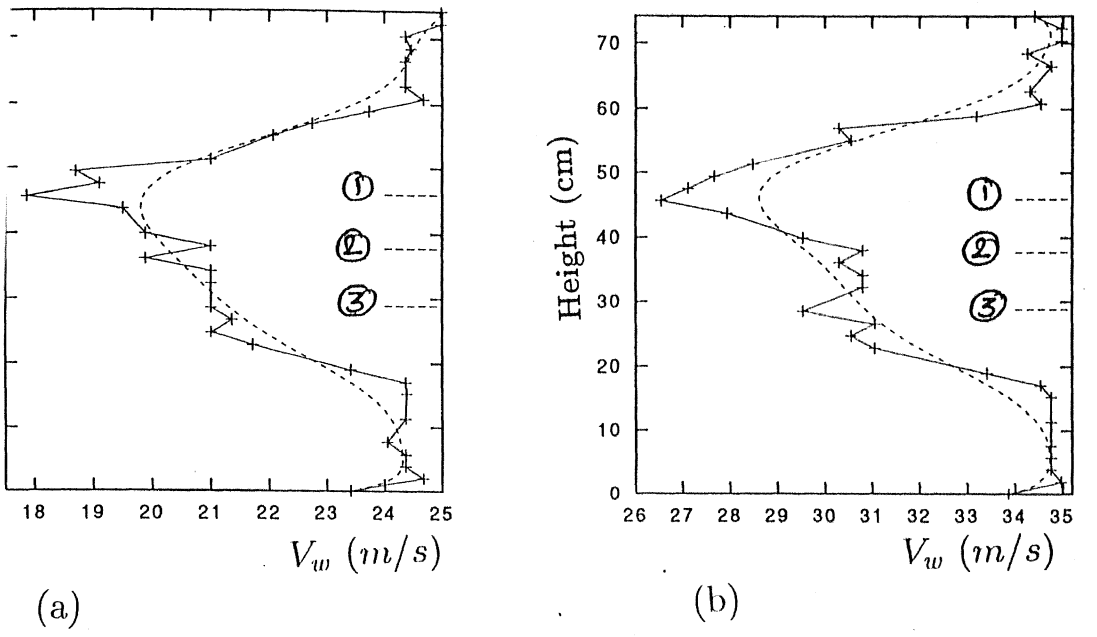

'igure 4.49 Velocity Profile from Wake Measurement; S/C = 0.5, $\alpha = 22.5^o$, , = 25 m/s, (b). $V_\infty = 35$ m/s, + Experimental, --- Bezier Apporoximation Curve, :ation of Top Airfoil, ② Location of Middle Airfoil, ③ Location of Bottom Airfoil.

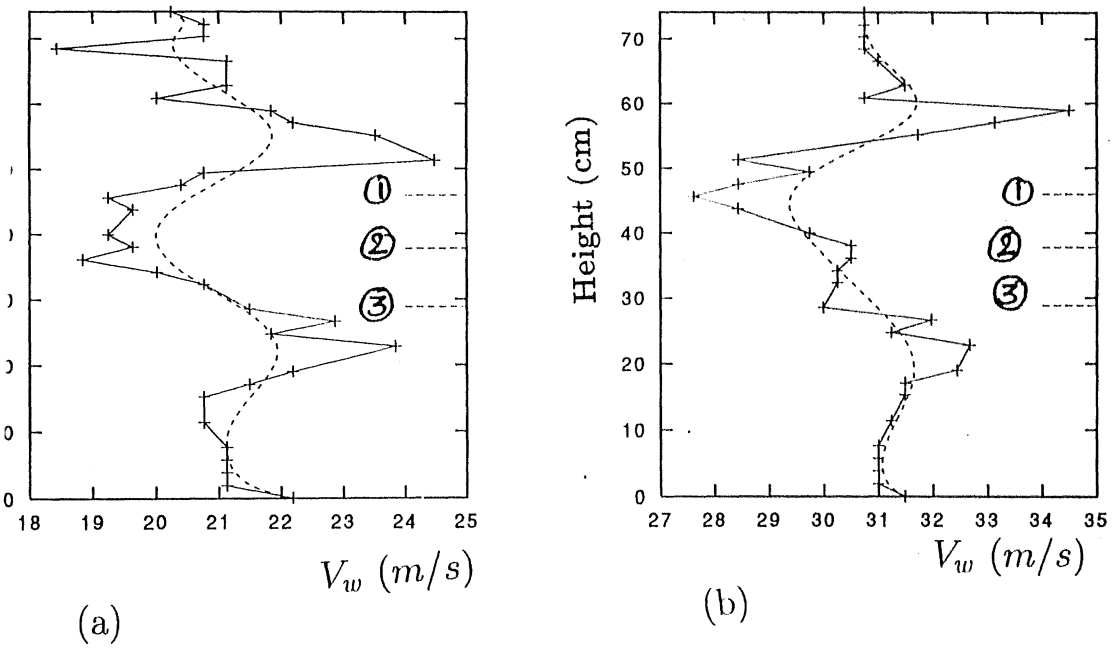

Figure 4.50 Velocity Profile from Wake Measurement; S/C = 0.5, $\alpha = 25^o$, $_\infty = 25$ m/s, (b). $V_\infty = 35$ m/s, + Experimental, --- Bezier Apporoximation Curve, ɔcation of Top Airfoil, ② Location of Middle Airfoil, ③ Location of Bottom Airfoil.

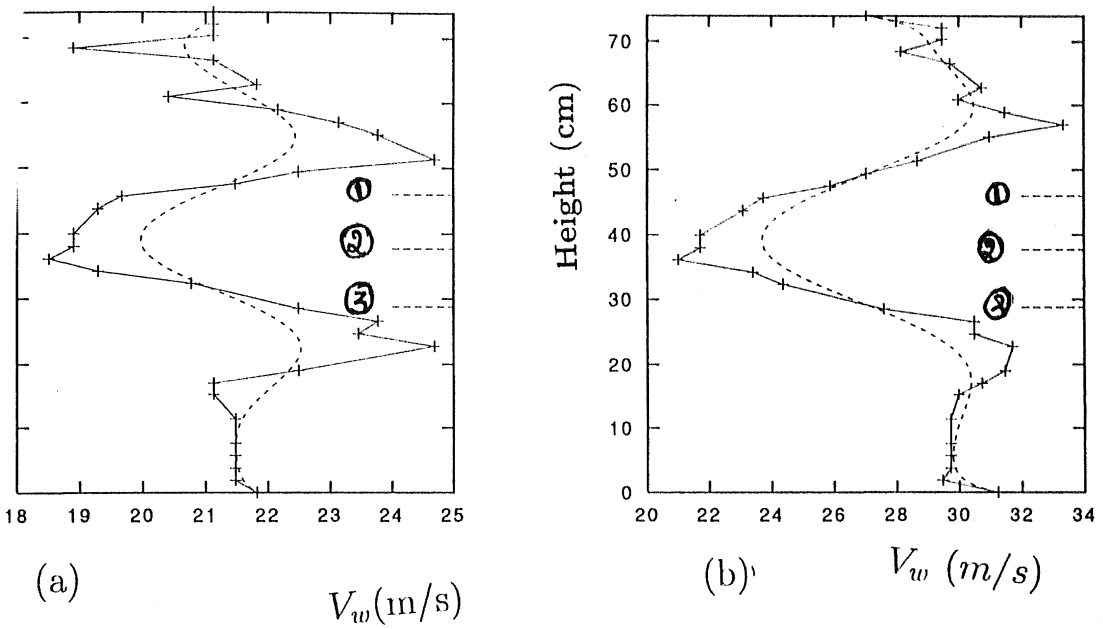

Figure 4-5 Velocity Profile from Wake Measurement; S/C = 0.5, $\alpha = 27.5°$, $_o = 25\ m/s$, (b). $V_\infty = 35\ m/s$, + Experimental, ... Bezier Apporoximation Curve, cation of Top Airfoil, ② Location of Middle Airfoil, ③ Location of Bottom Airfoil.

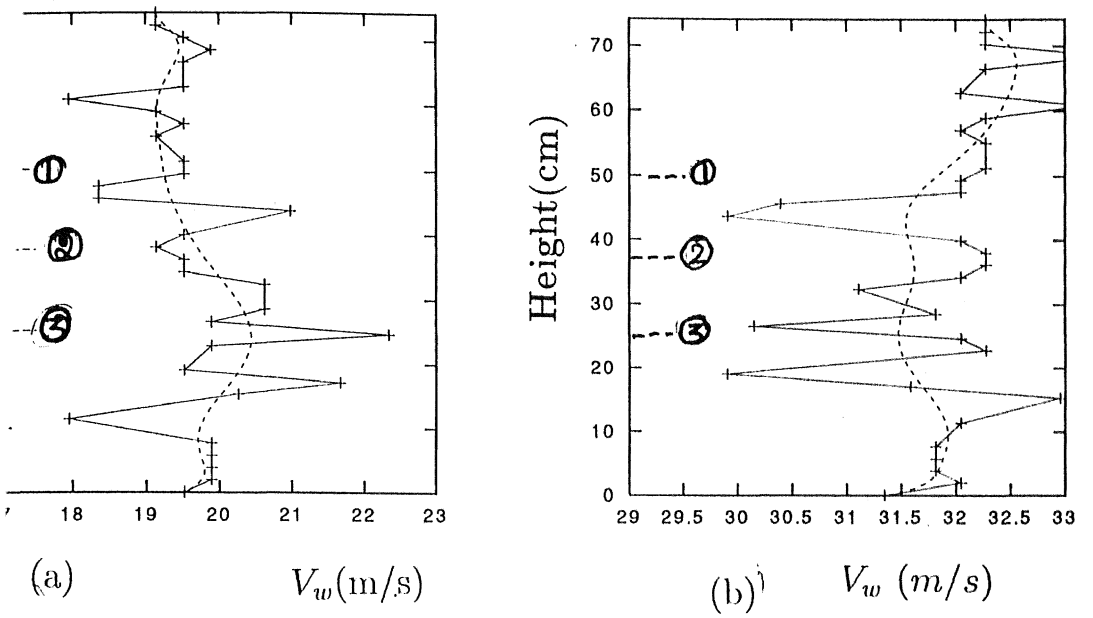

Figure 4.52: Velocity Profile from Wake Measurement; S/C = 0.7, $\alpha = 15^o$, $= 25\ m/s$, (b). $V_\infty = 35\ m/s$, + Experimental, ... Bezier Apporoximation Curve, ation of Top Airfoil, ② Location of Middle Airfoil, ③ Location of Bottom Airfoil.

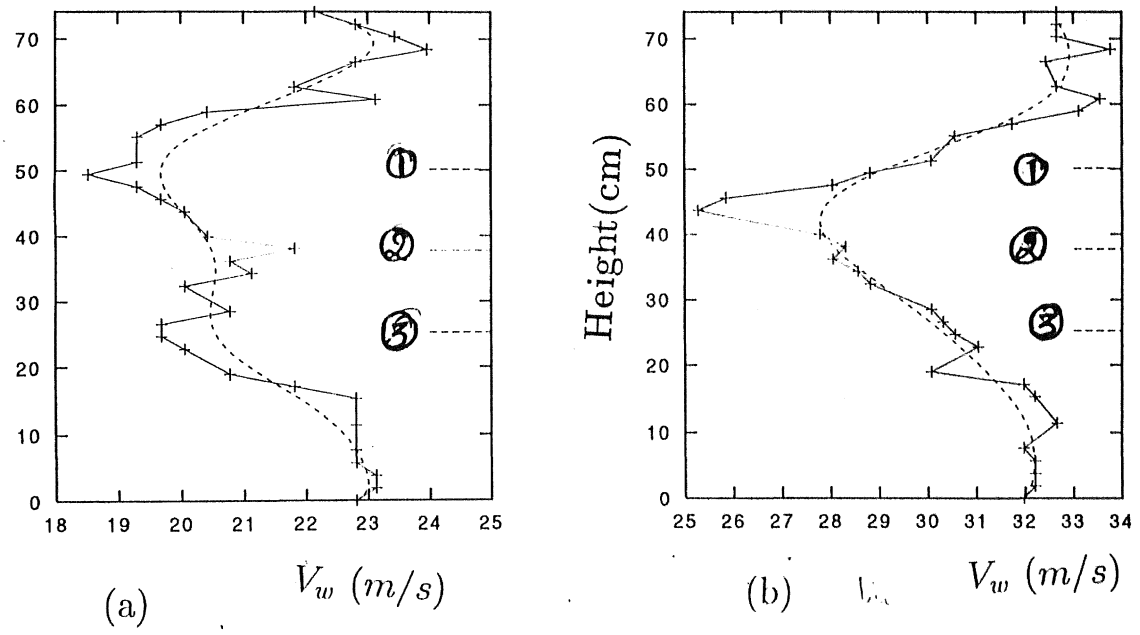

Figure 4.53: Velocity Profile from Wake Measurement; S/C = 0.7, $\alpha = 17.5^o$, $V_\infty = 25\ m/s$, (b). $V_\infty = 35\ m/s$, + Experimental, ... Bezier Apporoximation Curve, ocation of Top Airfoil, ② Location of Middle Airfoil, ③ Location of Bottom Airfoil.

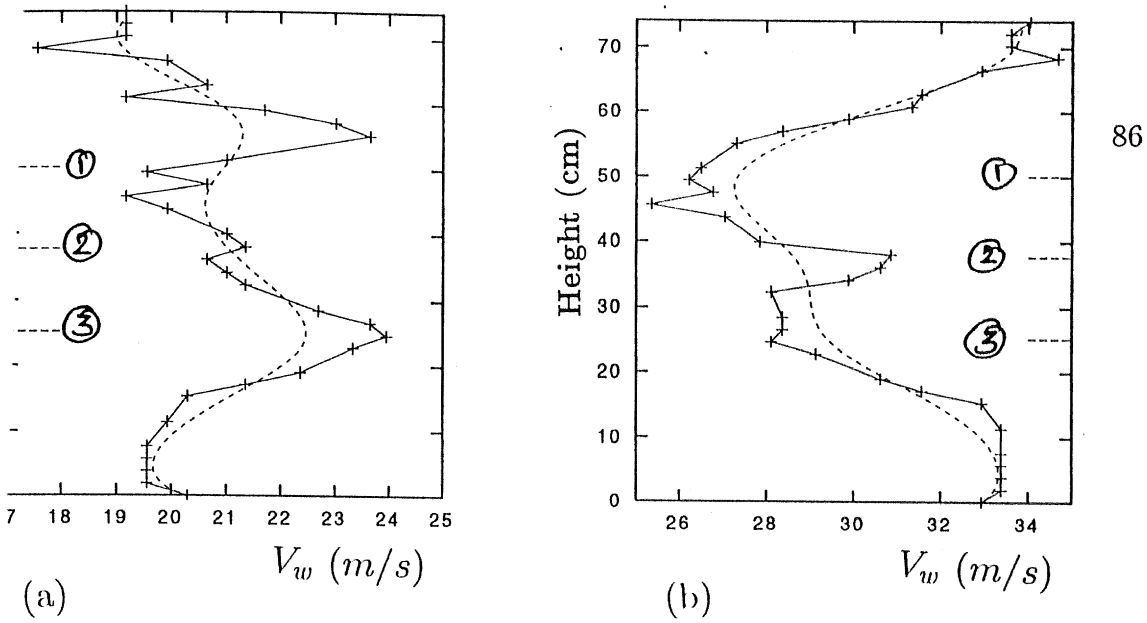

Figure 4.54: Velocity Profile from Wake Measurement; S/C = 0.7, $\alpha = 20^o$,
$= 25\ m/s$, (b). $V_\infty = 35\ m/s$, + Experimental, ... Bezier Apporoximation Curve,
ation of Top Airfoil, ② Location of Middle Airfoil, ③ Location of Bottom Airfoil.

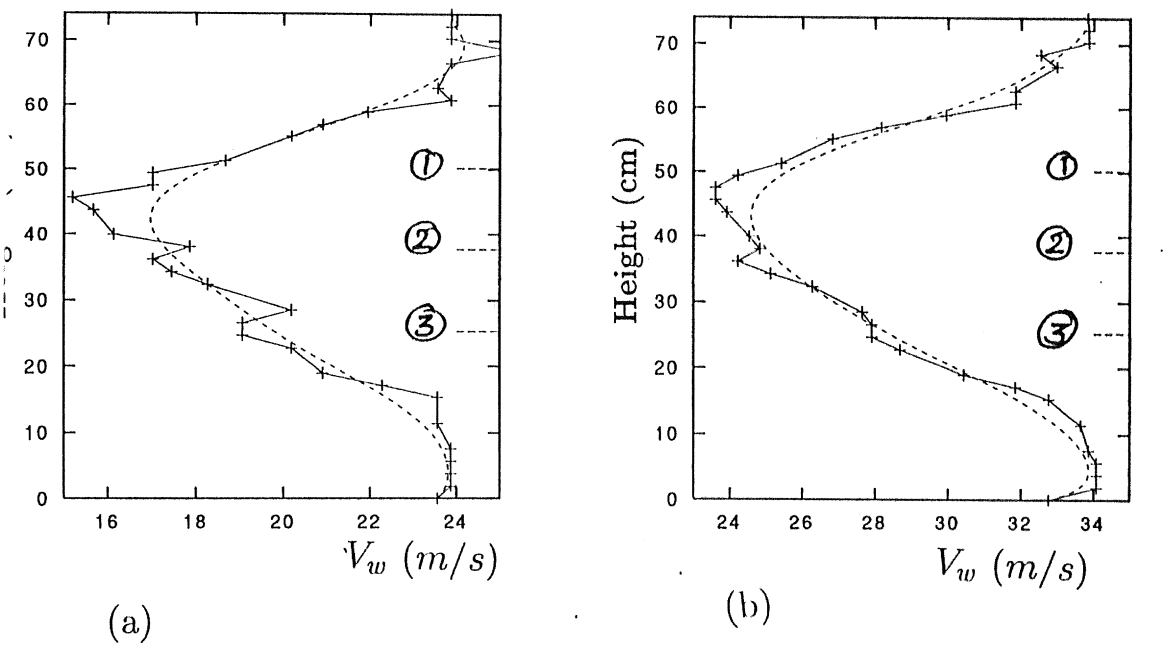

Figure 4.55: Velocity Profile from Wake Measurement; S/C = 0.7, $\alpha = 22.5^o$,
$_\infty = 25\ m/s$, (b). $V_\infty = 35\ m/s$, + Experimental, ... Bezier Apporoximation Curve,
cation of Top Airfoil, ② Location of Middle Airfoil, ③ Location of Bottom Airfoil.

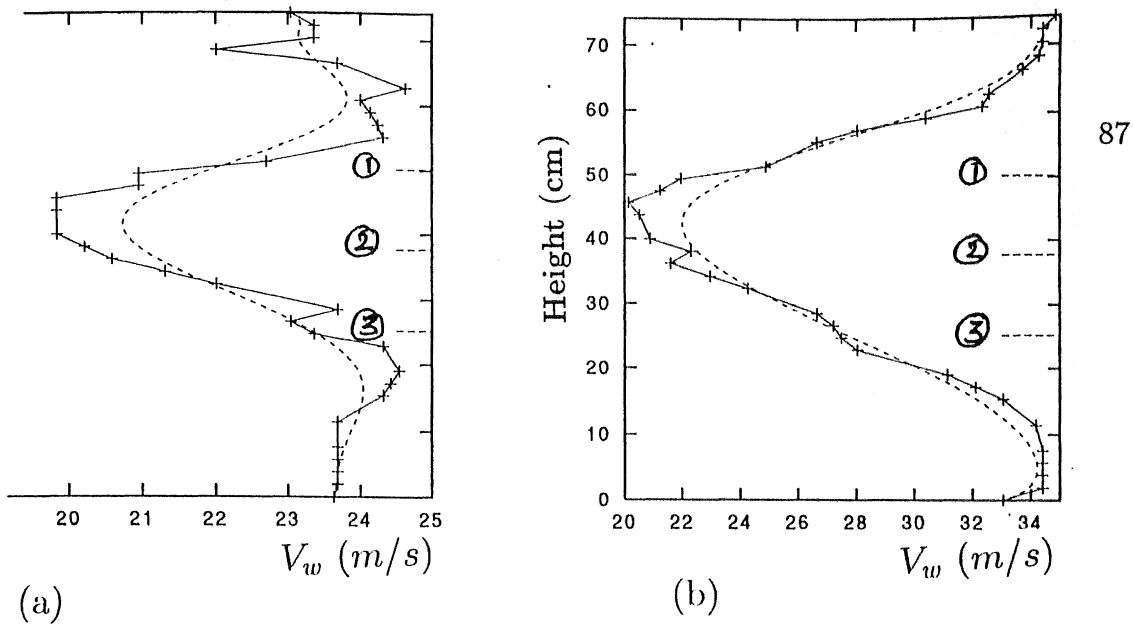

'igure 4.56: Velocity Profile from Wake Measurement; S/C = 0.7, $\alpha = 25^o$, = 25 m/s, (b). $V_\infty = 35$ m/s, + Experimental, ... Bezier Apporoximation Curve, ıtion of Top Airfoil, ② Location of Middle Airfoil, ③ Location of Bottom Airfoil.

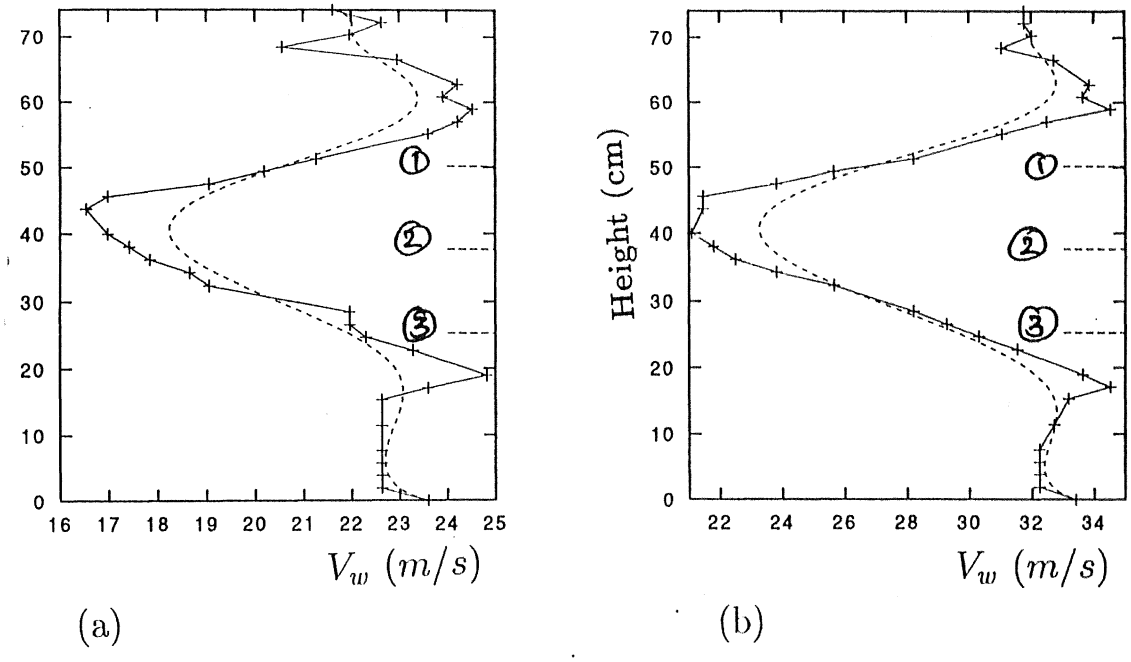

Figure 4.57: Velocity Profile from Wake Measurement; S/C = 0.7, $\alpha = 27.5^o$, $_\infty = 25$ m/s, (b). $V_\infty = 35$ m/s, + Experimental, ... Bezier Apporoximation Curve, ɔcation of Top Airfoil, ②Location of Middle Airfoil, ③Location of Bottom Airfoil.

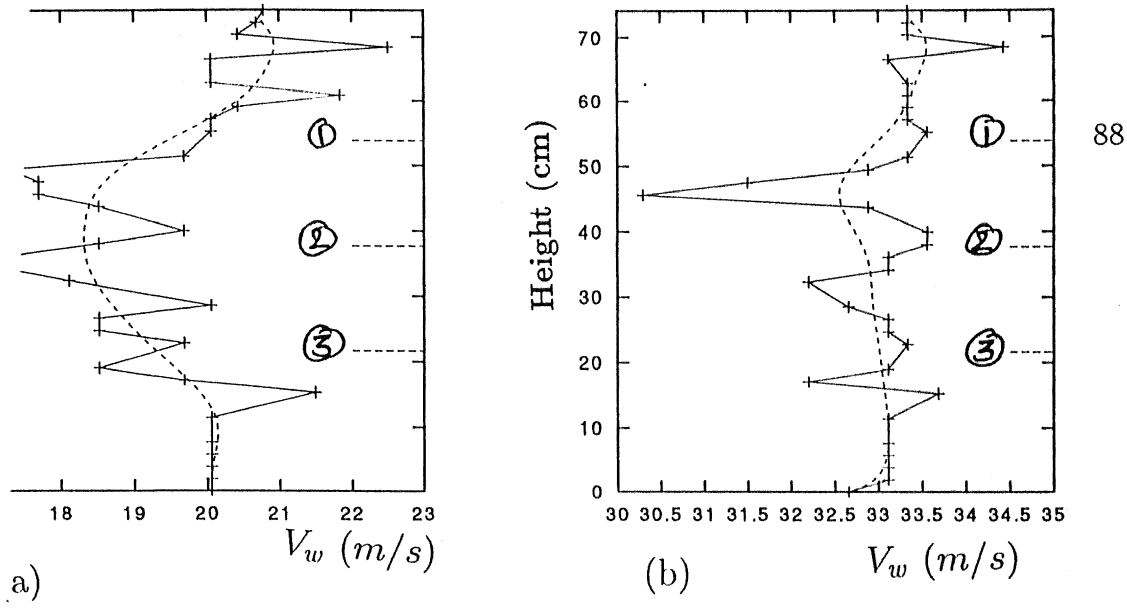

gure 4.58: Velocity Profile from Wake Measurement; S/C = 0.9, $\alpha = 15^o$,
= 25 m/s, (b). $V_\infty = 35$ m/s, + Experimental, --- Bezier Apporoximation Curve,
tion of Top Airfoil, ② Location of Middle Airfoil, ③ Location of Bottom Airfoil.

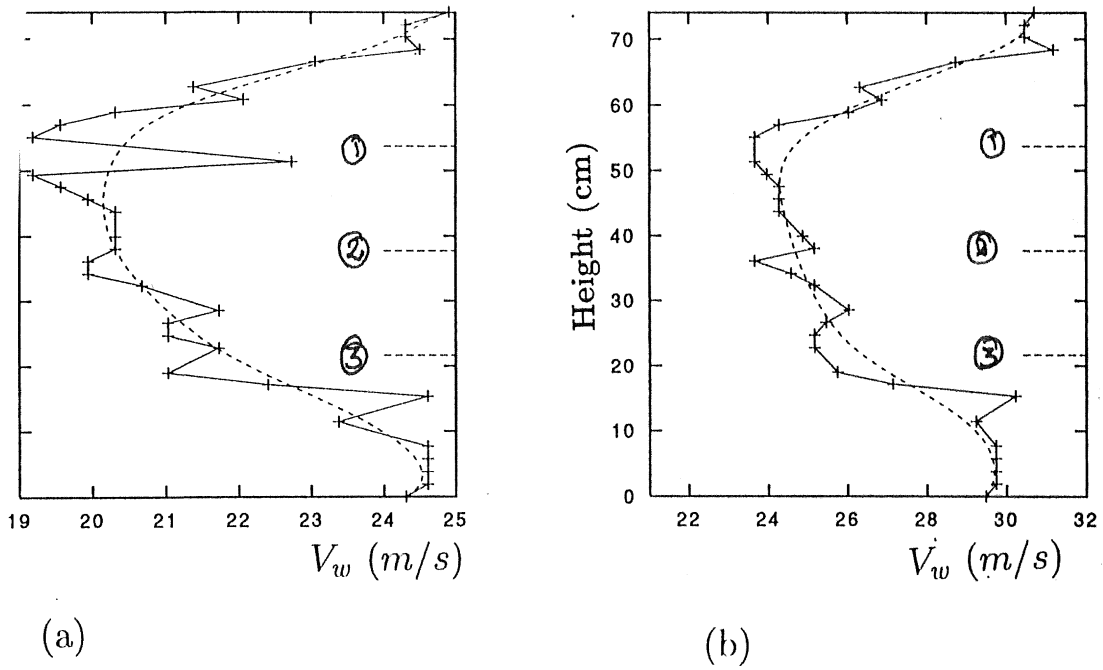

Figure 4.59: Velocity Profile from Wake Measurement; S/C = 0.9, $\alpha = 17.5^o$,
$_\infty = 25$ m/s, (b). $V_\infty = 35$ m/s, + Experimental, --- Bezier Apporoximation Curve,
)cation of Top Airfoil, ② Location of Middle Airfoil, ③ Location of Bottom Airfoil.

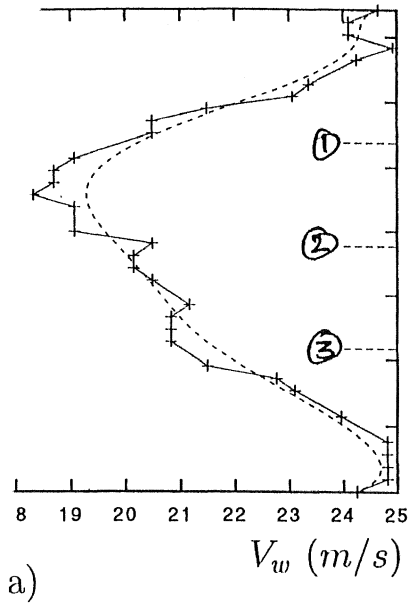

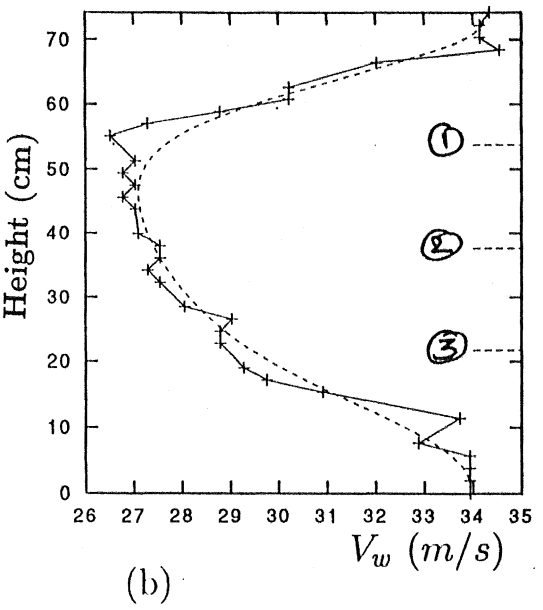

ıre 4.60: Velocity Profile from Wake Measurement; S/C = 0.9, $\alpha = 20^o$, 25 m/s, (b). $V_\infty = 35$ m/s, + Experimental, --- Bezier Apporoximation Curve, ɔn of Top Airfoil, ② Location of Middle Airfoil, ③ Location of Bottom Airfoil.

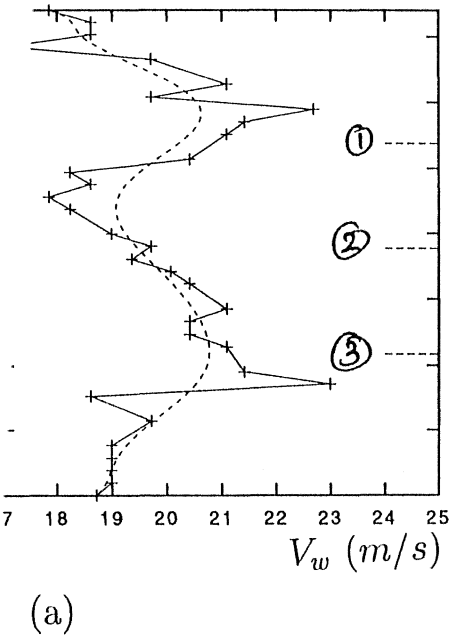

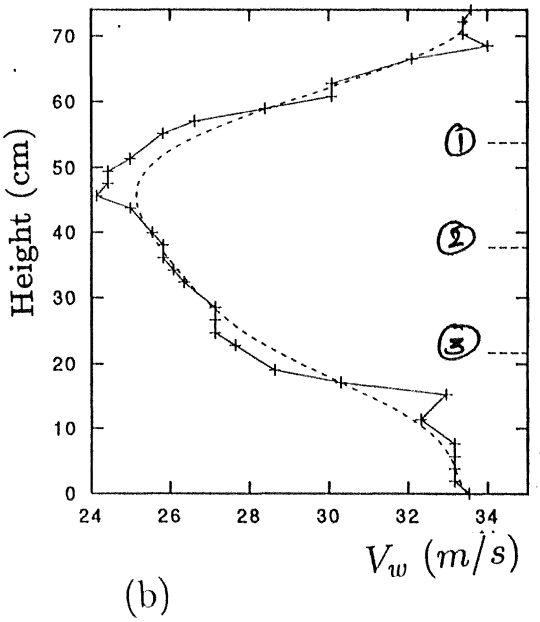

Figure 4.61: Velocity Profile from Wake Measurement; S/C = 0.9, $\alpha = 22.5^o$, $_\circ = 25$ m/s, (b). $V_\infty = 35$ m/s, + Experimental, --- Bezier Apporoximation Curve, cation of Top Airfoil, ② Location of Middle Airfoil, ③ Location of Bottom Airfoil.

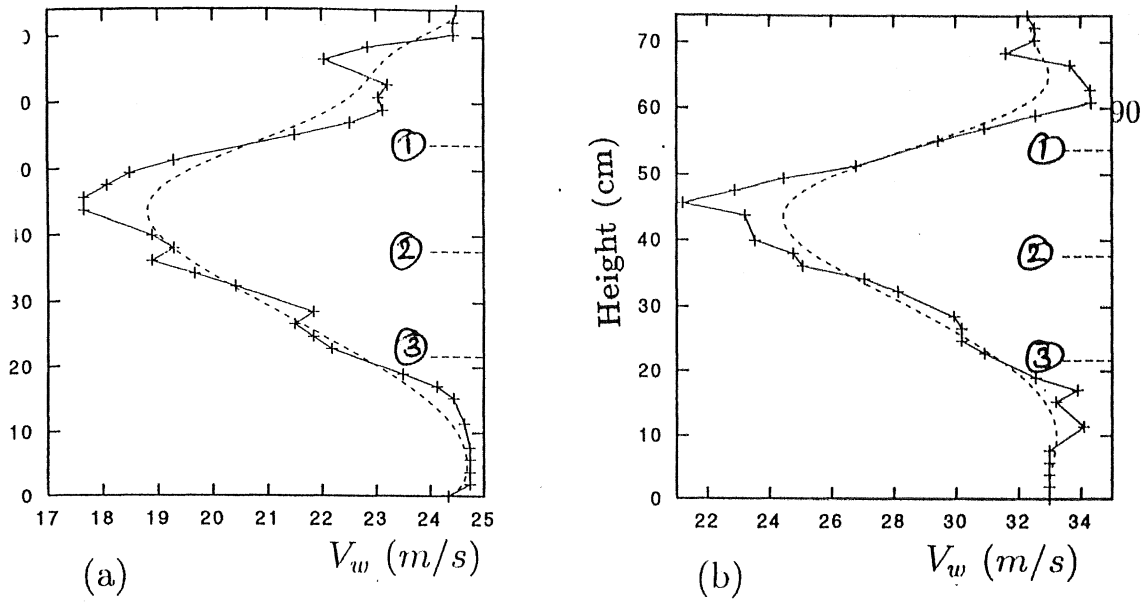

Figure 4.62: Velocity Profile from Wake Measurement; S/C = 0.9, $\alpha = 25^o$, $= 25\ m/s$, (b). $V_\infty = 35\ m/s$, + Experimental, ... Bezier Apporoximation Curve, ation of Top Airfoil, ② Location of Middle Airfoil, ③ Location of Bottom Airfoil.

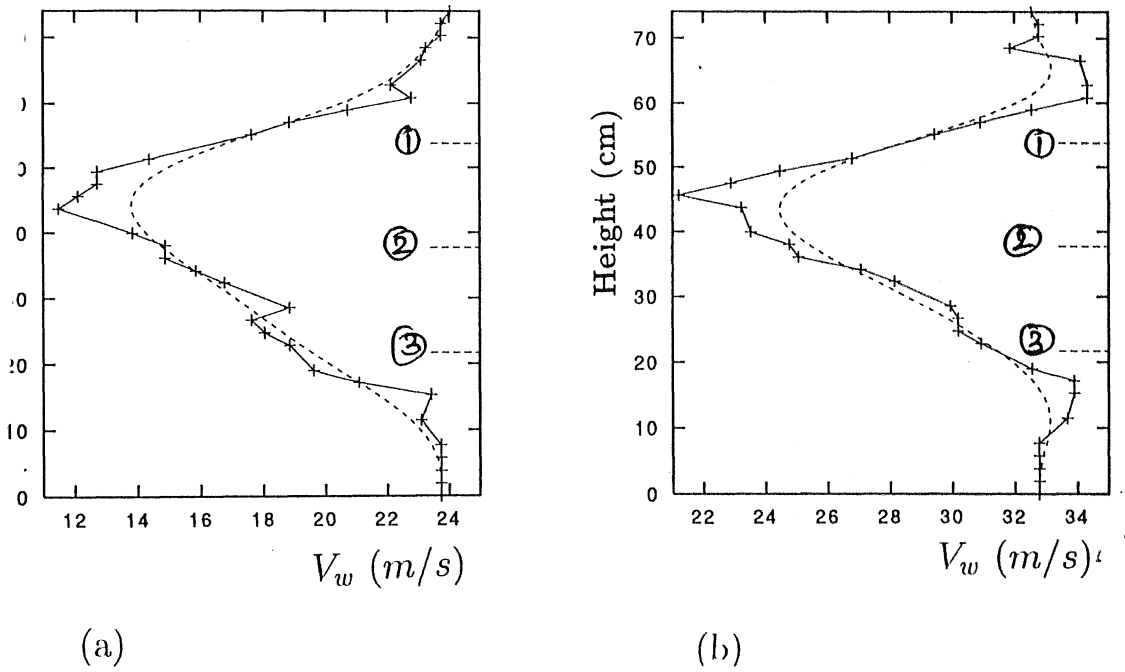

Figure 4.63: Velocity Profile from Wake Measurement; S/C = 0.9, $\alpha = 27.5^o$, $V_\infty = 25\ m/s$, (b). $V_\infty = 35\ m/s$, + Experimental, ... Bezier Apporoximation Curve, Location of Top Airfoil, ② Location of Middle Airfoil, ③ Location of Bottom Airfoil.

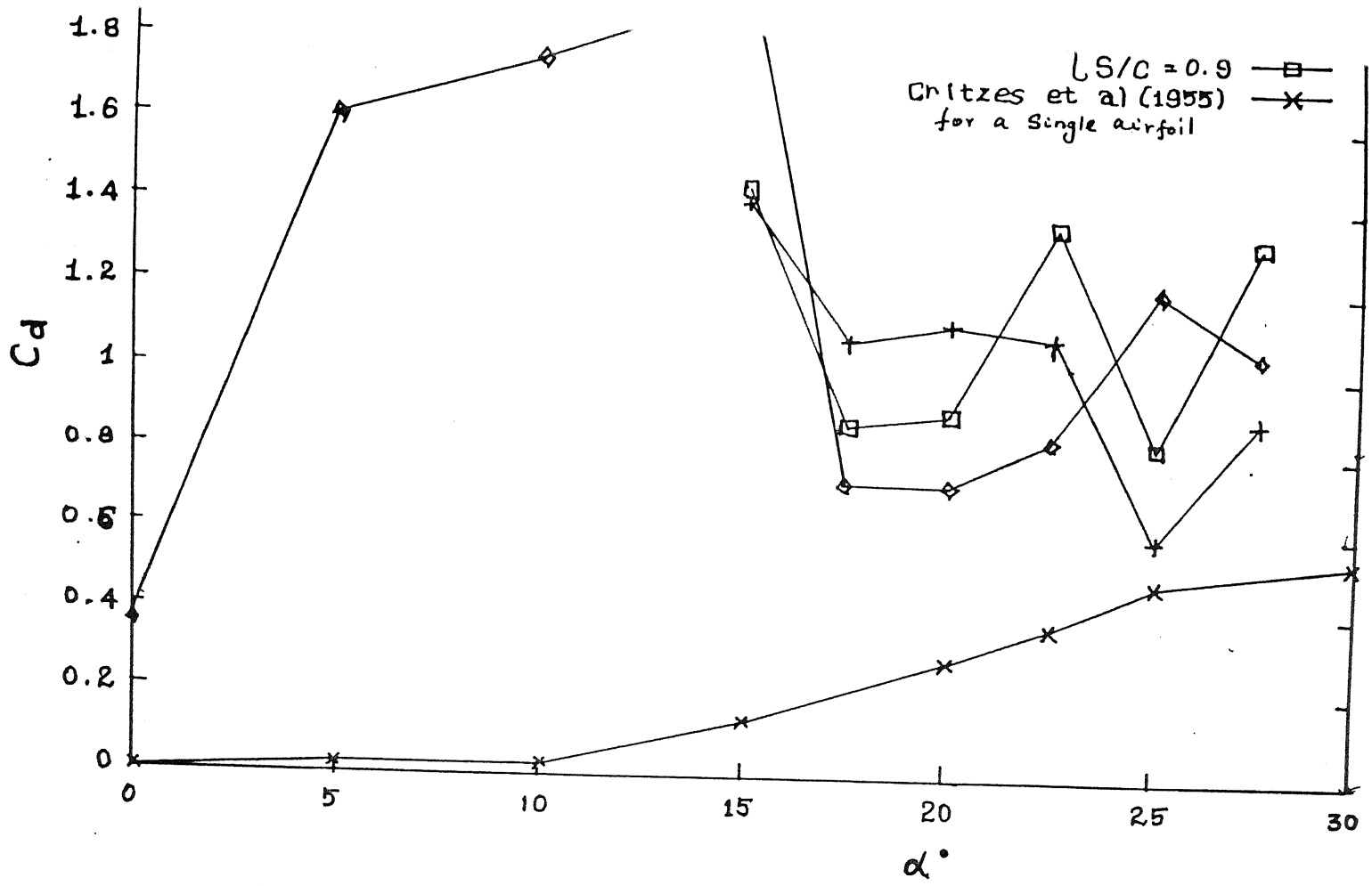

Figure 4.64: Drag vs α, $V_\infty = 25$ m/s

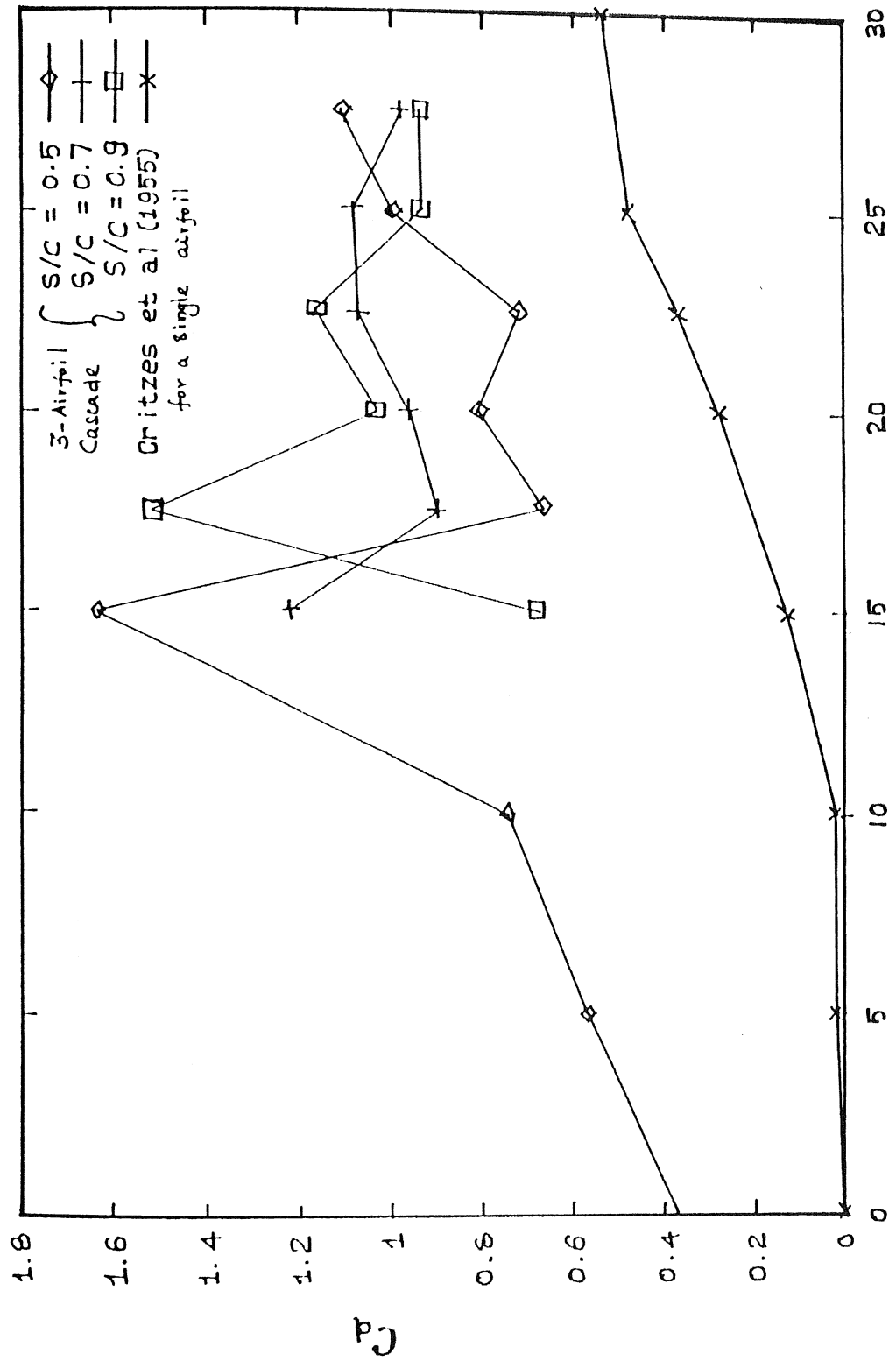

Figure 4.65: Drag vs α, $V_\infty = 35$ m/s

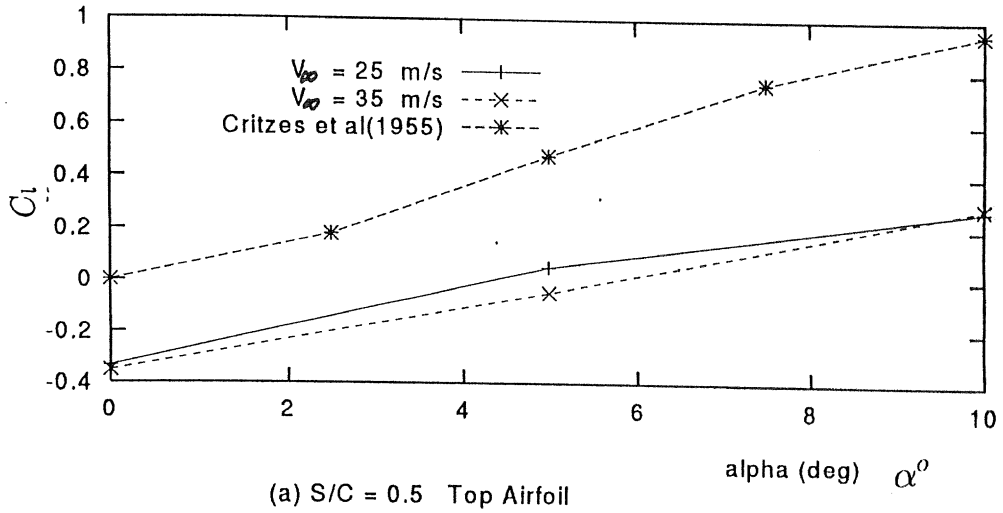

(a) S/C = 0.5 Top Airfoil

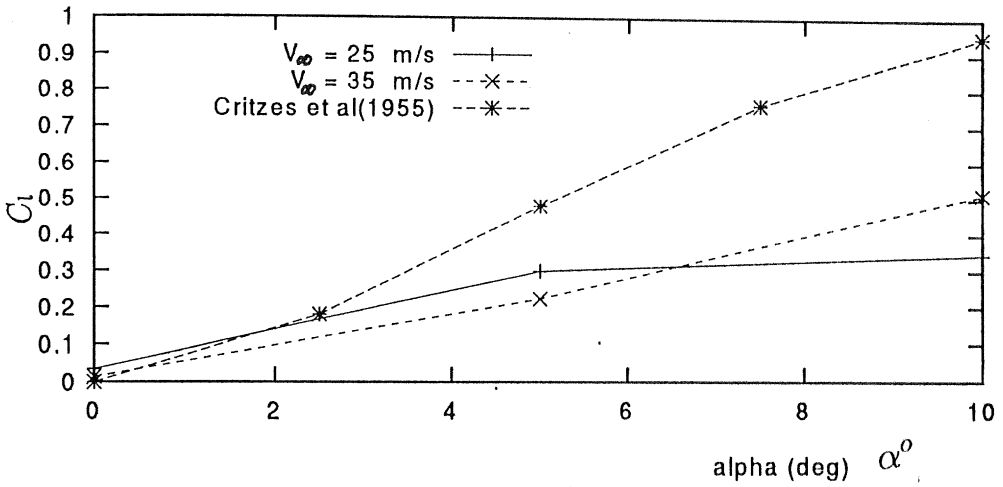

(b) S/C = 0.5 Middle Airfoil

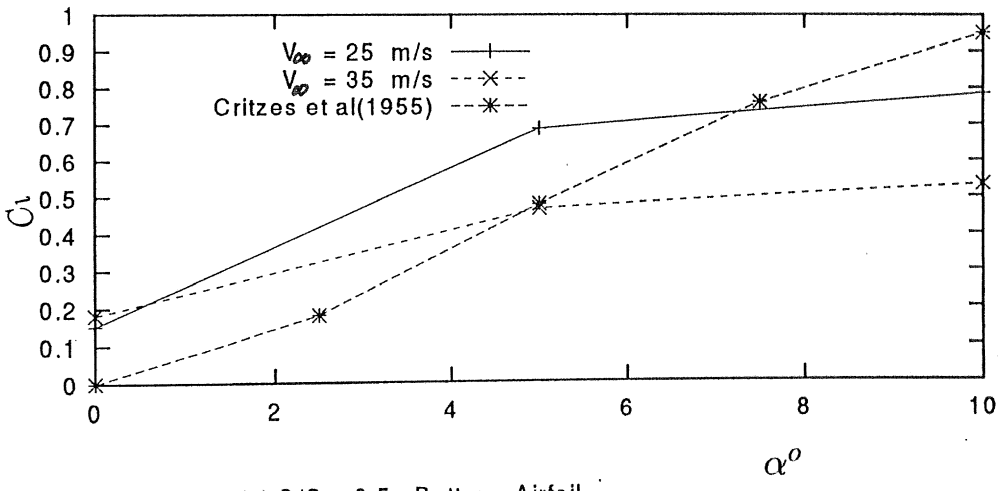

(c) S/C = 0.5 Bottom Airfoil

Figure 4.66: C_l *vs* α

pendix

ier approximation curves

curves and surfaces are credited to P.Bezier of the french car firm Regie Renault who ped it about (1962) and used them in his software system UNISERF, which has been ›y designers to define the outer panels of several Renault cars. These curves are known zier curves.

athematically for n+1 control points, the Bezier curve is defined for the following omial of degree n,

$$P(u) = \sum_{i=0}^{n} Pi\ Bi,n(u) \qquad 0 \leq u \leq 1 \qquad (1)$$

herer P(u) is any point on the curve and P_i is a control point. Bi,n are the Bernstein s polynomials. Thus, the Bezier curve has a Bernstein basis. The Bernstein polynomial

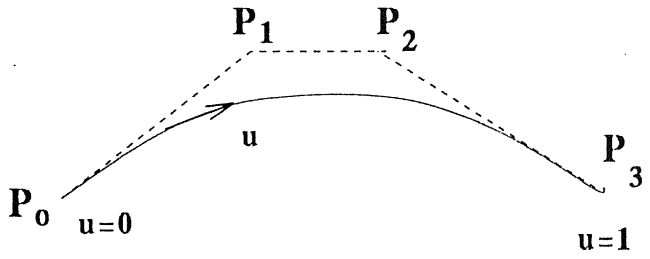

P_0, P_1, P_2, P_3 Control points

A Bezier curve

blending or basis function for the Bezier curve and is given by

$$B_{i,n(u)} = C(n,i)\ u^i\ (1-u)^{n-i} \qquad (2)$$

C(n,i) is the binomial coefficient

$$C(n,i) = \frac{n!}{i\ !(n-1)!} \qquad (3)$$

ng equation 2 and 3 and observing that C(n,o) = C(n,n) =1, equation 1 can be to give

$$P(u) = P_0(1-n)^n + P_1\ C(n,1)\ u(1-u)^{n-1} + P_2\ C(n,2)\ u^2(1-u)^{n-2}$$
$$+ \ldots\ldots + P_{n-1}\ C(n,n-1)u^{n-1}\ (1-u) + P_n u^n \qquad 0 \leq u \leq 1 \qquad (4)$$

haracteristics of Bezier curves are

e basis functions are real.

ıe degree of polynomial defining the curve segment is one less than the numbering defining polynomial points.

hey generally follow the shape of the defining polygon.

he first and last points of the curve are coincident with the first and last points of ıe defining polygon.

'he curve is contained within the convex hull of the defining polygon.

'he curve interpolates the first and last points. That is it passes through the first and ast points Po and Pn if we substitute u = 0 and 1 in eqn. 4

The curve is tangent to the first and last segments of the characteristic polygon.

eference,

Ibrahim Zeid(19991), CAD/CAM Theory and Practice., McGraw-Hill,Inc., New York.